The Electrochemical Detection of Acetaminophen and the Enantioselective Recognition of Tyrosine Enantiomers using a modified carbon-based electrode

Bronach Michelle Healy BSc. (Hons)

Department of Chemistry

National University of Ireland Maynooth

October 2022

Thesis Submitted to the National University of Ireland in Fulfilment of the Requirements for the Degree of Master of Science.

Supervisor: Prof. Carmel B. Breslin

Head of Department: Prof. Denis Rooney

Table of Contents

Declaration

I hereby certify that this thesis, which I now submit for assessment on the programme of study leading to the award of Master of Science, has not been submitted, in whole or in part, to this or any other University for any degree, and is, except where stated otherwise, the original work of the author.

Signed: Bríonach M. Healy Date: 27/10/2022

Acknowledgements

I would like to begin by thanking my supervisor, Professor Carmel Breslin, for her amazing support and guidance during my Masters. Throughout the past two years she was always at hand to help with any problems or queries I had and for that I am extremely grateful. Her approachable and friendly manner always put me at ease if I became stressed or unsure of anything, providing reassurance and encouragement at all times. I am very thankful to have had her as my supervisor.

I would also like to thank the staff of the chemistry department for making me feel welcome and being a great help during my time demonstrating.

Lastly, but by no means least, I would like to thank my family and my partner Rory. To my mam and dad thank you for encouraging me to complete a masters, thank you for supporting me emotionally and financially through not only my masters but my entire journey at Maynooth, thank you for everything. To Rory thank you for keeping me calm and stress free the past four months during writing. I could not have done it without any of you.

Abstract

The beginning of this thesis sees the development and characterisation of a β-cyclodextrin (β-CD) based electrochemical sensor for the electrochemical detection of acetaminophen (paracetamol) and the influence of the accompanying activation of the glassy carbon-based substrate. To incorporate the β-cyclodextrin onto the glassy carbon electrode, electropolymerisation from an aqueous solution of the β-CD monomer was carried out, attempting to form a polymeric β-CD film. The modified electrode was characterised using cyclic voltammetry, electrochemical impedance spectroscopy and scanning electron microscopy (SEM) coupled with electron dispersive X-Ray analysis (EDX). Optimum conditions for the formation of the sensor were obtained by selecting an ideal potential window, applied potential and also selecting the suitable number of cycles required for modification. A highly efficient sensor was formed when cycling occurred between -2.0 to 2.2 V (vs. SCE) cycled for 15 cycles. The role of the activation of the GCE was also investigated and found to greatly enhance the electrochemical performance of the sensor. It was found that cycling the GCE in a 1.0 M phosphate buffer solution (PBS) at pH 5.5, from -2.0 to 1.1 V (vs. SCE) for 5 cycles, produced a nearly identical voltammogram when compared to a voltammogram where both activation and the electropolymerizing processes on the GCE surface occurred. The modified sensor achieved good sensitivity towards acetaminophen at a neutral pH with a peak current density of 3.8 mA cm^{-2}, with the oxidation of acetaminophen being influenced by pH in which peak currents became lower in more alkaline solutions. In addition, a wide variety of interfering compounds was examined to establish their effect, if any, on the detection of acetaminophen using the β-CD modified GCE. The study concluded that the oxidation of acetaminophen was not influenced by the addition of any of the interference compounds and the sensor was capable of achieving high selectivity.

The final part of this thesis explores the development and characterisation of a chitosan and graphene-modified GCE (CS/GO- GCE) for the electrochemical enantioselective recognition of tyrosine enantiomers. Graphene was incorporated into the sensor by electrodeposition from an aqueous graphene nanoplatelet (GO) dispersed in a 5 mM β-CD solution to prevent agglomeration of the graphene sheets. The biopolymer chitosan was incorporated by electrodeposition from 1% chitosan hydrogel solution (CS) dissolved in 0.2 M acetic acid. The presence of GO and CS were confirmed using cyclic voltammetry, attenuated total reflectance Fourier transform infrared spectroscopy (ATR-FTIR) and potentiostatic measurements. Optimum conditions for development of the CS/GO-modified GCE involved investigating

solvent and polymer concentration of the chitosan hydrogel solution, analysis of the supporting electrolyte used and examining the time sensitive diffusion of molecules into the hydrogel. Electrodeposition of graphene was accomplished by cycling from -1.5 to 0.8 V (vs. SCE) for 5 cycles at 50 mV s^{-1} using cyclic voltammetry, whilst deposition of the adherent hydrogel polymer was achieved by potentiostatic measurements held for 5 min at -1.5 V (vs. SCE). FTIR spectra showed a combination of CS and GO characteristic peaks suggesting the GO become encapsulated in the CS polymer on the surface of the GCE. The CS/GO-modified GCE achieved good enantioselective recognition between the tyrosine (Tyr) enantiomers, with preferential binding towards L-Tyr displayed. The presence of the chiral hydrogel polymer enabled enantioseparation capability of sensor however it reduced the electrochemical sensitivity of the sensor.

Chapter 1: Introduction and Literature Review

1.1 Introduction

The thesis outlines two objectives 1. to develop a β-Cyclodextrin (β-CD) based sensor for the detection of acetaminophen (Paracetamol) and 2. to develop a chitosan/graphene (CS/GO) based sensor for the enantioselective recognition between enantiomers of the amino acid Tyrosine (Tyr). Paracetamol is a commonly used drug used to relieve mild to moderate fever and pain however, ingested in excess quantities can cause organ damage and even acute liver failure. The L enantiomer of tyrosine (L-Tyr) is a non-essential amino acid that plays an important role in synthesising hormones needed for sleep and mood regulation in the human body, whilst the D- Tyr does not act as a building block for these vital hormones. Therefore, the ability to achieve selective recognition between the two is of paramount importance in relation to human health.

In this chapter, an introduction to electrochemical sensors, the modification of these sensors and the analytes to be tested is given. The materials used in the modification processes and their electrochemical suitably to the sensor are also introduced and discussed in great detail. The second chapter details the relevant experimental techniques and apparatus employed, along with an overview of the theories and related equations used in this thesis.

The results and main findings for the β-CD modified sensor are presented and discussed in Chapter 3. Within this chapter the formation and characterisation of the β-CD modified sensor is investigated. The β-CD film is successfully formed through the proposed electropolymerisation of the β-CD monomer and the optimum parameters are obtained. The β-CD film is then analysed as a sensor for the detection of acetaminophen. An activated GCE without the presence of β-CD is also examined for the detection of acetaminophen, to investigate the role of the activation of the GCE.

In Chapter 4, the results and findings are presented and discussed for the CS/GO modified sensor. This chapter includes the formation and characterisation of CS/GO sensor in which the successful electrodeposition of both the graphene nanoparticles and chitosan hydrogel onto the surface of the GCE is achieved. The sensor was then analysed for the enantioselective recognition of tyrosine enantiomers and the optimum parameters are obtained by varying the solvent and polymer concentration. Chapter 5 presents the final conclusion of the thesis results and findings, relating to both modified sensors.

1.2 Electrochemical Sensors

The word sensor originates from the Latin word *sentire*, meaning to feel. A sensor is an appliance that can react and respond to an array of external stimulus, such as light, pressure and sound to name only a few. Any changes occurring within the sensor as a result of the surrounding stimuli is measured through the transmission of an electrical signal. This signal or impulse of the sensor provides feedback and information about the stimulus being investigated.

Electrochemical sensors are a special branch of sensors which employ electrodes as the transducer of the electrical impulse for analyte testing [1]. Electrochemical sensors are used to detect reactions that are electrochemical in nature where usually a reduction-oxidation reaction is taking place between an electrode and analyte [2]. The measurements typically relate to a change in current or potential within the electrochemical system. For amperometry-based sensors, where the measurement signal is current, the electrode employed as the sensor is designed to facilitate the electron transfer step, where the analyte is oxidised or reduced at the electrode-solution interface. Ideally, the electrode should possess high electronic conductivity, good long-term stability and a high-rate constant for the electron transfer step.

An ideal sensor system, whether it be chemical or even biological in nature, should also possess recognition ability. The recognition factor allows the sensor to differentiate and selectively identify the target analyte in a complex solution. As the electrodes are the sensor's transducer, they are responsible for translating the recognition of the bounded analyte into an understandable and quantifiable signal [3]. Many electrochemical and electro-analytical techniques, such as amperometry and cyclic voltammetry, are employed with electrochemical sensors. These devices are increasingly useful due to many beneficial factors; the electrode as the transducer of the system is thought to be a rather clean design accumulating no waste, the ability to measure target compounds in micro-volumes, cheap production costs and quick analysis of signal data are all advantageous factors. There are numerous applications of these electrochemical sensors over a range of industries, one example in the medical industry is seen in glucose sensors that are commercially available to patients suffering from diabetes, for the monitoring of glucose levels in the blood [1]. In agriculture, electrochemical sensors are used by modern day farmers to gain vital information relating to soil fertility. Factors such as soil nutrient levels and pH are two prevalent parameters determining soil quality that can be recognized by sensor electrodes within the soil due to particular ions they contain. In addition, the literature also commonly reports the use of electrochemical sensors in the removal of

contaminants and impurities from water as part of wastewater treatment processes [4]. Furthermore, electrochemical sensors have been used in the enhancement of other analytical techniques namely chromatography detectors. Overall electrochemical sensors being developed today are growing in precision, selectivity and sensitively [1].

1.3 Modification of Electrochemical Sensors

Two important parameters in the development of electrochemical-based sensors are selectivity and sensitivity and these are normally enhanced by modifying the surface of the electrode. This is an attractive way to achieve a greater binding of the target analyte. Most commonly the immobilisation of recognition compounds onto the electrode surface is carried out to increase the selectivity of the target compound. Surface electrode modifications were first introduced by Bard and Itaya back in 1978. Since that time an extensive amount of research has been undertaken in the design and planning of electrochemical sensors [5]. The substrate or working electrode which is employed to develop a sensor is normally either carbon, platinum, or gold, as indicated in Figure 1.1, but in more recent times screen printed electrodes have gained attention [6]. It is at this surface where the redox reaction occurs and where the analyte is bounded for recognition, therefore this surface is also the site for modification. Ultimately this site links the sensing region of the electrode with the sample.

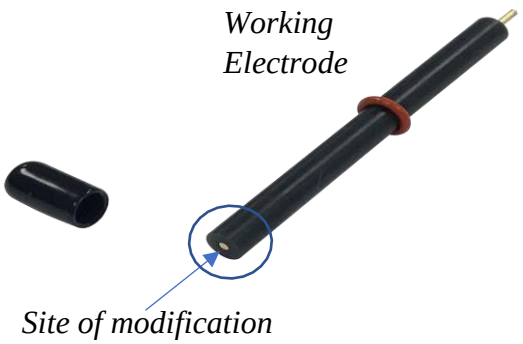

Figure: 1.1: A working electrode containing a GCE surface as the active site.

1.3.1 Nanoparticles and Nanostructures

The use of nanoparticles (NPs) and nanotechnology in the development of electrochemical sensors has gained a significant amount of interest from researchers in recent times. NPs are attractive materials due to their small cost, high surface area, good electrical and catalytic properties [7]. Within the branch of nanotechnology, the nanoparticles being manipulated and dealt with consist of atoms and molecules typically with a diameter of 100 nm or less. NPs can exist from either one type of nanomaterial or from different starting nanomaterials that are referred to as hybrid nanomaterials. Hybrids can possess combined physical-chemical properties and carry out multiple functions [7]. NPs can display a wide range of shapes and can even form in multiple dimensions (D), i.e., 1D, 2D and 3D. Studies have also found that these materials can greatly enhance the sensing element of the electrode by modifying morphological features and physiochemical properties such as optical properties.

The composition of NPs is not a simple one, they encompass three different layers; (1) The most outer layer or surface layer which is commonly functionalized using a range of compact molecules, metal ions and most frequently polymers. (2) The middle or shell layer, this layer surrounds the core of the NP but its chemical composition is different from the core itself. (3) Finally, the core, which exists as the central segment of the NP [8]. Nanoparticles are being deployed in sensor modification for two mains reasons; from a recognition viewpoint they improve the selectivity of the working electrode, they can also enhance sensitivity and from an efficiency viewpoint NPs result in increased surface area of the sensor, swift transport of mass and great control of the electrode microenvironment. In addition, the unique size of the NPs enables the production of electrodes to be more cost friendly by curtailing the materials required and waste generated. This is hugely beneficial to materials that are expensive to purchase such as platinum and gold. In turn, only a small sample size is required when NPs are incorporated into the sensor development process due to miniaturization. In general, the merging of nanotechnology with current electrochemical methods enables the creation of strong, dependable electrical appliances with waste and good process control [9]. There are many techniques used to modify the WE's surface with these NPs, one common method sees the particles incorporated into a matrix, typically a polymer of some sort, to create a nanocomposite film/polymer [8]. Other procedures involve depositing the NPs directly to the electrode surface through electrodeposition methods, following the NPs dispersion within a solution.

Many studies have reported positive findings in relation to selectivity and recognition ability of sensors modified with an array of NPs. One study conducted by Manjula et al. electrodeposited cerium niobium oxide nanoparticles (CNO NPs) onto the glassy carbon electrode (GCE) surface with the aim of detecting 4-Nitrophenol, a water toxin from industrial waste. Cerium is a rare earth metal and when oxidized to cerium oxide (CeO_2) possess remarkable redox properties, semiconductor characteristics and has a significant surface area making it a suitable electrochemical material. The addition of niobium (Nb) greatly increases the thermal and chemical stability. The modification of the GCE with the CNO NPs was found to improve the selectivity of 4-Nitrophenol sensitivity when compared to the unmodified/bare GCE, a CeO_2 modified electrode and even a niobium pentoxide (Nb_2O_5) modified electrode. The study also stated that the CNO NPs/GCE showed a strong rate of electron transfer and electrical conductivity. The high electron transfer factor is apparent when the charge transfer resistance (Rct) of the above-mentioned modified electrodes were compared, with CNO NPs found to display significantly lower Rct values [10].

In a different study an electrochemical sensor was developed using an electropolymerized DL-methionine (DL-met) polymer onto a GCE modified with gold nanoparticles (AuNPs), for the detection of paroxetine (PRX). PRX being an inhibitor of serotonin reabsorption within the human body. The research found many advantageous factors associated with the use of AuNPs and also the use of a conducting polymer in sensor development. The authors stated that the modified AuNPs/CGE increased the current peak of the target analyte by tenfold when compared to the bare unmodified GCE. This dramatic increase in current is due to the AuNPs boosted electron transfer and expanded surface area, hence enhancing sensor sensitivity. A further higher redox peak/ current peak was noted for poly(DL-met)/AuNPs GCE [11]. These examples are two of many studies displaying heightened sensitivity and increased recognition ability following the modification of the WE with NPs, also seen in studies that have introduced polymers to the modification process. The role of polymers in electrochemical sensor modification will be further discussed in Section 1.2.3.

NPs can be categorised into different groupings based on their morphology, sizing and characteristics properties. Three of the most well-known categories include metal NPs such as the gold NPs mentioned above, semiconductor NPs like the cerium-based NPs and finally carbon-based nanoparticles [6]. Carbon-based nanoparticles include some of the latest and most versatile NPs, with graphene being one of the most widely used material.

1.3.2 Graphene

Graphene (GR) was discovered in 2004 by a team of physicists lead by Andre Geim from Manchester University and is the world's first ever known two-dimensional (2D) crystal that is atomic in nature. In the search for graphene the team used a rather simple extraction approach. Through the technique of micromechanical cleaving, they successfully removed a single layer of atoms from three-dimensional (3D) graphite. Following this removal, the researchers then carried out exfoliation on the 2D graphene crystals that are held together by weak forces, to obtain independent graphene atomic sheets [12]. GR is an engrossing material and since its discovery has attracted immense attention from different fields due to its distinctive properties, including great mechanical strength, strong electrical conductance [13] and adaptive surface functionalities [14]. The charge build up on a material's surface is dependent on the material's conductivity. The degree of a material's conductivity or lack thereof can be classified under three categories: conductors, semiconductors and non-conductors. Conductors have the ability to disperse and lose charge almost instantaneously after receiving it whilst non-conductors will hold on to the charge for a much longer period of time, with some never dissipating the charge also called insulators. GR belongs to the class of semi-conductors, which fall in the intermediate between non-conductor and conductor conductivity values meaning they can dissipate charge under certain conditions [15].

This 2D graphene crystal is comprised of a single layer of sp^2 hybridized carbon atoms arranged in a hexagonal lattice [16], similar in shape to a honeycomb, as illustrated in **Fig. 1.2**. Within a single sheet of GR each carbon atom forms three sigma (σ) bonds with their neighbouring atoms. The sp^2 hybridization of the carbon atoms results in the delocalization of non-planar π bonds and this delocalization is what brings about GR's electrical conductivity [14].

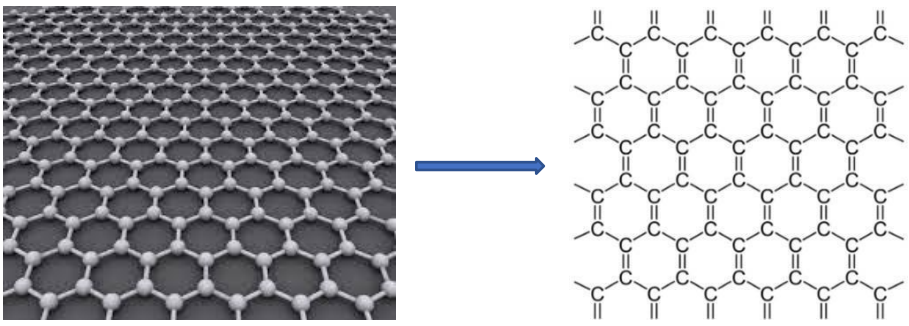

Figure 1.2: Crytsalline structure of a single graphene sheet in a hexagonal lattice [17].

GR can be classed based on the number of stacked sheets it contains; singe sheet/layer, few layers GR (2-10) layers and multilayer GR which is essentially a thin layer of graphite. The conductivity of GR (64 mS cm^{-1}) is noted to be 60 times greater than other carbon-based nanostructures such as single-walled carbon nanotubes (SWCNTs) and conveys great thermal stability over a wide temperature range. The surface area (2630 m^2 g^{-1}) of GR is large and is also reported to be larger than the surface area of SWCNTs [18]. This large surface area supplies an increase in active sites for the electrocatalytic reactions to occur by accommodating more target analytes, productively improving the sensor sensitivity [19].

Another amazing quality of this ultra-thin material is its strength, with studies showing that the breaking strength of GR is over 100 times higher than a film of steel possessing identical thickness. The recognition material used at the electrode surface should conduct a catalytic effect and catalyse the reaction of the solution [16]. GR has been credited in recent years as a significant potential catalyst that can be extremely beneficial to electrochemical sensors. Moreover, GR conducts a strong charge carrier mobility that enables fast electron transfer at the basal planes of GR layers, facilitating the electron transfer between the electrode sensing material and the target molecules [19]. Carbon-based materials have been largely used as modifiers of electrodes in electrochemistry as they possess a large potential window, low charge resistance, display a low background current, are cheap and show clear-cut redox peaks. As illustrated in **Fig. 1.3**, GR monolayers act as the building blocks of other carbon-based materials like graphite, carbon nanotubes (CNT), fullerenes and diamond and therefore GR can be considered the mother of all other graphitic materials [16].

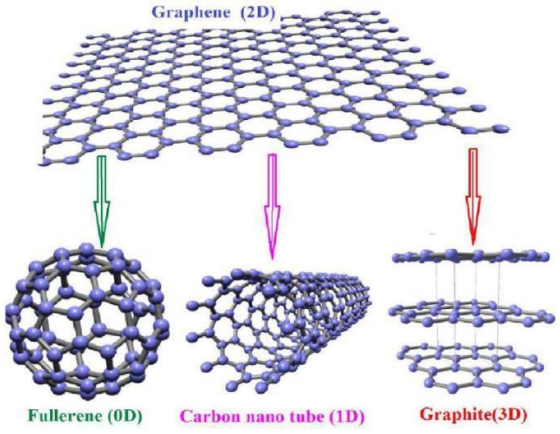

Figure 1.3: Carbon-based nanostructure materials with varying dimensions that can be formed from 2D graphene sheets as the building layers/blocks [20].

This research project used graphene nanoplatelets as the graphene-based material of choice. Different types of graphene nanoparticles are given different terminologies based on the materials thickness. Single sheet GR or nanosheet graphene is one atom thick with a diameter of just 0.345 nm [21] whilst GR nanoplatelets possess a thickness between 5-25 nm and typically under 10 nm [22].

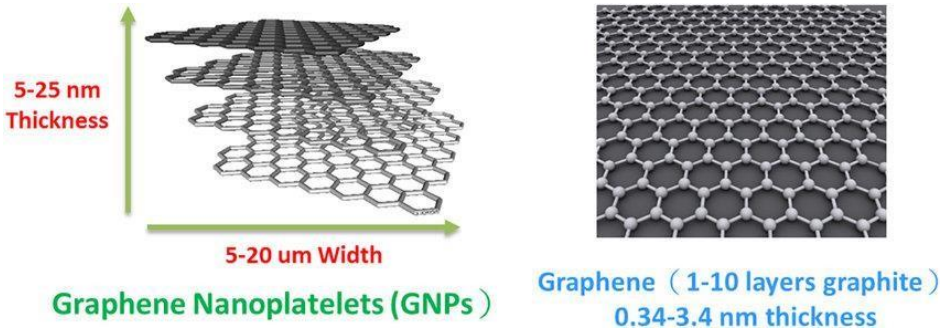

Figure 1.4: Comparison in material thickness, graphene nanoplatelets vs graphene nanosheet.

GR nanoplatelets are also extracted from graphite and it is possible that following this process GR nanoplatelets could contain some oxygen-containing groups. This would see the surface of the GR nanoplatelets exist very similar to the material graphene oxide, just greater in thickness.

Graphene oxide (GO) is a chemically modified version of graphene containing an abundant of oxygen-containing functional moieties, formed by the oxidation of graphene as seen below in **Fig. 1.5**. GO as a derivative of graphene is a hugely important one which also displays a large surface area, good electrical conductance and great intrinsic strength similar to graphene. However, following the oxidation process GO unlike graphene possess copious epoxide (C-O-C) and (C-OH) hydroxyl groups on the carbon rings [23] while the edges surrounding the sheets contain carbonyl (C=O) and carboxyl groups (-COOH). GO exhibits different adsorption properties when compared with GR due to its different chemical structure. GR is hydrophobic and non-polar in nature and is extremely hard to disperse in aqueous solutions. On the contrary GO displays hydrophilic tendencies and can form stable dispersions in aqueous media and displays polarity as the oxygen containing groups it contains causes the material to be strongly charged.

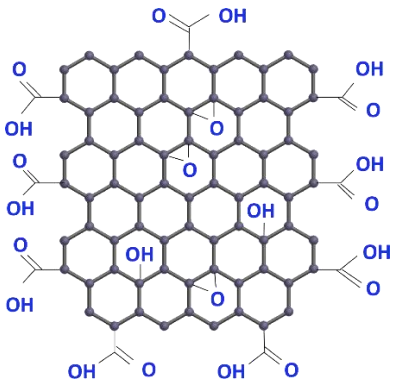

Figure: 1.5: Modified graphene with abundant oxygen-containing functional groups [24].

1.3.3 The Biopolymer Chitosan

Polymers are a type of macromolecule consisting of smaller molecules called monomers. These monomers are arranged in a repeating manner and can also be called repeating units which are held together by chemical bonds. The sum of monomers within a polymer can greatly differ and the recurrence of the repeating pattern or regularity of the polymer alongside orientation can also greatly vary. Polymers can exist naturally in nature, or they can be lab synthesised, both types are incorporated in some way across nearly each and every type of industry, this versatility being attributed to the numerous extraction/synthesis pathways and adjustability of polymers. Examples of everyday polymers can be found in our own homes such as polytetrafluoroethylene (PTFE), commonly known as Teflon, which is employed as a non-stick coating on utensils, irons and boilers to name but a few. Within the medical industry polyacrylates and polybutylene are two polymers commonly used in the manufacturing of medical devices [25]. In the field of electrochemistry natural occurring polymers or biopolymers have been involved in the latest developments of electrochemical sensors such as gelatin, albumin and chitosan.

Chitosan is a naturally occurring linear polysaccharide derived from the alkaline deacetylation of chitin, commonly sodium hydroxide is used as the alkylating agent. Chitin itself is a large polysaccharide that exists as a structural component of the exoskeletal systems of crustaceans and arthropods and is also found within the cell wall of yeast and fungi. The structural role of chitin is similar to the role of the protein keratin in human nails, skin and hair providing strength and healing properties. Chitin was first extracted from fungi in 1811 by Braconnot and was

coined the name ‘chitin’ originating from the Greek meaning for tunic or cover [26]. Chitosan is a biopolymer comprising of repeating units of D-glucosamine and N-acetyl-D-glucosamine, connected by β (1-4) bonds [27] and in solution can be used to form many substances such as gels, films, particles etc. In this research project, a chitosan solution was utilised as a hydrogel matrix in order to immobilize graphene nanoplatelets, for the detection of the amino acid tyrosine (L/D). In general, chitosan is an ideal material for immobilisation purposes due to its adsorption ability, environmentally friendly nature, remarkable layer-growing capability, increased permeability, availableness and biocompatibility [26].

Chitosan consists of a primary amino group located at the second carbon (C2) and primary and secondary hydroxyl groups located on the sixth and third carbon (C6,C3), respectively, **Fig. 1.6**. The acetamide functional group and the glycosidic linkage found in chitosan are also accepted as reactive functional groups. The presence of such groups permit a variety of modifications forming polymers with advanced properties and characteristics [28].

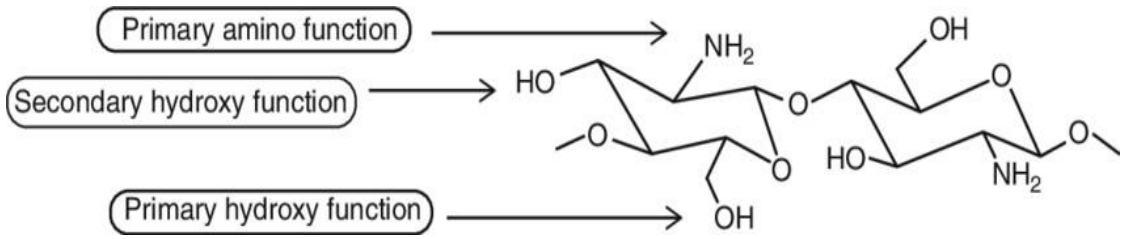

Figure 1.6: The chemical structure of chitosan and the reactive functional groups it contains [29]. The structure of chitosan contributes to the physical and chemical behaviours that chitosan exhibits including solubility, hydrogel formation capability and enantioselectivity of the natural polymer.

Chitosan is soluble in most acidic aqueous solutions with this property being attributed to the great number of protonated amino groups it contains in acidic media with the p*K*a value of chitosan reported to be typically around 6.5 [28]. Protonation of the amino groups results in an increase in cationic species along the polymer which in turn increases the polarity and magnitude of electrostatic effects which ultimately increases the solubility [30]. Chitosan begins to exhibit solubility when half or more of all these amino groups become protonated, whilst it displays poor solubility in basic and neutral solutions, limiting some applications of chitosan [28].

Chitosan-based hydrogels can be produced through a method called cross-linking, either chemical or physical cross-linking to be exact. Physical crosslinking can occur due to the cation nature of chitosan in solution that sees anions or negatively charged polymers ionically interacting with chitosan to form a hydrogel. An alternative method of physical crosslinking is the addition of a base, such as sodium hydroxide or sodium carbonate into the chitosan solution. This addition leads to a rise in pH levels causing chitosan to become deprotonated and form gels through hydrogen bonding, hydrophobic effects and through weak Van der Waals forces. [31]. In terms of chemical crosslinking, various polymerization methods have been employed, such as radial and photopolymerization, reactions using enzymes, the use of crosslinking agents, such as aldehydes, that form covalent bonds and also self-assembly cross-linking without the use of any cross-linkers [32]. Chemical cross-linking is a stronger and permanent form of cross-linking, whereas physical cross-linking involves much weaker bonds being formed [33]. As mentioned above, chitosan exhibits solubility in acids, typically it is dissolved in aqueous solution with the help of a monocarboxylic acid. In this study, chitosan was aided in dissolution by the monocarboxylic acid acetic acid and formed a hydrogel matrix through chemical cross-linking. The chemical cross-linking of chitosan occurs due to the interactions of the hydroxyl (OH) and amine groups (NH_2) located on the polymer chain backbone. These interactions form strong and irreversible covalent bonds that link polymers chains together. This is the simplest method of chemical cross-linking and occurs when chitosan's own polymeric chains react together to form a hydrogel [32].

Highly conductive graphene nanoplatelets were incorporated into the hydrogel to provide an electrical conductive element to the polymer as chitosan itself is a non-conducting material [34]. This incorporation was made possible due to the remarkable adsorption properties of chitosan previously mentioned. Another fascinating property of the chitosan-based hydrogel that was significant in the detection of the target analyte was the ability of the hydrogel to swell. Polymers that can form hydrogels possess hydrophilic functional groups, in the case of chitosan it contains the hydrophilic amino group and hydrophilic hydroxyl group shown above in **Fig. 1.6**. These 'water-loving' or hydrophilic groups tend to mix well with water and allow the adsorption of water or aqueous fluids by the hydrogel, causing the hydrogel to expand in size and uptake a larger volume of solution, as evident in **Fig. 1.7**. This characteristic process of hydrogel swelling can be accounted for by the cross-linking polymeric structure that prevents the hydrogels from destructing or breaking during this process [32]. This increase of volume

size means more analyte solution can enter into the graphene-containing hydrogel matrix increasing detection of the target analyte.

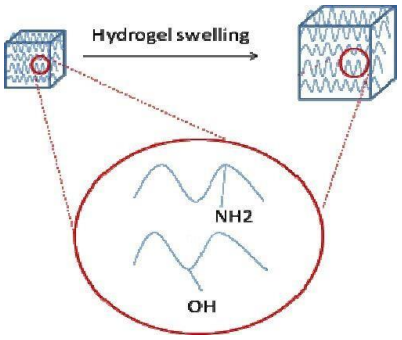

Figure: 1.7: Swelling process of chitosan hydrogel due to the presence of hydrophilic groups [32].

Within the pharmaceutical industry over 40% of the drugs produced are chiral molecules [35], meaning they exist as optical isomers that are non-superimposable mirror images of one another referred to as enantiomers. The chemical composition of enantiomers are the exact same with the only distinguishing property being the direction in which the plane of polarized light rotates. One enantiomer will rotate this light to the right in solution known as the 'dextrorotatory' or D enantiomer. Whilst the other enantiomer will rotate the light in the opposite direction to the left known as the 'Levorototary' or L enantiomer [36]. As the chemical compositions are identical the pair therefore have identical chemical and physical properties, for example thermodynamic properties such as reaction rates with non-chiral reactants are identical between the L and D forms of enantiomers. Differences between the two forms only come into play when the enantiomers are introduced to other molecules that are also chiral such as chiral recognition molecules. Individual enantiomers will fit differently into other chiral molecules like certain enzymes, amino acids and proteins and chiral polymers. This unique fit or interaction between different enantiomers with other chiral agents can explain why so often one enantiomer can smell and taste so dissimilar to the other and why they can have dramatically different effects as drugs [37].

Chiral separation is increasing in demand as it is highly important to isolate L and D enantiomers as one enantiomer could act as the safe and effective form of the drug while the other form could be non-effective or potentially harmful and even toxic if ingested. The need to develop separation methods that are both effective and eco-friendly is one of the many challenges faced in today's world of analytical science [35]. Natural polymers or polysaccharides such as chitosan, cellulose and chitin have been widely used as chiral ligands

for the separation of enantiomers that offer a more environmentally conscious approach with them being a renewable and sustainable source of chirality [38]. The chitosan polymer is one that is optically active in nature, meaning it has chirality. This property arises from the presence of asymmetrically substituted carbon atoms, which enable the self-assembly of helicoidal or spiral-like formations [39]. Chitosan in its solid state forms an ordered fibrillar structure containing a high magnitude of crystallinity and can adopt a diversity of shapes. Experimental data have shown that the helicoidal structure is composed of an elongated two-fold helix to be exact, arranged in zigzag formation [40] shown below in **Fig 1.8**. The fibrillar structure is extremely flexible enabling the polymer to twist, turn and twitch at any one moment in time. The helicoidal structure is what drives the polymer's ability to act as a chiral recognition molecule as it provides stereoselective recognition sites for different enantiomers [39]. Furthermore, in acidic solutions chitosan has been shown to form not one but a variety of different helical conformations observed in the solid state including a relaxed two-fold, a 4/1 and five-fold helix further increasing the chiral diversity of the chitosan polymers in solution. Preferred helical conformation and the ability to interchange between helical forms is dependent on the degree of acetylation carried out on the chain of chitosan [40].

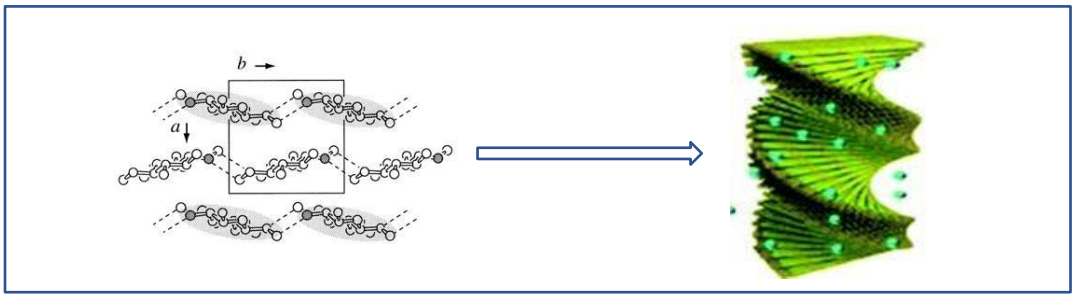

Figure 1.8: Zigzag formation of chitosan polymers taking up a systematic helicoidal conformation [41].

Many studies have achieved enantiomer recognition with chiral polysaccharides using electrochemical techniques. For example, one study investigated the enantioseparation of tryptophan using a chitosan/deoxyribonucleic acid (DNA)-based modified GCE. The study found that the modified electrode portrayed a stronger binding affinity to the L enantiomer over the D. The findings were based on an electrochemical technique that resulted in different oxidation peaks for each, with the peak current of highest value representing which enantiomer had a greater binding ability with the chiral interface [42].

In the study presented in this thesis, the enantiorecognition of the amino acid tyrosine (Ty) in its L and D enantiomer form is investigated. Tyrosine enantiomers can serve very different functions and have important roles in relation to human health, the exact roles of which will be discussed with detail in Section 1.3. Cyclic voltammograms were used to identify a preferred binding interaction between the enantiomers and the chiral chitosan polymer based on the lowest potential value recorded for each. Cyclic voltammograms and the corresponding electrochemical technique will be discussed with great detail in the next chapter.

1.3.4 β-Cyclodextrin

Cyclodextrins (CDs) are cyclic polysaccharides that can be produced by the degradation of starch by enzymes, commonly the enzyme glucotransferase is used [43]. The amylaceous origins of CDs make them biodegradable with non-toxic products that are tolerated remarkably well by the environment [44]. These polysaccharide structures consist of d-glucopyranose units connected by 1,4 glycosidic bonding [45]. CDs are divided into three distinct forms based on minor structural differences, alpha CD (α-CD), beta CD (β-CD) and gamma CD (γ-CD). The structural differences of α-, β- or γ-CDs arise from the different number of glucopyranose units each contains with α-CD containing six, β-CD seven and γ-CD eight units [46]. All three forms take a truncated cone or torus shape with both ends open, as depicted in **Figure 1.9**. This shape results from the chair conformation adopted by the glucose units. This conformation sees all secondary hydroxyl groups situated on one edge of the cone and all primary hydroxyl groups located on the other edge. The side of secondary groups (-OH) tend to slightly open up more than the side with the primary groups (-OH), this is why the cavities possess a 'V' shape [47].

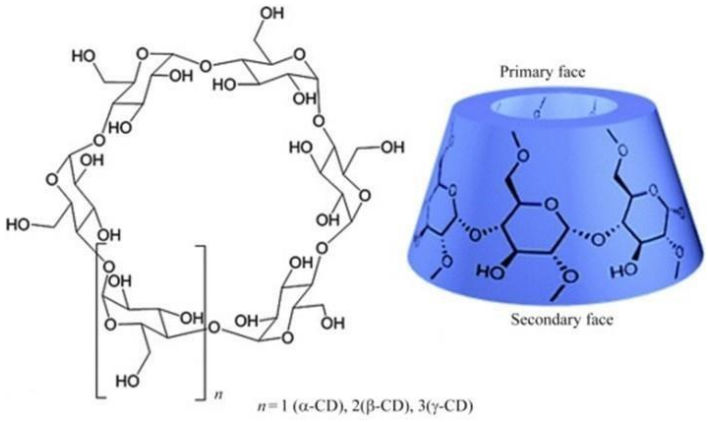

Figure 1.9: Cyclodextrin structure and toroidal shape cone [48].

The structure of CDs is amphiphilic in nature containing a hydrophilic outer layer and an internal hydrophobic cavity decorated with hydrogen atoms. Due to the bifunctional structure, CDs are able to encapsulate molecules that typically dissolve poorly in water, into the hydrophobic cavity they contain. The molecules that become encapsulated or trapped within this cavity are referred to as 'guest' molecules while the cyclodextrin itself is called the 'host' molecule, with the binding interaction known as an 'inclusion complex' [45]. These inclusion complexes have widely been used as molecular recognition systems due to correlating the shape and match of guest and host molecules [49]. The inclusion complex provides a quantitative analysis of the equilibrium between the guest-host system formed in an aqueous solution with most inclusion complexes arranged in a 1:1 (CD:guest) ratio [50]. β-CD is the most used CD due its large cavity diameter of 0.8 nm, easy production, ease of access and has the cheapest price of all three forms [51].

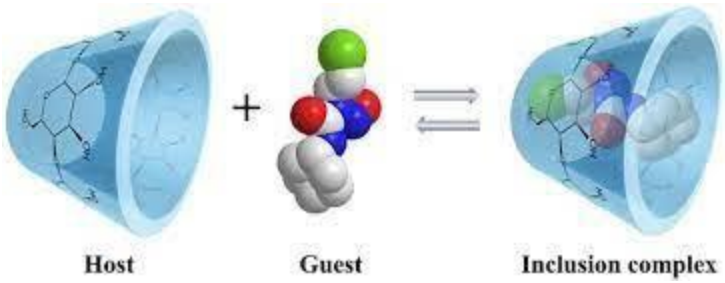

Figure 1.10: Inclusion complex that is formed between cyclodextrin (host) molecule and the guest molecule.

There is no one simple proposal that can describe the binding interactions of the CD and guest molecules in solution. However, there is a general understanding that intermolecular forces such as Van der Waals forces and hydrophobic effects play a crucial role in inclusion complexation. In this binding scenario the hydrophobic moieties of the guest become included within the internal CD cavity that is also hydrophobic in nature. Other intermolecular bonding including dipole-dipole, charge-transfer and hydrogen bonding have also been proposed for certain guest molecules, displaying the importance of the guest molecules characteristics also. In terms of guest properties, the size of the molecule or the size of the hydrophobic regions it contains must also match with the diameter of the CD cavity in order to achieve stable and strong binding [52].

They ability of CDs to incorporate a huge variety of organic molecules with differing shapes and polarity [53] makes them compelling materials in the development of sensors to give high

selective and sensitive detection of target analytes. CDs are often merged with a variety of materials with the hope of immobilizing the material onto an electrode surface in sensor modification. This combination method results in the production of a CD array with additional characteristics used to bind and encapsulate the target analyte through the formation of an inclusion complex, giving high sensitivity and selectivity. In this study graphene nanoplatelets were added to a CD solution acting as the combination material, enhancing the electronic conduction of the CD array. The weak intermolecular binding between the CD and the analyte is suitable for facilitating electron transfer during the redox reaction in solution, yet strong enough to actually trap and hold the target analyte in close proximity to the surface of the electrode for detection [52].

Electrochemical polymerization or electropolymerisation is an easy, straightforward and efficient technique used to produce polymers and indeed CD polymers have been reported [54]. The process begins by the oxidation of the monomer following this the polymer starts to grow into a polymer film situated on the surface of the carbon-based electrode. In many cases, polymerisation begins with oxidation of the monomer to produce a radical cation. The growth of the polymer film is understood to occur because of the coupling of these radical cations either with one another or with a neutral monomer. The monomer oxidation process being initiated by an electrical method is considered a green or eco-friendly chemical technique avoidant of the use of harmful oxidizing agents and allows for the control of polymer synthesis in real time [55].

Typically, the electrochemical method employed is either galvanostatic or potentiostatic in nature, and in this study cyclic voltammetry was used to attempt the electropolymerisation of β-cyclodextrin. The chemical and physical characteristics of the synthesized polymers are controlled by the conditions of the technique used such as applied potential, scan rate, number of cycles etc. [56]. The potential window is important as the extent of the potential should be great enough to initiate monomer oxidation yet avoid the overoxidation or secondary reactions which can obstruct the polymer forming process or result in unwanted reactions [55]. With either type of electrochemical method, a suitable electrode is chosen and the polymerization is performed in an electrolyte solution of the monomer [56]. For the electropolymeization of β-CD in this study, the monomer solution was supported in an electrotype solution of KCl, with the KCl providing ions to enhance conductivity of the solution.

The proposed mechanism for the electropolymerisation of β-CD is depicted in **Fig. 1.11**. Here the CD monomer is oxidised electrochemically to give the reactive radical cation, which then couples with neighbouring CD monomers. The corresponding cyclic voltammogram is also provided in **Fig. 1.11**. The origins of these peaks were not explained by Pereira et al. [56] but the authors did suggest that the peaks were all associated with the electropolymerisation reactions.

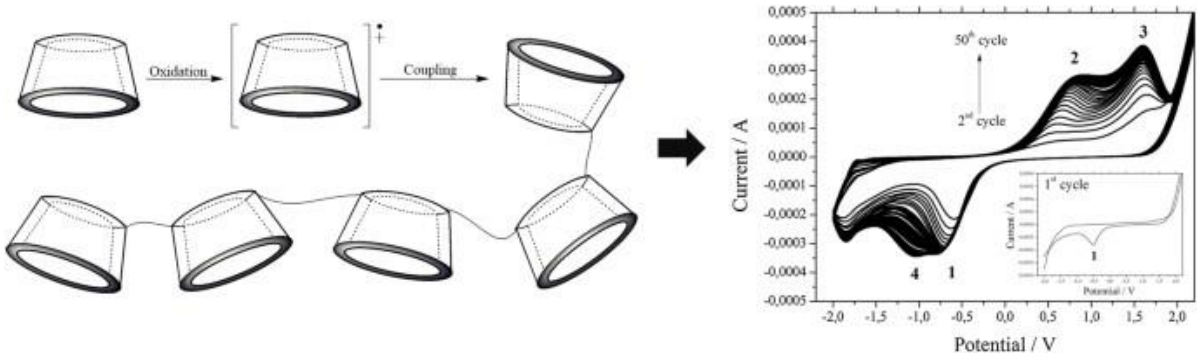

Figure 1.11: Electropolymerisation of β-cyclodextrin through initial oxidation step followed by radical cation coupling. Cyclic voltammetry was the electrochemical technique of choice as depicted by the cyclic voltammogram (CV) [56].

1.4 Paracetamol

Acetaminophen also known by the common brand name Paracetamol, **Figure 1.12**, is both an antipyretic and analgesic drug, used to relive moderate pain and reduce fever [57]. It is likely the most used medication for common pain ailments such as headaches, menstrual cramps, muscle and joint pain to name a few and is found in hundreds of products worldwide [58].

The history of paracetamol is a rather long and complicated one. Its discovery like many other important science discoveries was accidental. In the late 1880's two doctors treating a patient for intestinal worms mistakenly administered acetanilide instead of the drug naphthalene. Although the acetanilide had little effect on the parasites, it had a dramatic effect in reducing the patient's fever. Following this discovery, acetanilide was introduced to medicine in 1886 given the name 'antifebrin' [59], translating to antifever. Not long after its introduction, it was found that the drug displayed high toxicity levels with the most worrying level being

methemoglobinemia [59]. Methemoglobinemia refers to a condition where hemoglobulin in the blood is unable to bind to oxygen leading to impaired release of oxygen to tissues [60]. Research then began on derivatives of acetanilide that were hopefully far less toxic. Two compounds soon came to light that seemed to satisfy safety levels, phenacetin and N-acetyl-p-aminophenol (paracetamol). These derivatives were tested thereafter through a series of clinical trials conducted by the German scientist Joseph Von Mering. It is reported that Von Mering made an incorrect inclusion of the trial's results and stated that paracetamol had a similar toxicity level to the original drug acetanilide. As a result, phenacetin became the first derivative administered by doctors in the 1887. It was not until years later in 1948 that it was found that paracetamol is actually the primary active metabolite of both acetanilide and phenacetin and does not cause Methemoglobinemia at all. This revelation kicked off the start of paracetamol's career, being introduced to the pharmaceutical market in 1955 as an analgesic drug [59].

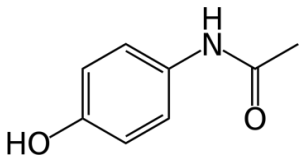

Figure 1.12: The molecular structure of Acetaminophen (Paracetamol) [61].

Paracetamol, when ingested in the recommended dosage shows good cardiovascular and gastrointestinal safety [57] and is a relatively safe drug. However, if taken outside of recommended guidelines in large doses or for a prolonged time it can cause liver damage and, in some cases, can result in comas and even death. In the United States alone paracetamol plays a role in 50% of all acute liver failures [62]. Liver toxicity or hepatotoxicity is caused by the formation of a metabolite N-acetyl-p-benzoquinone which cause protein adducts to form on proteins found in the mitochondria. The formation of the protein adducts causes a cascade of intracellular reactions that ultimately results in a change in the member of the mitochondria releasing intercellular proteins, which leads to the fragmentation of DNA and the onset of necrosis within the liver. Inflammation of the liver results from the necrosis, as highlighted in **Figure 1.13** [63].

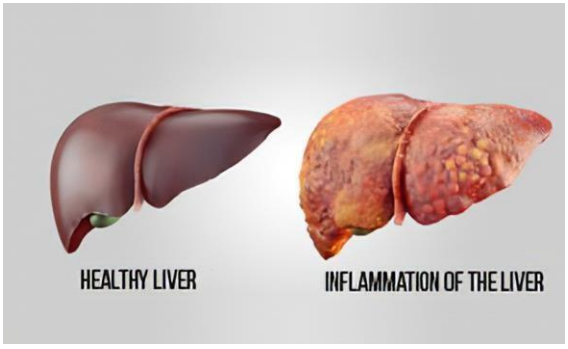

Figure: 1.13: Inflammation of the liver resulting from hepatotoxicity caused by the excessive ingestion.

Paracetamol exists on the market as both prescription only strengths and non-prescription medication, meaning the general public can simply access certain strengths of the drug from over-the-counter at pharmacies. In one recent published report by Sebastine and Wakeman [64], it was stated that in the year 2000 there were approximately 400 tons of paracetamol prescribed, just in England alone. The need to monitor the quantity of paracetamol for pharmaceutical quality control purposes and for the health of the general public is therefore paramount. Electroanalytical techniques have been used extensively for the determination of paracetamol as they provide a straightforward and sensitive method of determining paracetamol levels in tablet form, in human blood and in pharma formulations [65]. Furthermore, it is known in the literature that paracetamol can form an inclusion complex with β-CD [66] and therefore it was anticipated that the electropolymerised β-CD would provide a high concentration of suitable hosts to include the paracetamol molecules to give improved sensing.

1.5 Tyrosine

Tyrosine is one of twenty amino acids (AA) found in the human body and belongs to the aromatic amino acid family [67]. It exists as a non-essential AA meaning that the body itself can synthesize tyrosine and diet can provide a source, commonly found in milk-based products and fermented foods like wine and yoghurt [68]. Tyrosine is produced in the liver by the hydroxylation of the essential amino acid phenylalanine. This internal formation of tyrosine occurs when there is a low source of tyrosine coming from diet [69].

The enantiomers of tyrosine, which can polarise light in different directions, as shown in **Fig 1.14**, have different functions due to their differing optical isomer structures. It is widely understood that L-tyrosine (L-Tyr) acts as one of the primary building blocks for several neurotransmitters such as dopamine, epinephrine and norepinephrine etc. These hormones play important roles in sleep and mood regulation and therefore are implicated in human mental health. Whereas the D enantiomer of tyrosine (D-Tyr) is not used as a building block in protein formation but instead is used as a chemical reagent that promotes protein growth and it can act as a probe to investigate the dynamics of proteins [70]. D-Tyr has also been known to reduce melanogenesis in human cells, a process that involved the production of melanin pigments that are visible on skin. As a result, D-Tyr has been introduced to cosmetic formulations to help treat hyperpigmentation on skin caused by UV radiation and by Melanocyte-stimulating hormone (MSH) treatment [71].

The L enantiomer of tyrosine is of more importance in relation to human health and bodily regulation whereas D-Tyr, although useful in terms of protein studies and more recently cosmetic studies, is not as crucial to bodily functions. Therefore, the enantioseparation of the two is highly important.

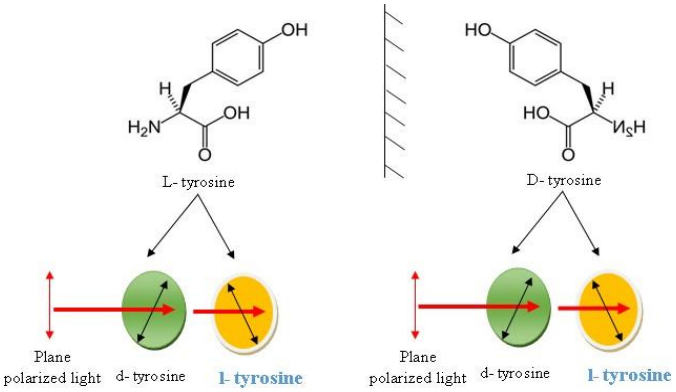

Figure 1.4: Tyrosine enantiomers characterised by the plane of polarized light. The L enantiomer polarizes to the left while the D enantiomer polarizes to the right.

1.6 Bibliography

1. Simões, F.R.; Xavier, M.G. *6 - Electrochemical Sensors*; Elsevier Inc., 2017;

2. Shetti, N.P.; Nayak, D.S.; Reddy, K.R.; Aminabhvi, T.M. *Graphene-clay-based hybrid nanostructures for electrochemical sensors and biosensors*; Elsevier Inc., 2018; ISBN 9780128153949.

3. Keçili, R.; Denizli, A. *Molecular Imprinting-Based Smart Nanosensors for Pharmaceutical Applications*; Elsevier Inc., 2021; ISBN 9780128221174.

4. Chugh, B.; Thakur, S.; Singh, A.K.; Joany, R.M.; Rajendran, S.; Nguyen, T.A. *Electrochemical sensors for agricultural application*; INC, 2021; ISBN 9780128245545.

5. Hussain, C.M.; Keçili, R. Electrochemical techniques for environmental analysis. *Mod. Environ. Anal. Tech. Pollut.* **2020**, 199–222, doi:10.1016/b978-0-12-816934-6.00008-4.

6. Li, M.; Li, Y.T.; Li, D.W.; Long, Y.T. Recent developments and applications of screen-printed electrodes in environmental assays-A review. *Anal. Chim. Acta* **2012**, *734*, 31–44, doi:10.1016/j.aca.2012.05.018.

7. Canevari, T.C. *Application of hybrid nanomaterials for development of electrochemical sensors*; Elsevier Ltd., 2022; ISBN 9780128237885.

8. Khan, I.; Saeed, K.; Khan, I. Nanoparticles: Properties, applications and toxicities. *Arab. J. Chem.* **2019**, *12*, 908–931, doi:10.1016/j.arabjc.2017.05.011.

9. Rassaei, L.; Marken, F.; Sillanpää, M.; Amiri, M.; Cirtiu, C.M.; Sillanpää, M. Nanoparticles in electrochemical sensors for environmental monitoring. *TrAC - Trends Anal. Chem.* **2011**, *30*, 1704–1715, doi:10.1016/j.trac.2011.05.009.

10. Manjula, N.; Pulikkutty, S.; Chen, T.W.; Chen, S.M.; Fan, C.H.; Ali, M.A.; Al-Hemaid, F.M. Electrochemical sensor based on cerium niobium oxide nanoparticles modified electrode for sensing of environmental toxicity in water samples. *Colloids Surfaces A Physicochem. Eng. Asp.* **2022**, *637*, 128277, doi:10.1016/j.colsurfa.2022.128277.

11. Al-Mhyawi, S.R.; Ahmed, R.K.; El Nashar, R.M. Application of a conducting poly-methionine/gold nanoparticles-modified sensor for the electrochemical detection of

paroxetine. *Polymers (Basel).* **2021**, *13*, doi:10.3390/polym13223981.

12. Graphene, I.; Carbon, H.O.; Geim, A.; Novoselov, K. Graphene: Electronic Properties. **2007**, *10*, 1–6.

13. Mittal, S.K.; Goyal, D.; Chauhan, A.; Dang, R.K. Graphene nanoparticles: The super material of future. *Mater. Today Proc.* **2020**, *28*, 1290–1294, doi:10.1016/j.matpr.2020.04.260.

14. Barua, S.; Geng, X.; Chen, B. *Graphene-based nanomaterials for healthcare applications*; Elsevier Inc., 2020; ISBN 9780128178409.

15. Of, H.; Circuits, H. 9 Handling and Clean Rooms 1.0., doi:10.1016/B978-0-8155-1423-7.50011-0.

16. Chaudhuri, B. *Biopolymers-graphene oxide nanoplatelets composites with enhanced conductivity and biocompatibility suitable for tissue engineering applications*; Elsevier Inc., 2018; ISBN 9780128136911.

17. Fiala, P.; Bartušek, K.; Dědková, J.; Kadlec, R.; Dohnal, P. Experimental measurement of nanolayers via electromagnetic, near infrared, and gamma radiation. *Meas. Sci. Rev.* **2019**, *19*, 144–152, doi:10.2478/msr-2019-0020.

18. Raj, M.A.; John, S.A. *Graphene-modified electrochemical sensors*; Elsevier Inc., 2018; ISBN 9780128153949.

19. Yusoff, N. *Graphene-polymer modified electrochemical sensors*; Elsevier Inc., 2018; ISBN 9780128153949.

20. Kamel, S.; El-Sakhawy, M.; Anis, B.; Tohamy, H.A.S. Graphene's Structure, Synthesis and Characterization; A brief review. *Egypt. J. Chem.* **2020**, *63*, 593–608, doi:10.21608/ejchem.2019.15173.1919.

21. Ahmad, H.; Fan, M.; Hui, D. Graphene oxide incorporated functional materials: A review. *Compos. Part B Eng.* **2018**, *145*, 270–280, doi:10.1016/j.compositesb.2018.02.006.

22. de Sousa, D.E.S.; Scuracchio, C.H.; de Oliveira Barra, G.M.; de Almeida Lucas, A. *Expanded graphite as a multifunctional filler for polymer nanocomposites*; Elsevier Inc., 2015; ISBN 9780323265034.

23. Li, J.; Kuang, D.; Feng, Y.; Zhang, F.; Xu, Z.; Liu, M. A graphene oxide-based electrochemical sensor for sensitive determination of 4-nitrophenol. *J. Hazard. Mater.* **2012**, *201–202*, 250–259, doi:10.1016/j.jhazmat.2011.11.076.

24. Alkhouzaam, A.; Qiblawey, H. Novel polysulfone ultrafiltration membranes incorporating polydopamine functionalized graphene oxide with enhanced flux and fouling resistance. *J. Memb. Sci.* **2021**, *620*, 118900, doi:10.1016/j.memsci.2020.118900.

25. Gad, S.E. Polymers. *Encycl. Toxicol. Third Ed.* **2014**, *3*, 1045–1050, doi:10.1016/B978-0-12-386454-3.00912-X.

26. Annu; Raja, A.N. Recent development in chitosan-based electrochemical sensors and its sensing application. *Int. J. Biol. Macromol.* **2020**, *164*, 4231–4244, doi:10.1016/j.ijbiomac.2020.09.012.

27. Karrat, A.; Amine, A.; Karrant, A.; Amine, A. Recent advances in chitosan-based electrochemical sensors and biosensors. *Arab. J. Chem. Environ. Res.* **2020**, *07*, 66–93.

28. Aranaz, I.; Alcántara, A.R.; Civera, M.C.; Arias, C.; Elorza, B.; Caballero, A.H.; Acosta, N. Chitosan: An overview of its properties and applications. *Polymers (Basel).* **2021**, *13*, doi:10.3390/polym13193256.

29. Ramawat, K.G.; Mérillon, J.M. Polysaccharides: Bioactivity and biotechnology. *Polysaccharides Bioactivity Biotechnol.* **2015**, 1–2241, doi:10.1007/978-3-319-16298-0.

30. da Silva Alves, D.C.; Healy, B.; Pinto, L.A. d. A.; Cadaval, T.R.S.; Breslin, C.B. Recent developments in Chitosan-based adsorbents for the removal of pollutants from aqueous environments. *Molecules* **2021**, *26*, doi:10.3390/molecules26030594.

31. Yang, Y.; Chen, G.; Murray, P.; Zhang, H. Porous chitosan by crosslinking with tricarboxylic acid and tuneable release. *SN Appl. Sci.* **2020**, *2*, 1–10, doi:10.1007/s42452-020-2252-z.

32. Ahmadi, F.; Oveisi, Z.; Samani, M.; Amoozgar, Z. Chitosan based hydrogels: Characteristics and pharmaceutical applications. *Res. Pharm. Sci.* **2015**, *10*, 1–16.

33. Xiong, S.; Marin, L.; Duan, L.; Cheng, X. Fluorescent chitosan hydrogel for highly and selectively sensing of p-nitrophenol and 2, 4, 6-trinitrophenol. *Carbohydr. Polym.* **2019**,

225, 115253, doi:10.1016/j.carbpol.2019.115253.

34. Martins, A.M.; Eng, G.; Caridade, G.; Mano, F.; Reis, R.L. Electrically Conductive Chitosan/Carbon Sca ff olds for Cardiac Tissue Engineering. **2014**.

35. Mabrouk, M.; Hammad, S.F.; Abdella, A.A.; Mansour, F.R. Enantioselective chitosan-based racemic ketoprofen imprinted polymer: Chiral recognition and resolution study. *Int. J. Biol. Macromol.* **2022**, *200*, 327–334, doi:10.1016/j.ijbiomac.2021.12.167.

36. Reading, F. Classification and Properties. 862–875.

37. Brakel, J. van *Substances: The ontology of chemistry*; Elsevier B.V., 2012; Vol. 6; ISBN 9780444516756.

38. Kolcsár, V.J.; Szőllősi, G. Chitosan as a chiral ligand and organocatalyst: Preparation conditions-property-catalytic performance relationships. *Catal. Sci. Technol.* **2021**, *11*, 7652–7666, doi:10.1039/d1cy01674a.

39. Iftime, M.M.; Marin, L. Chiral betulin-imino-chitosan hydrogels by dynamic covalent sonochemistry. *Ultrason. Sonochem.* **2018**, *45*, 238–247, doi:10.1016/j.ultsonch.2018.03.022.

40. Cunha, R.A.; Soares, T.A.; Rusu, V.H. The Molecular Structure and Conformational Dynamics of Chitosan Polymers : An Integrated Perspective from Experiments and Computational Simulations. **2012**.

41. Lizundia, E.; Nguyen, T.; Maclachlan, M.J. and chitosan. **2021**, 796–817, doi:10.1039/d0tc05381c.

42. Sun, Y.; He, J.; Zhang, D.; Sheng, Y.; Xu, D.; Zhang, R.; Bradley, M. Synergistic effects of chitosan and DNA self-assembly films on the chiral discrimination of tryptophan enantiomers. *Microchem. J.* **2021**, *165*, 106118, doi:10.1016/j.microc.2021.106118.

43. Abdellatif, F.H.H.; Abdellatif, M.M. *Utilization of sustainable biopolymers in textile processing*; Elsevier Ltd, 2021; ISBN 9780323852043.

44. Fink, J. *Drilling muds*; 2021; ISBN 9780323854382.

45. Patel, D.; Talele, D.; Pathak, D.; Misra, A. *Polymers Used in Peyer's Patch Targeting*; INC, 2021; ISBN 9780128196595.

46. Mangelings, D.; Eeltink, S.; Vander Heyden, Y. *Recent developments in liquid and*

supercritical fluid chromatographic enantioseparations; 2020; Vol. 8; ISBN 9780444640703.

47. Parmar, V.; Patel, G.; Abu-Thabit, N.Y. *Responsive cyclodextrins as polymeric carriers for drug delivery applications*; Elsevier Ltd., 2018; ISBN 9780081019979.

48. Zhou, J.; Ritter, H. Cyclodextrin functionalized polymers as drug delivery systems. *Polym. Chem.* **2010**, *1*, 1552–1559, doi:10.1039/c0py00219d.

49. Hashidzume, A.; Takashima, Y.; Yamaguchi, H.; Harada, A. *1.12 Cyclodextrin*; 2017; Vol. 1; ISBN 9780124095472.

50. Cid-Samamed, A.; Rakmai, J.; Mejuto, J.C.; Simal-Gandara, J.; Astray, G. Cyclodextrins inclusion complex: Preparation methods, analytical techniques and food industry applications. *Food Chem.* **2022**, *384*, 132467, doi:10.1016/j.foodchem.2022.132467.

51. Purwar, R. *Antimicrobial textiles*; Elsevier Ltd., 2018; ISBN 9780081024911.

52. Healy, B.; Yu, T.; da Silva Alves, D.C.; Okeke, C.; Breslin, C.B. Cyclodextrins as supramolecular recognition systems: Applications in the fabrication of electrochemical sensors. *Materials (Basel).* **2021**, *14*, doi:10.3390/ma14071668.

53. Sifaoui, H.; Modarressi, A.; Magri, P.; Stachowicz-Kuśnierz, A.; Korchowiec, J.; Rogalski, M. Formation of β-cyclodextrin complexes in an anhydrous environment. *J. Mol. Model.* **2016**, *22*, doi:10.1007/s00894-016-3061-6.

54. Qin, Q.; Bai, X.; Hua, Z. Electropolymerization of a conductive β-cyclodextrin polymer on reduced graphene oxide modified screen-printed electrode for simultaneous determination of ascorbic acid, dopamine and uric acid. *J. Electroanal. Chem.* **2016**, *782*, 50–58, doi:10.1016/j.jelechem.2016.10.004.

55. Liao, C. Electrochemical polymerization. *Chem. Bull. / Huaxue Tongbao* **2000**, *63*, 37–41, doi:10.1007/978-3-319-95987-0_3.

56. Pereira, A.C.; Oliveira, A.E.F.; Bettio, G.B. β-Cyclodextrin electropolymerization: mechanism, electrochemical behavior, and optimization. *Chem. Pap.* **2019**, *73*, 1795–1804, doi:10.1007/s11696-019-00732-x.

57. Healy, B.; Rizzuto, F.; de Rose, M.; Yu, T.; Breslin, C.B. Electrochemical determination

of acetaminophen at a carbon electrode modified in the presence of β-cyclodextrin: role of the activated glassy carbon and the electropolymerised β-cyclodextrin. *J. Solid State Electrochem.* **2021**, *25*, 2599–2609, doi:10.1007/s10008-021-05044-3.

58. Crockard, A. Clinical management. *J. Spinal Disord.* **1999**, *12*, 86, doi:10.1080/00002517-199902000-00024.

59. Jozwiak-Bebenista, M.; Nowak, J.Z. Paracetamol: Mechanism of action, applications and safety concern. *Acta Pol. Pharm. - Drug Res.* **2014**, *71*, 11–23.

60. Oxel, S. Best practice Best practice. *J. Pendidik.* **2000**, *46*, 33–34.

61. Tepe, O.; Tunç, Z.; Yıldız, B.; Şahin, M. Efficient Removal of Paracetamol by Manganese Oxide Octahedral Molecular Sieves (OMS-2) and Persulfate. *Water. Air. Soil Pollut.* **2020**, *231*, doi:10.1007/s11270-020-04620-z.

62. Shankar, K.; Mehendale, H.M. Acetaminophen. *Encycl. Toxicol. Third Ed.* **2014**, *1*, 26–29, doi:10.1016/B978-0-12-386454-3.00215-3.

63. Ramachandran, A.; Jaeschke, H. *Acetaminophen*; Elsevier Inc., 2017; ISBN 9780128043219.

64. Sebastine, I.M.; Wakeman, R.J. Pharmaceutical Substances in the UK. *Process Saf. Environ. Prot.* **2003**, *81*, 229–235.

65. Annadurai, K.; Sudha, V.; Murugadoss, G.; Thangamuthu, R. Electrochemical sensor based on hydrothermally prepared nickel oxide for the determination of 4-acetaminophen in paracetamol tablets and human blood serum samples. *J. Alloys Compd.* **2021**, *852*, 156911, doi:10.1016/j.jallcom.2020.156911.

66. El-Kemary, M.; Sobhy, S.; El-Daly, S.; Abdel-Shafi, A. Inclusion of Paracetamol into β-cyclodextrin nanocavities in solution and in the solid state. *Spectrochim. Acta - Part A Mol. Biomol. Spectrosc.* **2011**, *79*, 1904–1908, doi:10.1016/j.saa.2011.05.084.

67. Li, H.; Yang, Z.; Gao, Z. *Protein tyrosine nitration: Chemistry and role in diseases*; 1st ed.; Elsevier B.V., 2020; Vol. 13; ISBN 9780444642936.

68. Kapalka, G.M. Substances Involved in Neurotransmission. *Nutr. Herb. Ther. Child. Adolesc.* **2010**, 71–99, doi:10.1016/b978-0-12-374927-7.00004-2.

69. Litwack, G. *Metabolism of Amino Acids*; 2018; ISBN 9780123838643.

70. Gao, F.; Ma, S.; Xiao, X.; Hu, Y.; Zhao, D.; He, Z. Sensing tyrosine enantiomers by using chiral CdSe/CdS quantum dots capped with N-acetyl-L-cysteine. *Talanta* **2017**, *163*, 102–110, doi:10.1016/j.talanta.2016.10.091.

71. Park, J.; Jung, H.; Jang, B.; Song, H.K.; Han, I.O.; Oh, E.S. D-tyrosine adds an anti-melanogenic effect to cosmetic peptides. *Sci. Rep.* **2020**, *10*, 1–11, doi:10.1038/s41598-019-57159-3.

Chapter 2: Experimental

2.1 Introduction

This chapter outlines the experimental techniques and instrumentation utilised throughout this research project. Theoretical background information on the techniques is also provided. In addition, all chemicals and solutions relating to such experiments are described.

2.2 Experimental Techniques

A variety of electrochemical and electroanalytical techniques were implemented throughout the course of this research including cyclic voltammetry (CV), electrochemical impedance spectroscopy (EIS), potentiostatic techniques, scanning electron microscopy (SEM) and infrared spectroscopy (FT-IR). A brief overview of the above techniques is outlined below.

2.2.1 Cyclic Voltammetry

Cyclic voltammetry (CV) is a powerful type of voltammetry widely employed to investigate the oxidation and reduction processes of electroactive species. The technique of CV provides an insightful method to study the electron transfer processes of molecular species [1]. Cyclic voltammetry is conducted by applying a potential sweep to a working electrode (WE) in both oxidation and reduction directions [2], as illustrated in **Fig. 2.1**. Both directions are indicated by two potential limits or an optimised potential window. The potential applied is scanned at a constant rate referred to as the scan rate and the resultant current arises from the change in electron transfer kinetics and the diffusion of the redox species at a concentration gradient in solution [2]. The potential can be applied for a chosen number of cycles typically between five and fifteen cycles. Over the course of these cycles, information on the build-up of polymer layers or modifications to the surface of the electrode can be obtained. The resulting change in current vs. potential is visualised as a graph called a voltammogram, **Fig. 2.1**.

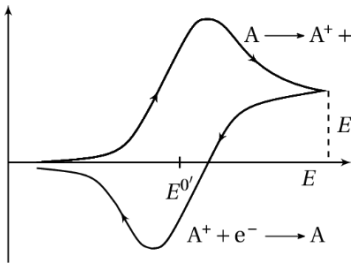

Figure 2.1: Voltammogram of a reversible redox reaction of species A

An example of a voltammogram for a simple redox reaction for species A is given above in **Fig. 2.1**; the forward potential sweep sees species A oxidised to A^+ producing an anodic peak. The reverse sweep sees species A^+ subsequently reduced back to A producing a cathodic peak [3]. CV was essential in this project for the attempted production of the electrochemical polymer (beta-cyclodextrin polymer[β-CD]) and the electro-deposition of various absorbents (graphene) at the working electrode surface carried out under varying conditions, including pH, concentrations, scan rate studies and different cycle numbers.

2.2.2 Potentiostatic Techniques

Potentiostatic measurements were carried out for the electrodeposition of chitosan containing KCl salt ions onto the WE surface. The potentiostatic technique used in this study involved a constant potential applied to the WE for a fixed period of time typically 5 min, with current (A) recorded as a function of time (s).

As mentioned above CV was carried out for the creation and deposition of polymers. Whereas, through potentiostatic methodology, a constant controlled potential method can yield a swift nucleation and a gradual particle growth process, resulting in a thinner and finer film grain. Furthermore, both chemical and physical behaviours of these films can be more easily and precisely controlled [4]. In this study the chitosan solution to be electrodeposited was viscous in nature and this one-step potentiostatic method was ideal for the deposition of fine layers/films of chitosan onto the WE surface, avoiding the creation of a heavy chitosan polymer that may ultimately peel off. The reaction taking place at the WE surface is a hydrogen evolution reaction (HER). As the solvent for the chitosan solution is acetic acid, it in turn becomes deprotonated at the electrode surface causing the production of hydrogen gas to occur. It is believed that potentiostatic technique delivers a tight adhesion between the grown polymer

and surfactant which can aid in the HER activity, which is required for the deposition of chitosan.

2.2.3 Impedance Measurements

Impedance measurements allow the user to study an array of characteristics of an electrochemical system including diffusion co-efficients, rates of electron transfer, charge transfer resistance and capacitance to mention a few. For this study, Electrochemical Impedance Spectroscopy (EIS) was deployed as a means to carry out impedance investigations, involving the application of a sinusoidal potential applied in a waveform manner alternating between negative and positive potentials. Impedance studies are usually conducted over a frequency range similar to other spectroscopy methods, with frequency referring to the speed at which the potentials change between the electrodes in the cell. The analysis of both the magnitude and phase of the sinusoidal voltage that results in the alternating current (AC) provides information on parameters such as the resistance and capacitance of the system [5].

The resistive and capacitive character of the cell is contingent to the frequency. Low frequencies see the charge transfer restricted by the capacitance as a result of the slow diffusion of ions. Whereas, at more higher frequencies the charge transfer is restricted by electron-transfer kinetics. Analysing the currents response over a frequency range enables the separation of processes, occurring at different times into either electronic or ionic processes within one system. Hence, the main mechanisms of the electrochemical cell which contribute to the resistance and capacitance of the system are ionic and electronic in nature, respectively. The resultant current can be broken into two current outputs, an in phase and out of phase current output. The in-phase component corresponds to the resistance experienced and the out phase relates to the capacitance experience by the system [5].

The experimental data can be represented by a Complex Impedance Plot called a ‘Nyquist Plot’, comprising of a negative imaginary component (Z_{im}) plotted against the real component (Z_{re}). The imaginary part is plotted on the Y-axis and the real part is plotted on the X-axis [6], as shown in **Fig. 2.2**.

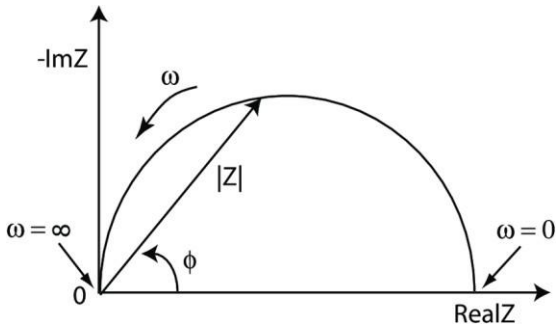

Figure 2.2: Example of simple Nyquist Plot or Complex Impedance cartesian plot.

Another commonly used graphical representation of impedance data is a Bode plot. A Bode plots conveys the changes in the magnitude and phase shift occurring in the set frequency range, unlike a Nyquist plot where the frequency is not shown. Normally, bode plots exist in two graphs rather than one. The bode plot consists of the logarithmic of frequency plotted on the X-axis versus the logarithmic of the absolute impedance values or phase angle [7] on the Y-axis, as illustrated in **Fig. 2.3**.

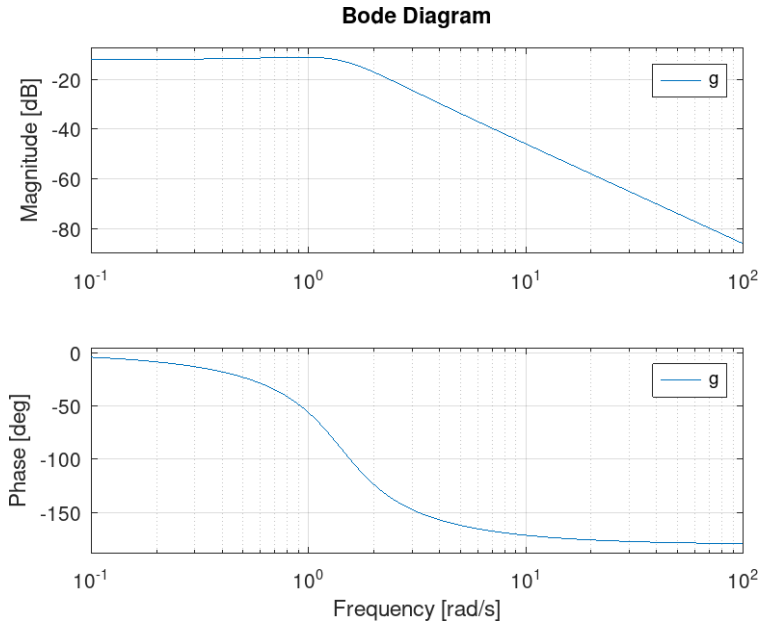

Figure 2.3: Bode diagrams representing EIS data, with the magnitude of the impedance (top) and phase angle (bottom) plotted as a function of frequency (on a logarithmic scale).

Within this study, EIS techniques were utilised in order to extract information on the charge transfer resistance and capacitance of the polymeric films. Precise experimental details are provided in Section 3.3.2.1.

2.2.4 Scanning Electron Microscopy

Scanning Electron Microscopy (SEM) allows the user to visualise and characterise the surface and microstructure of samples through the use of electrons. The process of SEM involves the transmission of electrons from an electron gun across the samples surface, scattered signals arising from the interplay of the sample and electrons are then detected by energy transducers that convert the energy of the signals into electronic analysis, such as graphs and images. Within a SEM a vacuum can also be found which enables the electrons to travel a greater distance as electrons can typically only travel short distances [8]. The ideal sample for an SEM would be typically dry, containing a hard surface and be a good electrical conductor. Traditional SEMs require such an ideal sample, however it can be noted the development of Environmental SEMs in recent years can be used to view both non-conductive and wet samples [9]. Any limitations caused by conductivity can be overcome by coating the sample in a fine metal layer to make it more electrically conductive and give rise to good signals. Gold, and alloys of gold and palladium are often used for the deposition of this metal film. The process of this deposition is called sputter coating and can be accomplished by bombarding a metal coating containing disc with ionized gas particles, so that these ionized particles hit the samples surface and extract atoms which in turn are placed evenly over the samples surface [10].

SEM is a useful tool for obtaining the morphology of surfaces. However, the elemental composition of a sample surface requires further in-dept study commonly achieved through the technique of energy dispersive X-Ray analysis or EDX, often coupled together with scanning electron microscopy (SEM-EDX). In EDX the sample's surface atoms become excited after being struck with a beam of electrons. This causes the emission of the X-rays of specific wavelengths that are based on the nature and characteristics of the atomic structure of the elements within the sample. Therefore, this technique provides an insightful method to study the chemical composition of the surface of samples. Modern SEMs contain an EDX X-ray spectrometer within, responsible for the production of these X-rays [11].

This study used EDX to confirm the presence of oxygenated species during the attempted polymerisation of the polymer[β-CD] at a glassy carbon electrode (GCE), while SEM was employed to study the morphology of the resulting polymer[β-CD]/activated GCE. SEM/EDX was also employed to characterise the electrodeposited graphene. The samples were prepared by forming the polymers onto a smooth flat glassy carbon electrode surface through CV and potentiostatic procedures. The samples were thoroughly rinsed with deionised water and then slowly dried under a heat lamp and left overnight to further dry. For the SEM and EDX analysis the acceleration voltage implemented was 20 keV.

2.2.5 Fourier Transform Infrared Spectroscopy (FT-IR)

Fourier Transform Infrared (FT-IR) spectroscopy is a type of vibrational spectroscopy that can be useful as an analytical technique to investigate mechanisms of bonding on surfaces. FT-IR spectroscopy induces molecular vibrations which are known to be directly linked to the symmetry of molecules and can therefore provide details of how exactly a molecule is bonding on a certain surface and what type of chemical bonds are present in the sample [12]. FT-IR is the most widely used method of Infrared spectroscopy (IR) praised for its high accuracy, sensitivity, speed and ease of handling.

A source within FT-IR produces infrared radiation that passes through an interferometer before being transmitted to the sample. The energy transmitted by the interferometer to the sample will either go through or bounce-off the surface of the sample. The infrared radiation is absorbed at specific wavelengths depending on the functional groups of the molecules being analysed. Different molecules are easily detected and identified by FT-IR as different molecules will have unique infrared spectra. The beam of radiation then continues to pass until it reaches the detector where a mathematical conversion called Fourier transformation is carried out. This conversion can provide more accuracy of the measure of radiation passed through the sample than compared to normal dispersive IR spectrometry, making FT-IR an advantageous and useful analytical technique [13].

FTIR was used to study the electrodeposited chitosan films and the oxidation and activation of glassy carbon during the formation of the polymer[β-CD] at the glassy carbon substrate.

2.3 Instrumentation, Software and Ancillary Apparatus

A Solartron Potentiostat Model 1285 was used to carry out cyclic voltammetry and potentiostatic measurements. The software used to collect and display the electrochemical data from the Potentiostat was Scribner Associates CorrWare and to analyse the data Scribner Associates CorrView was used. Both software programmes were used for Windows Version 9.0. A Solartron Frequency Response Analyser Model 1255B was used to undertake impedance studies, alongside the Solartron Potentiostatic Model 1287. The impedance data were collected using Scribner Associates ZPlot software, Windows Version 9.0, while data analysis was performed using Scribner Associates ZView software. Further data analysis was carried out using Microsoft Excel 2019. Information related to the remaining analytical techniques are given below in the **Table 2.1**, whilst the apparatus employed for the more ancillary daily processes is outlined in **Table 2.2**.

Table 2.1: Model details for used analytical techniques.

Equipment	***Model***
SEM	Leica Stereoscan 440/Joel 840 SEM/Hitachi S400
EDX	Tescan Mira XMU VPFE
FT-IR	Nicolet TM iS50 FTIR

Table 2.2: Model Information from Ancillary equipment.

Equipment	***Model***
Electronic Balance	Sartorius Model TE214S
pH Meter	Mettler Toledo
Sonication	Branson 1510

2.4 Chemicals and Solutions

All chemicals were supplied as high purity analytical reagents by Sigma-Aldrich and used without any further purifications. The GCE were obtained from IJ Cambria. The first step in any experimental procedure involved the thorough polishing of the bare GCE, and for this a 1 μm monocrystalline diamond suspension solution was used with a microcloth. The surface of the GCE was polished to give a mirror-like finish. The attempted electropolymerisation of β-CD was carried out using a 5 mM β-CD solution in a 0.1 M phosphate buffer (PBS) at a pH of 5.5. The solution was sonicated to aid dissolution. For comparative purposes and to explore the role of the activated GCE, the GCE was activated using the same cycling conditions and solutions that were used to form the polymer[β-CD], but in the absence of β-CD.

For the creation of the chitosan polymer, 10 ml of a 1% chitosan solution was dissolved in 0.2 M acetic acid with the addition of 0.5 g of potassium chloride (KCl). For the production of the graphene solution, 10 ml of a graphene solution dissolved in a 5 mM β-CD solution was used. The immobilisation of graphene within the chitosan layer was carried out using 10 ml of a 5 mM β-CD solution dissolved in PBS at pH 5.5 with the addition of 18 mg of graphene nanoplatelets.

2.5 The Electrochemical Cell Setup

A standard three electrode cell set-up was employed as the electrochemical set-up of all experiments, comprising of a working electrode (WE), a reference electrode (RE) and an auxiliary or counter (CE) electrode. The cell itself was a small glass cylinder enclosed with a ridged Teflon lid that contained openings to allow all the electrodes to be positioned in the solution with connections to the potentiostat, as shown in **Fig. 2.4.**

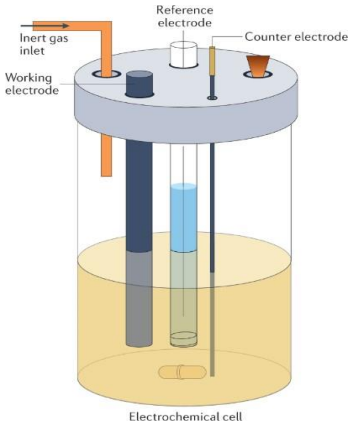

Figure 2.4: A standard three-electrode cell set-up

The reference electrode used was a silver silver chloride (Ag/AgCl) electrode or a saturated calomel electrode (SCE) acting as a constant and controlled potential, remaining unchanged throughout the experiment. In the three-electrode system the potential of the working electrode is measured relative to the reference potential [14]. Ultimately, it provides a standard for the electrochemical measurements of the working electrodes, as they respond to changes in the electrolyte solution within the cell. Within electroanalytical chemistry, the Ag/AgCl system has been used over the past one hundred years and is more frequently employed in comparison to other reference electrode systems due to its stability, reproducibility and more eco-friendly behaviour [15].

The WE used for this study was a glassy carbon electrode (GCE). The glassy carbon is also commonly known as polymeric carbon, produced by the process of thermal degradation of chosen polymer resins. The glassy carbon material possesses an extraordinarily strong thermal stability and more uniquely great resistance to chemical processes. For example, it has been observed that the extent of oxidation of glassy carbon in water vapour, oxygen and even carbon dioxide was lower when compared to various other carbon-based materials [13]. This property is ideal for this study as the majority of the electrochemical processes conducted involves the oxidation of absorbents or analytes on the WE surface, as well as oxidation of the WE itself. However, oxidation of the WE is not desired in most cases and implementation of a GCE as the WE thus enables a level of protection from the oxidation process due to its thermal stability. All reactions or chemical processes occurring in the electrolyte solution took place at the active site of the WE, i.e., the glassy carbon interface. The Auxiliary or Counter Electrode (CE) consisted of a platinum wire (Pt) and provided a route for the electric current to flow. Within this cell configuration the current passes between the WE and CE [11], whereas the potential is measured between the WE and RE as described above. The cell set-up was connected to a

potentiostat, **Fig. 2.5**. The potentiostat supplied and controlled the WE's potential. Within this analytical instrument it is a circuit that is responsible for the generation of the potential and also the measuring of the corresponding current changes.

Prior to each experiment, the WE was polished to a mirror finish and free from any remaining material or impurities. This was achieved using the polishing diamond paste previously described in Section 2.4. Following polishing the WE was sonicated in deionised water, rinsed with deionised water and finally dried. The RE was frequently serviced by ensuring the inner liquid solution was full with a concentrated solution of super-purum KCl. Both the CE and RE were rinsed with deionised water in-between experiments.

Figure 2.5: A schematic of the electrochemical set-up used to record experimental measurements.

2.6 Electrode Kinetic Analysis

The technique of cyclic voltammetry is a valuable analytical tool as mentioned earlier in Section 2.2; however, it can also reveal information about the kinetics of the system's reactions. In particular, the reaction kinetics can identify if the process occurring is under diffusion or adsorption control and can also provide information on the reversibility behaviour of the reaction. For a reversible reaction, a mathematical equation called the Randles-Sevcik equation can predict if a redox couple undergoes diffusion in solution rather than being absorbed on the WE surface.

The equation calculates this prediction by relating the cyclic voltammetry peak current with the square root of the scan rate deployed [16], as shown in Eq. 1.

$$i_p = (2.69 \times 10^{5})\, n^{3/2} D^{1/2} v^{1/2} c_o \qquad Eq\ (1)$$

Here, i_p is the peak current density (A cm^{-2}), n represents the electron stoichiometry, D is the diffusion coefficient ($cm^2\ s^{-1}$), v is the scan rate (V s^{-1}) and C corresponds with the concentration of the analyte (mol cm^{-3}).

From **Eq. 1**, the peak current i_p is directly proportional to the square root of the scan rate as well as analyte concentration and the diffusion coefficient of the analyte. When the plot of the square root of the scan rate vs. current produces a linear plot this indicates that the redox reaction obeys the Randles-Sevcik equation and is therefore ruled to some degree by a diffusion controlled-process. From this linear plot the slope of the line representing the diffusion process can be found to give the diffusion coefficient of the analyte or indeed other parameters in the Randles-Sevcik equation. This equation was employed in Section 6.3.1 to calculate the diffusion coefficient of paracetamol and L/D tyrosine at the GCE surface.

In reversible redox reactions, the word 'reversible' suggests that the rate of electron transfer is fast, whilst preserving equilibrium at the WE/electrolyte solution interface. In this system the current is governed only by diffusional mass transport where the peak potentials and separation are not dependent on scan rate. Whereas the term 'irreversible' suggests that a slow reaction takes place. For irreversible systems, the peak potential and separation move to more excessive potentials that are dependent on increasing scan rate. The peak current for an electrochemical irreversible reaction is given in **Eq. 2**, where the additional term α is the charge transfer coefficient and n_α represents the number of electrons transferred during the rate-determining step.

$$i_p = (2.99 \times 10^{5})\, n\, (\alpha n_\alpha^{1/2})\, D^{1/2} C\, v^{1/2} \qquad \textbf{\textit{Eq (2)}}$$

Reactions whose rate of electron transfer falls between the two extremes of either reversible or irreversible systems, are referred to as quasi-reversible. The voltammograms of quasi-reversible systems have intermediary plots determined by a combination of mass-transport and

charge transfer rates. Within quasi-reversible reactions the relationship between the square root of the scan rate and peak current may not be proportional, and hence CV will not yield a linear plot with a zero intercept. As a result of this non-linearity the diffusion coefficient must be determined from an alternative route [17]. Shown in **Fig. 2.6** are two CV plots depicting quasi-reversible reactions with different rates of electron transfer.

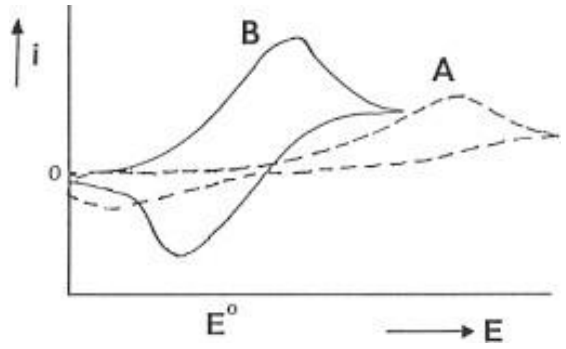

Figure 2.6: Quasi-reversible electron transfer reactions A and B illustrating different rates of electron transfer, with A exhibiting a higher rate of electron transfer.

2.7 Bibliography

1. Elgrishi, N.; Rountree, K.J.; McCarthy, B.D.; Rountree, E.S.; Eisenhart, T.T.; Dempsey, J.L. A Practical Beginner's Guide to Cyclic Voltammetry. *J. Chem. Educ.* **2018**, *95*, 197–206, doi:10.1021/acs.jchemed.7b00361.

2. Coffman, A.J.; Lu, J.; Subotnik, J.E. A grid-free approach for simulating sweep and cyclic voltammetry. *J. Chem. Phys.* **2021**, *154*, doi:10.1063/5.0044156.

3. Wurster, B. Two-Dimensional Metal-Organic Networks as a New Class of Electrocatalysts. *Thesis* **2015**, *6783*.

4. Zhang, Z.; Wu, Y.; Zhang, D. Potentiostatic electrodeposition of cost-effective and efficient Ni–Fe electrocatalysts on Ni foam for the alkaline hydrogen evolution reaction. *Int. J. Hydrogen Energy* **2022**, *47*, 1425–1434, doi:10.1016/j.ijhydene.2021.10.150.

5. Warriner, K.; Namvar, A. *Biosensors for foodborne pathogen detection*; Third Edit.; Elsevier, 2019; Vol. 4; ISBN 9780444640475.

6. Mei, B.A.; Munteshari, O.; Lau, J.; Dunn, B.; Pilon, L. Physical Interpretations of Nyquist Plots for EDLC Electrodes and Devices. *J. Phys. Chem. C* **2018**, *122*, 194–206, doi:10.1021/acs.jpcc.7b10582.

7. Faika, T.; Kim, T.; Khan, M. An Internet of Things (IoT)-Based Network for Dispersed and Decentralized Wireless Battery Management Systems. *2018 IEEE Transp. Electrif. Conf. Expo, ITEC 2018* **2018**, *11*, 342–346, doi:10.1109/ITEC.2018.8450161.

8. de Assumpcão Pereira-da-Silva, M.; Ferri, F.A. *Scanning Electron Microscopy*; Elsevier Inc., 2017; ISBN 9780323497794.

9. Williams, H. SEM for conductive and non-conductive specimens. *Phys. Educ.* **2021**, *56*, doi:10.1088/1361-6552/ac1503.

10. Goldberg, M.W.; Allen, T.D. *Imaging the Cell: Electron Microscopy – Scanning Electron Microscopy in Cell Biology*; Elsevier Ltd., 2022; ISBN 9780128216187.

11. Raval, N.; Maheshwari, R.; Kalyane, D.; Youngren-Ortiz, S.R.; Chougule, M.B.; Tekade, R.K. *Importance of physicochemical characterization of nanoparticles in pharmaceutical product development*; Elsevier Inc., 2018; ISBN 9780128179093.

12. Peak, D. *Fourier Transform Infrared Spectroscopic Methods of Soil Analysis*; Elsevier Inc., 2013; ISBN 9780124095489.

13. Undavalli, V.K.; Ling, C.; Khandelwal, B. *Impact of alternative fuels and properties on*

elastomer compatibility; Elsevier Inc., 2021; ISBN 9780128183144.

14. H Kara, O.A.M.A. 済無*No Title No Title No Title*; 2014; Vol. 7; ISBN 9780444519580.

15. Sarvestani, M.R.J.; Madrakian, T.; Afkhami, A. Developed electrochemical sensors for the determination of beta-blockers: A comprehensive review. *J. Electroanal. Chem.* **2021**, *899*, 115666, doi:10.1016/j.jelechem.2021.115666.

16. Henstridge, M.C.; Laborda, E.; Dickinson, E.J.F.; Compton, R.G. Redox systems obeying Marcus-Hush-Chidsey electrode kinetics do not obey the Randles-Ševčík equation for linear sweep voltammetry. *J. Electroanal. Chem.* **2012**, *664*, 73–79, doi:10.1016/j.jelechem.2011.10.015.

17. Wang, H.; Sayed, S.Y.; Luber, E.J.; Olsen, B.C.; Shirurkar, S.M.; Venkatakrishnan, S.; Tefashe, U.M.; Farquhar, A.K.; Smotkin, E.S.; McCreery, R.L.; et al. Redox Flow Batteries: How to Determine Electrochemical Kinetic Parameters. *ACS Nano* **2020**, *14*, 2575–2584, doi:10.1021/acsnano.0c01281.

18. Hashidzume, A.; Takashima, Y.; Yamaguchi, H.; Harada, A. *1.12 Cyclodextrin*; 2017; Vol. 1; ISBN 9780124095472.

19. Cid-Samamed, A.; Rakmai, J.; Mejuto, J.C.; Simal-Gandara, J.; Astray, G. Cyclodextrins inclusion complex: Preparation methods, analytical techniques and food industry applications. *Food Chem.* **2022**, *384*, 132467, doi:10.1016/j.foodchem.2022.132467.

Chapter 3: Formation and Characterisation of the β-CD-modified GCE and its Interactions with Acetaminophen and the Role of the Activated GCE

3.1 Introduction

Polymer-based electrochemical sensors overall enhance the determination of target molecules by supporting immobilisation of materials such as dyes, fluorophores and nanoparticles and through the modification of their chemical or physical properties to allow for greater recognition of the target analyte [1]. This chapter describes the proposed electropolymerisation of β-CD [2] at the electrode surface for the determination of the target analyte acetaminophen. The role of the GCE activation process is also discussed.

3.2 Experimental

The apparatus and computer software utilised for the experiments mentioned in this chapter are previously described in Section 2.4. All chemicals were supplied as Analar grade reagents from Sigma-Aldrich and were used without any further purification or modification. All solutions were prepared fresh prior to each experiment. For pH changes of solutions diluted concentrations of HCl and NaOH were used, and all experiments were carried out at room temperature. A 3 mm glassy carbon electrode (GCE) rod was used in all experiments with this rod being contained in epoxy resin and inserted into a Teflon holder. Electrical conductivity was accomplished through the presence of a copper plate at the base of the carbon sample. Before each experiment was carried out the GCE was polished and sonicated using the methodology described in Section 2.4. For the auxiliary electrode a platinum wire (Pt) was used and for the reference electrode a saturated calomel electrode (SCE) was employed during the voltammetry experiments. For the differential pulse voltammetry (DPV) experiments a silver-silver chloride (Ag/AgCl) reference electrode was utilised. To analyse the surface of the β-CD modified GCE and the activated GCE a Hitachi S-3200-N SEM was used, whilst energy dispersive X-ray (EDX) investigations were conducted using an Oxford Instrument INCAc-act EDX system. A Varian FTS-7000 FTIR spectrometer containing a Pike Miracle ATR diamond crystal was used to obtain all ATR-FTIR results. Samples were let dry fully prior to any analysis. A Cary 50 UV-visible spectrometer was utilised to probe the interactions between acetaminophen and the β-CD in the phosphate buffer solution.

For all cyclic voltammetry experiments a Solartron 1287 Potentiostat was employed with a CHI Potentiostat being used for DPV experiments. The DPV experiments were recorded using a pulse amplitude of 50 mV, a pulse width of 0.1 s, a sampling width of 0.05 s and pulse period

of 0.3 s, an increment of 3 mV. Electrochemical impedance spectroscopy measurements were performed in the phosphate buffer solution at a fixed potential of 0.3 V (*vs* SCE) using a Solartron (Model SI 1287) Potentiostat coupled to a Solartron frequency response analyser (Model 1255). The frequency was varied from 65 kHz to 5 mHzusing a potential perturbation of 10 mV. All data were recorded following a 120 min polarisation period to ensure steady-state conditions. The data were fitted to equivalent circuits, where the errors in the fitted elements were less than 3.5 %. All the experiments were repeated for at least three times and the standard error (SE = $\rho/n^{1/2}$, where ρ is the standard deviation and n represents the number of repeated experiments) is shown as error bars on the relevant plots.

3.3 Results and Discussion

β-CD has been widely used in electrochemical sensor development due to its ability to form inclusion complexes with certain molecules, resulting in the encapsulation or immobilisation of materials that increases sensitivity and selectivity in the detection of analytes [3]. Nevertheless, the β-CD is normally drop cast on the surface of sensors and is easily lost and dissolved during the detection of analytes in aqueous solutions [4], especially over longer immersion times in the aqueous electrolyte. Through the electrochemical technique of cyclic voltammetry, it is believed that β-CD begins to form a film or polymer on the electrode surface, this technique being referred to as electropolymerisation. It is further believed that this polymer is highly adherent to the electrode and therefore it should remain stable and not prone to dissolution, making these β-CD polymeric materials interesting in the development of electrochemical sensors. In this chapter, acetaminophen is used as a model analyte to determine if these electropolymerised polymers of β-CD, if indeed formed, can be employed as sensors.

3.3.1 Electropolymerisation of β-CD and Activation of the GCE

The proposed electropolymerisation of β-CD was carried out by cycling the electrode from −2.0 to 2.2 V (*vs.* SCE) in a slightly acidic phosphate buffer solution (PBS) with a pH of 5.5, containing a 5 mM β-CD solution, as shown in **Fig 3.1 (a)**. Two anodic peaks can be noted at approximately 0.6 V and 1.6 V (*vs.* SCE) and as the cycle number increases so too does the

intensity of the peaks. A strong reduction peak is also evident at about −0.6 V (*vs*. SCE), also this peak grows in intensity as the cycle number increases. As described in Section 1.2.3 electropolymerisation is understood to arise from the formation of radical cations that bring about coupling reactions either between radical cations themselves or between radical cations and a neutral monomer. These coupling reactions result in the formation of the polymeric structure deposited on the electrode surface [5]. In fact, the cathodic peak at −0.6 V (*vs*. SCE) has been directly linked to the extent of polymerisation. A dark black flat film/coating was observed on the surface of the electrode once cycling was complete, as seen in **Fig. 3.2.**

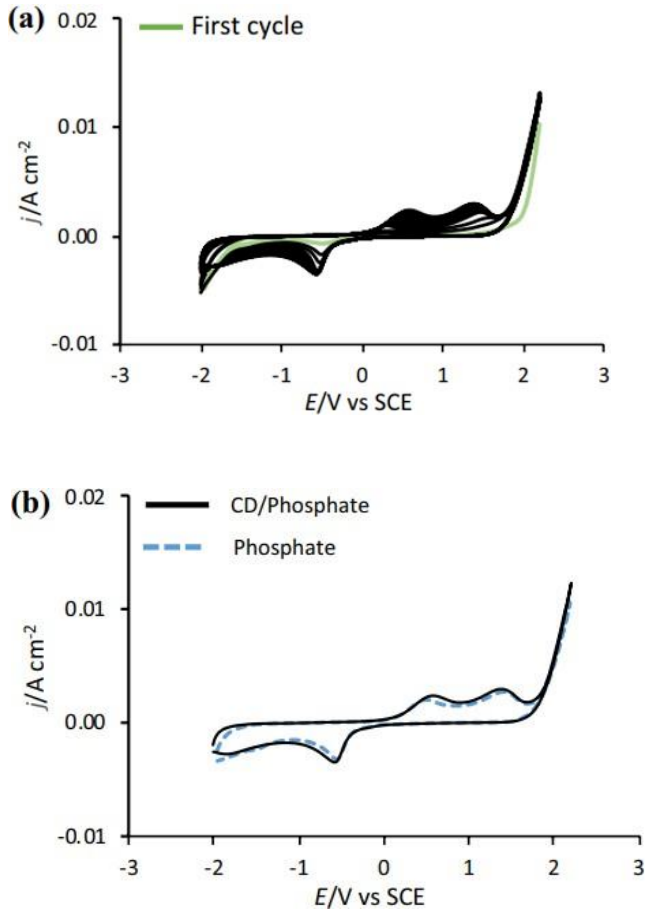

Figure 3.1: Cyclic voltammograms recorded at 100 mV s^{-1} **(a)** in a 5 mM β-CD and 0.1 M phosphate, cycles 1 to 20 and **(b)** in 5 mM β-CD in 0.1 M phosphate and also in 0.1 M phosphate.

Nevertheless, as seen in **Fig. 3.1 (b)**, almost identical voltammograms were observed on cycling the GCE in the PBS without the presence of the β-CD and with the presence of β-CD. This shows how the cycling process itself actually activates the GCE with this activation

brought about by changes in the microstructure of the GCE such as the forming of new active edges planes and the forming of a graphite oxide layer that contains numerous oxygen-containing moieties. The reduction peak at around −0.6 V (*vs*. SCE), is more likely to be associated with the reduction of oxides that were formed during the GCE cycling to rather high potentials. The current of the peaks related to this reduction wave increase with cycling while the potentials of these peaks become slowly more negative as cycling continues.

Figure 3.2: A dark black flat film/coating observed on the surface of the electrode.

The chosen supporting electrolyte has also been seen to play a part in the activation process [6] and this is evident in **Fig. 3.3** where the GCE was cycled in the presence of β-CD with chloride and sulphate as the supporting electrolytes. The supporting electrolyte provides or increases the conductive properties of the solution and forms stable complex ions which enable the current to pass through the solution [7]. Similar to above, nearly identical voltammograms were obtained, one in the presence of β-CD and one in the absence, suggesting that the observed redox peaks are associated with oxidation and activation of the GCE. The voltammogram representing the chloride supporting electrolyte is significantly different to sulphate and phosphate solution voltammograms. The characteristic oxidation peaks seen prior to the oxygen evolution reaction with the phosphate and sulphate solutions are no longer present, whilst the reduction peaks appear greater in size during the reverse of the cycle. The initiation of the oxygen evolution reaction happens at a lower overpotential in the chlorine system and the reaction of the solution is a complex one containing more than one intermediate step. This reaction sees the formation of adsorbed species, $OH^{\bullet}$ radicals and the production of gaseous molecules. Also, the Cl^- ions in solution can couple with the OH^- ions resulting in numerous intermediate compounds including $ClOH^-$ [8]. There is no precise mechanism of chloride ions

reacting with $OH^{\bullet}$ species that has been proposed, but there is a general assumption that the chloride ions are analogous to the reaction with radical $OH^{\bullet}$ species that were homogenously formed [9]. The onset of this reaction within the chloride system is highly likely to alter both the activation of the GCE electrode and possibly the electropolymerisation of the β-CD monomers. Furthermore, the activation process of the GCE may also be affected by the chloride, phosphate and sulphate anions.

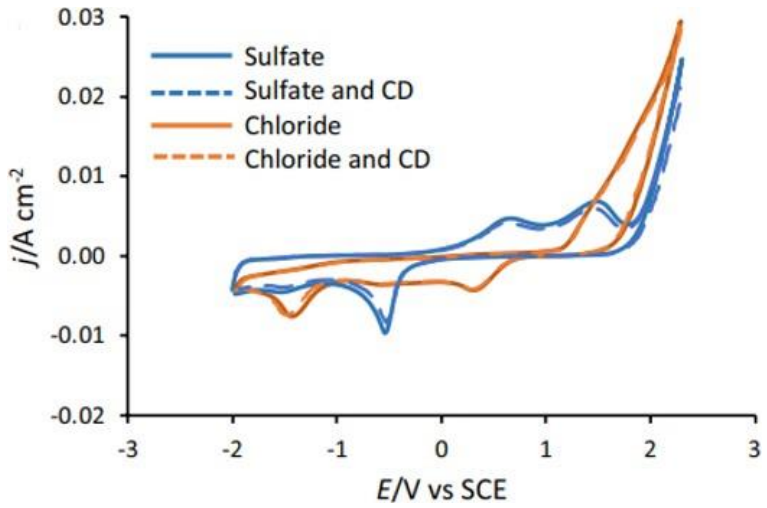

Figure 3.3: Cyclic voltammograms recorded at 100 mV s^{-1} in the presence and absence of 5 mM β-CD in 0.1 M NaCl and 0.05 M Na_2SO_4.

The glassy carbon electrode is a non-graphitizing form of carbon which incorporates glassy and ceramic characteristics with properties of graphite. It is referred to as glassy carbon as its appearance is simply glass like with a shiny reflective surface and is well-used as an electrode material due to its key properties such as the ability to resist both high temperatures and chemical attacks and it is impermeable to liquids and gases [10]. The electrochemical sensing ability of the bare glassy carbon electrode (GCE) for acetaminophen without the presence of β-CD and hence without any modification was investigated initially and the corresponding data are shown below in **Fig 3.4.**

From the voltammogram in **Fig 3.4** it can be observed that the bare GCE alone did have a sensing ability for acetaminophen, but with a low peak current at approximately 0.64 V (*vs*. SCE). However, upon modification with β-CD it can be seen that a much higher level of detection was achieved with the oxidation peak at 0.40 V (*vs*. SCE). This is to be expected as many studies found upon modification of the glassy carbon electrode with various materials, a

higher level of detection is achieved for the target analyte [11,12]. Furthermore, there is a considerable shift of 0.24 V in the peak potential, indicating that the oxidation of acetaminophen becomes more thermodynamically favoured upon modification of the electrode. In addition, the GCE was tested in a phosphate buffer solution (PBS) which evidently produced an extremely low signal with no detection of acetaminophen or any other peaks. This is due to the fact that the PBS does not undergo any redox reaction, but instead keeps the pH of the solution constant and acts as a means of dissolution for the analyte, with some studies even finding the PBS to enhance the oxidation process of analytes [13].

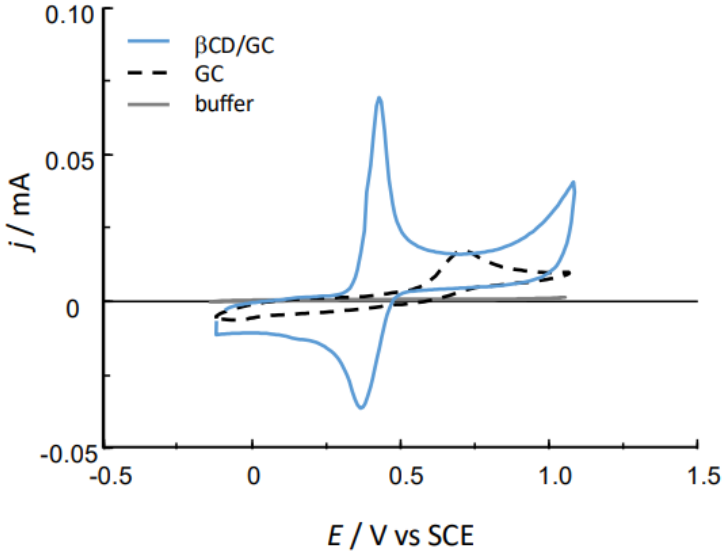

Figure 3.4: Cyclic voltammogram recorded at 100 m V s^{-1} cycled from –0.2 V to 1.1 V (*vs.* SCE) in an acetaminophen solution, 0.5 mM, for (a) β-CD modified GCE and **(b)** a bare GCE, whilst for (c) a bare GCE was cycled in 0.1 M phosphate buffer.

It clearly appears from **Fig. 3.4** that the β-CD modified GCE enhances considerably the detection of acetaminophen, and this is consistent with the formation of an inclusion complex between the β-CD and the acetaminophen molecule. The potential interactions between acetaminophen and the β-CD in the solution phase was explored using UV-visible spectroscopy and a typical plot is presented in **Fig. 3.5**. The spectra show the UV-visible data recorded for acetaminophen in the absence and presence of a 3-fold and 30-fold excess of β- CD in the phosphate buffer. The addition of excess β-CD gives rise to an increase in the absorbance at λ_{max} and this can be explained by an increase in the solubility of acetaminophen as it is included within the hydrophobic CD cavity. Nevertheless, the activation of the GCE

during the cycling of the electrode to very high potentials into the oxygen evolution region may also promote the oxidation of acetaminophen and this is explored in Section 3.2.5.

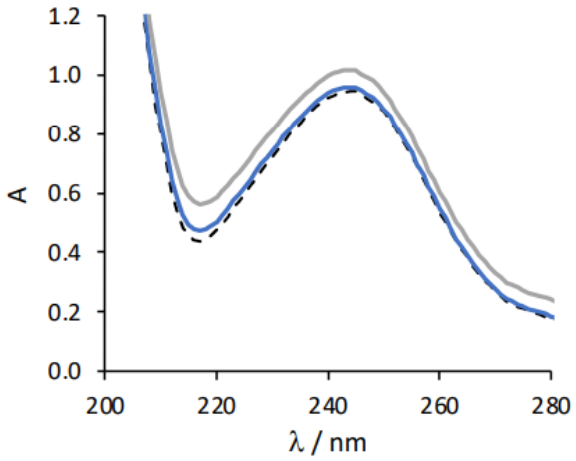

Fig. 3.5: (a) UV-visible spectra recorded for 0.01 mM acetaminophen in the absence (dashed trace), and presence of a 3-fold (blue) and 30-fold (grey) excess of βCD in a phosphate buffer.

3.3.2 ATR-FTIR

ATR-FTIR techniques were carried out to investigate the relationship between the β-CD and the surface of the activated GCE. **Fig 3.6** displays the FTIR data obtained, showing the spectrum of β-CD alongside the β-CD modified and the activated GCE. The spectrum of β-CD shows the symmetric and antisymmetric O–H stretching, with a broad peak centred at 3230 cm^{-1}. Bands representing C–O stretching at 1038 cm^{-1}, C–O–C stretching at 1153 cm^{-1}, C–H stretching at 2930 cm^{-1} and bending vibrations of O–H at 1028 cm^{-1} are also evident.

The FTIR data recorded for the activated and β-CD modified GCE showed highly similar spectra. For both spectrums broad bands can be noted in the 3000 to 3400 cm^{-1} region and can relate to O–H stretching vibrations, implying the possible presence of basal and edge hydroxyl groups. The remaining bands in the regions of 1400-1800 cm^{-1} can be designated to oxygen-containing functional groups including carboxyl, carbonyl and ketone groups [14]. Particularly the band present at 1056 cm^{-1} can be assigned to C–OH stretching vibrations while the band at band 1650 cm^{-1} can be ascribed to C=C stretching and the vibrational frequency at 1214 cm^{-1} is usually associated with C–O–C. The band observed at 1200 cm^{-1} accounts for the

presence of phenolic compounds with lower wavenumber bands that are characteristic with the bending movements of C=C.

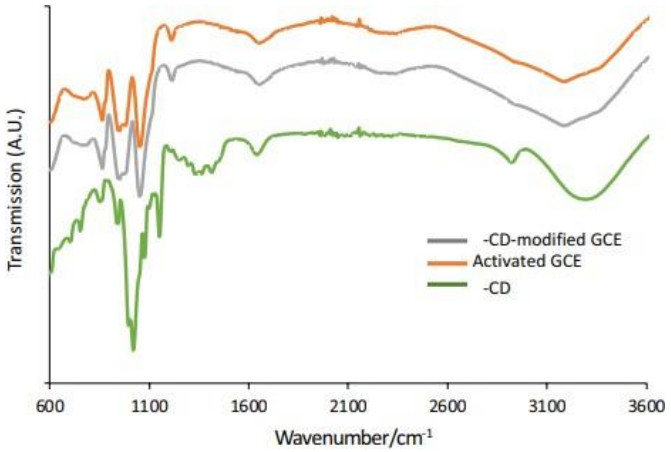

Figure 3.6: FTIR data recorded for β-CD (green), β-CD-modified (grey) and activated GCE (orange).

Although similarities exist between the spectra of the β-CD and the β-CD modified sensor, it remains difficult to confirm the presence of the electropolymerised β-CD. In both spectra similar functional groups can be noted such as the C–O and O–H due to observed vibrations whilst the spectrum of the activated and β-CD modified electrode appear almost identical.

3.3.3 EDX Studies

EDX studies were carried out on both the β-CD-modified GCE and the activated GCE in an attempt to determine if there were any variations in the oxygen and carbon contents. The results are tabled below in **Table 3.1**. The pristine carbon consisted of a freshly polished GCE with no exposure to the solution and this was employed as a control in the experiments. Element analysis of pristine carbon showed the material constituted of 100% carbon, whereas all other surfaces of the modified GCEs showed a notable oxygen content. For the activated and β-CD-modified GCE an oxygen content of close to 30% was recorded, while a much lower level of 12% was observed when using a sulfonated β-CD. The sulfonated β-CD was used during these studies as it is easily and readily detected by EDX. Surprisingly enough, there was no detection of sulphur once this β-CD , with numerous OH groups replaced by SO^{-}_{3}, was added to the PBS.

This evidently shows that the sulfonated β-CD is not electropolymerised at the GCE. Although the electropolymerisation of the sulfonated β-CD may be slower that the unsubstituted β-CD, it should nevertheless polymerise as it possess greater solubility and has OH groups available. With the absence of a sulphur signal coupled with the similar % of carbon and oxygen for the activated and β-CD modified GCE, it is proposed that the oxidation of the GCE surface is the primary reaction that takes places as the GCE is electrochemically cycled in the PBS. Reaction pathways have been reported in the literature that led to the formation of these oxidising groups like ketones, carbonyl, carboxylic and aldehydes. One study suggested that in acidic media the electrophilic addition of water happens at the conjugated π-system of carbon, which is followed then by the oxidation and condensation reactions [15]. The PBS used in this study had a pH of 5.5 providing the reaction mechanisms with the necessary acidic conditions.

Sample	%Carbon	%Oxygen
Pristine GCE	100	-
Activated GCE	70.8 ± 2.3	29.1 ± 1.9
β-CD/GCE	75.3 ± 1.9	24.4 ± 1.5
Sulfonated β-CD/GCE	87.6 ± 0.3	12.3 ± 0.3

Table 3.1: Elemental analysis obtained for GCE cycled in 0.1 M phosphate buffer for 20 cycles at 50 mV s^{-1} from –2.0 to 2.2 V vs. SCE and in the presence of 5 mM β-CD and 5 mM sulfonated β-CD. Data averaged over 5 sites on the surface.

3.3.4 SEM Analysis

Scanning electron microscopy (SEM) was employed to study the morphology of the activated and the β-CD modified GCE. **Fig 3.7(a)** and **(b)** show SEM data taken after the GCE was cycled in the PBS from –2.0 to 2.2 V (*vs.* SCE) at a scan rate of 100 mV s^{-1} and cycled in the presence and absence of the β-CD, respectively. On comparison of these two SEM micrographs with the micrographs of pristine GCE in **Fig 3.7(e)** it is observed that the surface appears much rougher in texture showing cracking-like characteristics that are more evident on cycling without the presence of the β-CD. In terms of the β-CD electropolymerisation at the GCE, there is no definite evidence to determine that this has occurred however the globules evident in **Fig 3.7(a)** could possibly be related to β-CD deposits.

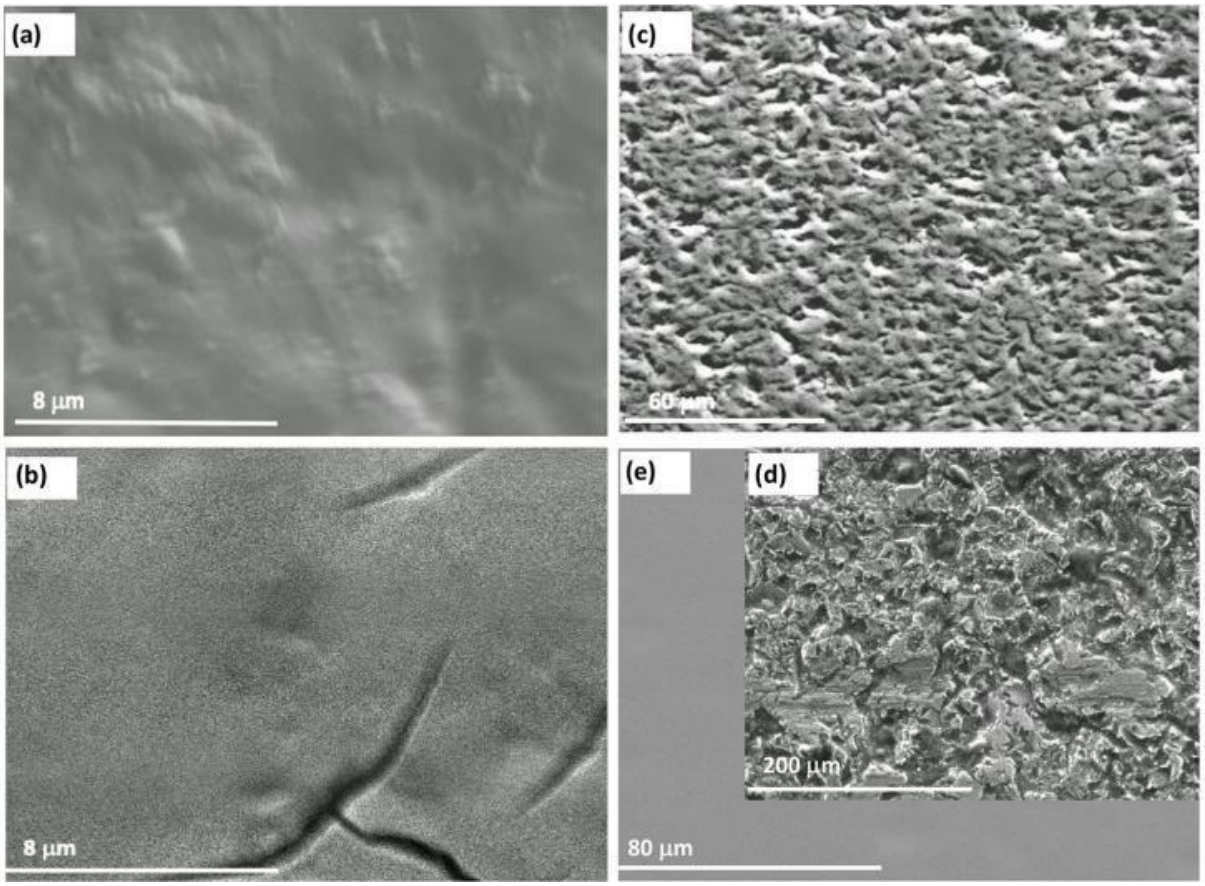

Figure 3.7: SEM micrographs recorded for GCE formed in 0.1 M phosphate between –2.0 and 2.2 V vs. SCE in the **(a)** presence of 5 mM β-CD at 100 mV s^{-1} and **(b)** absence of β-CD at 100 mV s^{-1}, **(c)** presence of 5 mM β-CD at 50 mV s^{-1}, **(d)** absence of 5 mM β-CD at 50 mV s^{-1} and (**e**) pristine GCE before cycling.

As the scan rate is decreased from 100 mV s^{-1} to 50 mV s^{-1} (i.e., cycled from –2.0 to 2.2 V (*vs.* SCE) at a scan rate of 50 mV s^{-1}) the morphology of the surface begins to change as illustrated in **Fig 3.7(c).** In this scenario, the surface of the GCE takes on an etched surface characteristic of dissolution and corrosion of the GCE. Even though the surface morphologies in the phosphate only solutions are alike to the β-CD phosphate solutions, more significant etching is clearly evident in the absence of the β-CD. This observation may imply that the β-CD somewhat protects or shields the surface to a certain degree, during cycling at these high potentials. Similar findings have been disclosed by a study examining the electrochemical corrosion of the GCE. The study concluded that in acidic media the GCE gets degraded by a ring opening reaction in the graphitic structure resulting in the formation of oxides on the surface [14].

3.3.5 Electrochemical Impedance Analysis

In order to study the conducting properties of the modified GCE electrodes, electrochemical impedance spectroscopy was employed. The data were recorded in a neural pH 7.0 phosphate buffer solution. In **Fig. 3.8** the impedance spectra recorded at 0.35 V (*vs*. SCE), which corresponds to the potential vicinity where acetaminophen is oxidised, are compared for the unmodified and cyclodextrin modified GC electrodes. The impedance response clearly shows that the modification of the GCE with the polymeric β-CD does not lead to any significant increase in the resistance of the electrode. Instead, the modified β-CD GCE electrode remains conducting. The impedance data were fitted to the equivalent circuit depicted in **Fig. 3.8**, where R_s corresponds to the solution resistance, R_{CT} is the charge transfer resistance and CPE_1 and CPE_2 are constant phase elements. The complex impedance of the CPE element is given in **Eq. 1**, where *A* is the surface area, ω is the angular frequency ($2\pi f$) and the exponent *n* can vary from 0 to 1. This expression corresponds to a resistor for *n* values of 0, an ideal capacitor when $n = 1$, an inductor with $n = -1$, while $n = 0.5$ is characteristic of a diffusional process. In this analysis the CPE was used to represent a non-ideal capacitor, giving $0.8 \leq n < 1$, and diffusion processes, with *n* close to 0.5.

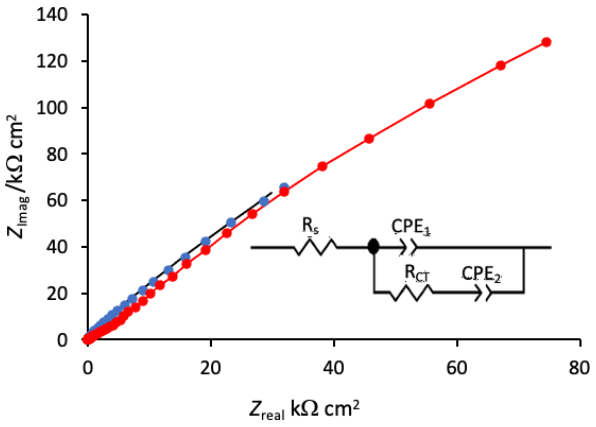

1

Fig. 3.8: Impedance spectra recorded at 0.35 V vs SCE for GC and β-CD modified GC in a phosphate buffer solution, inset shows the equivalent circuit employed in fitting the data.

$$Z_{CPE} = \frac{1}{\omega^n A} e^{-i\frac{\pi}{2}n}$$

The equivalent circuit elements are summarised in **Table 3.2**. It is seen from this analysis, that the β-CD modified GCE has only a slightly higher charge transfer resistance, making it suitable as an electrochemical sensor. The CPE_1 component with $n > 0.8$ can be related to the double

layer capacitance. While the CPE_1 has a value typical of a double layer capacitance for the GC electrode, the double layer capacitance is significantly higher for the β-CD modified GCE. This is consistent with the accumulation of ions at the β-CD polymer, as the primary and secondary hydroxyl groups can provide coordination sites for the chelation of ions [16]. The CPE_2 term corresponds to a nearly ideal diffusional term, with n = 0.55, for the β-CD modified GCE.

Table 3.2: Summary of fitted circuit elements for GC and poly-β-CD/GC recorded at 0.32 V vs SCE in 0.1 M phosphate buffer.

System	R_{CT}/ kW cm^2	CPE_1/ F cm^{-2}	n_1	CPE_2/ $W^{-1}s^n$ cm^{-2}	n_2
GC	5660	2.41×10^{-5}	0.83	3.12×10^{-5}	0.67
β-CD/GC	6130	1.27×10^{-4}	0.91	4.77×10^{-5}	0.55
Activated GC	5930	3.44×10^{-4}	0.92	4.68×10^{-5}	0.53

Nevertheless, as illustrated in **Table 3.2**, the fitted equivalent circuit elements are similar for both the activated GCE and the β-CD modified GCE. The high capacitance values are also seen with the activated electrode and may be associated with the presence of oxygenated groups that can attract ions. As mentioned earlier, the oxidation of carbon-based substrates occurs when polarised to high potentials and this has been reported with GCE [17] and indeed other carbon-based electrodes [18,19]. At such high potentials beyond the oxygen evolution reaction, $OH^{\bullet}$ radicals are produced, and these can attack the C–C bonds. This in turn gives rise to the formation of oxygen-containing groups [20]. This is consistent with the elemental analysis in **Table 3.1** and may be responsible for the increase in the capacitance of the activated GCE compared to the unmodified GCE.

3.3.6 Redox behaviour of acetaminophen at β-CD-modified and activated GCE

The electrochemical performance of the sensors with modified GCE surfaces for acetaminophen determination were investigated using the modified electrodes in the chloride, sulphate and phosphate solutions. The greatest acetaminophen detection was achieved using

the phosphate electrolyte solution, while as predicted the chloride-based system exhibited the lowest of all peak currents observed (data not shown).

The cyclic voltammograms recorded for the modified and unmodified electrodes that were formed by cycling in the phosphate systems are depicted in **Fig 3.9.** The voltammograms representing the modified electrodes cycled in phosphate solution with and without β-CD are compared with the unmodified GCE. The unmodified GCE shows the normal irreversible diffusion-controlled character of acetaminophen, displaying a wide oxidation wave focused at around 0.55 V (*vs*. SCE). Moreover, the reverse reduction peak is missing which indicates that a slow irreversible redox reaction is taking place. These data are congruent with the forming of N-acetyl benzoquinone imine arising from the oxidation of acetaminophen which subsequently undergoes a hydrolysis reaction, as represented in **Scheme 1**.

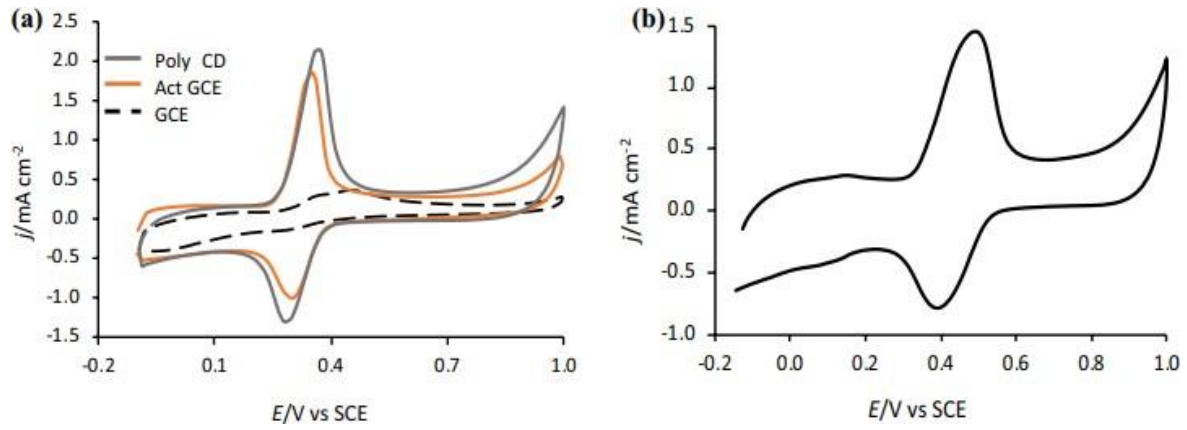

Figure 3.9: Cyclic voltammograms recorded at 100 mV s^{-1} scanning from –0.2 to 1.0 V in 1.0 mM acetaminophen in a neutral phosphate buffer at **(a)** GCE, activated GCE and at β-CD/GCE and **(b)** extended activation period, with β-CD/GCE formed by cycling between –2.0 and 2.2 V vs. SCE at 50 mV s^{-1} for 20 cycles.

On the contrary, the oxidation peaks for the modified GCEs occur at much lower overpotentials being centered at about 0.35 V (*vs*. SCE). In addition, the reduction peak waves are considerably higher with values close to 1.95 ± 0.08 mA cm^{-2} and 1.78 ± 0.09 mA cm^{-2} for the β-CD/GCE and activated GCE , respectively, compared to a significantly lower current density value of 0.2 mA cm^{-2} for the unmodified GCE.

The thin symmetric redox wave peaks present at the activated GCE and the β-CD/GCE agree with an adsorption-controlled mechanism where the acetaminophen is contained at the electrode surface. However, once a longer period of activation and oxidation of the GCE

happened due to cycling for longer via a slower scan rate of 50 mV s^{-1} between the potential window of –2.0 to 2.2 V (*vs.* SCE) for 20 cycles, what was noted was lower peak currents, wider peaks and higher peak potentials, as seen in **Fig 3.9(b).** This observation proposes that a slower electron transfer rate is occurring. Furthermore, greater background currents are seen with a wide wave emerging in the region of 0.0 to 0.2 V (*vs.* SCE). The presence of this wide wave is also seen with cycling in the PBS, implying that it is related with surface bound redox groups produced during the prolonged activation and oxidation of the GCE surface. In fact, the increase in capacitance is compatible with the forming of extremely porous surface layers seen earlier in the SEM micrograph **Fig 3.7(c).**

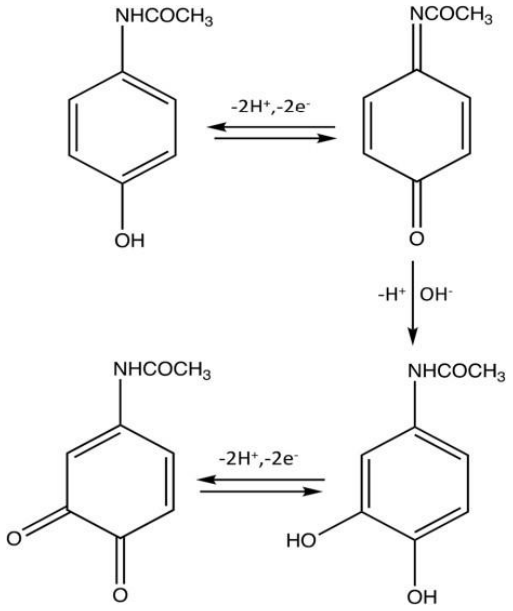

Scheme 1: The oxidation of acetaminophen followed by a hydrolysis reaction.

In **Fig 3.9(a)** the data recorded is characteristic of an analyte that is confined to the surface. The experimental ΔEp values were in the vicinity of 45 mV at the slow scan rates. This value being close to a typical adsorbed species which has a theoretical value of ΔEp = 0 mV for the reversible electron transfer. In addition, the ratio of $j_{p(ox)}/j_{p(red)}$ is relatively close to unity at the lower rates of scanning. This suggest that the N-acetyl benzoquinone imine formed from electrochemical oxidation is quite stable and does not undergo a significant amount of hydrolysis following oxidation. Thus, it can be ultimately reduced back to acetaminophen.

Although the conversion of N-acetyl benzoquinone imine to acetaminophen is evident at high scan rates for a diversity of electrodes, in this instance it is seen at slow scan rates at the rate of 15 mV s^{-1}, implying that it is certainly protected from extensive hydrolysis. The protection from hydrolysis is possibly linked to the adsorption of the N-acetyl benzoquinone at both the modified β-CD/GCE and the activated GCE surface. It seems that the microstructure alterations such as the modified edge planes and oxygen-containing functional moieties that were formed during the activation of the GCE, facilitate acetaminophen and N-acetyl benzoquinone imine adsorption. In addition, the deposited or potentially electropolymerised β-CD can also enhance the adsorption through the formation of an inclusion complex, encapsulating the acetaminophen and its oxidised counterpart N-acetyl benzoquinone at the electrodes surface.

3.3.7 Scan Rate Studies

Scan rate studies were conducted to investigate the rate determining step and to determine if the reaction was under adsorption or diffusion control. The relationship between the scan rate and the oxidation peak current for both the modified β-CD GCE and the activated GCE is displayed in **Fig. 3.10.** Linear relationships were recorded for both the β-CD modified and the activated GCE, as seen in **Fig. 3.10**. The linear regression equation of the β-CD-modified GCE was deduced as Ep/mV = (0.015 ± 0.001)υ + (0.225 ± 0.091) with a R^2 value of 0.98. The equivalent equation of the activated GCE was Ep/mV = (0.016 ± 0.001)υ + (0.151 ± 0.052) with a R^2 value of 0.99. Both relationships and data obtained are consistent with the oxidation of acetaminophen being governed by an adsorption-controlled process.

Transportation of an analyte from a bulk liquid phase to a liquid-solid interface occurs in two steps. Firstly, the analyte diffuses from the bulk fluid phase to the sublayer or subsurface, and secondly adsorption of the adsorbate at the interface occurs. If a situation arises where a diffusion flux or diffusion equilibrium is established between the bulk and sublayer during mass transfer of the analyte, the reaction will consequently be deemed to be governed as a diffusion-controlled process. This diffusion step will also be the rate-determining step [21,22], meaning the rate at which this first step occurs controls or determines the overall rate of the reaction. For an adsorption-controlled process, the adsorption of the analyte at the surface is

the rate determining step. The rate at which the molecules orient and adsorb at the interface/electrode surface determines the overall speed of the entire adsorption process [23].

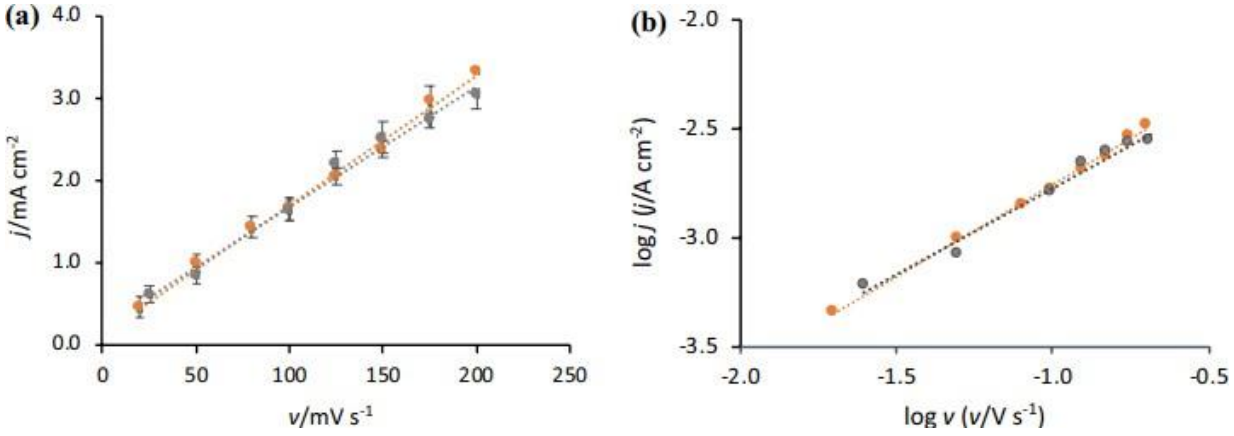

Figure 3.10: (a) Plot of peak current as a function of scan rate and **(b)** logarithm of peak current as a function of the logarithm of scan rate, recorded in 1.0 mM acetaminophen, for the β-CD GCE (grey) and activated GCE (orange).

For a diffusion-controlled event, a linear relationship would be observed between the logarithm of the peak current and the logarithm of the scan rate with a slope of 0.5. Whilst under an adsorption-controlled process a linear plot will be obtained between the logarithm of both the peak current and the scan rate with an ideal slope of 1.0 [24]. The latter was seen in this study as the logarithm of the peak current was plotted as a function of the logarithm of the scan rate and showed a linear relationship for both the modified and activated electrodes. The slopes of the plots were measured as 0.85 and 0.78 for the activated and the β-CD-modified GCEs, respectively, slightly deviating from the ideal value of 1.0 for a surface or adsorption-controlled process. In particular, the 0.78 value produced by the β-CD-modified GCE suggests that a mixed adsorption-diffusion controlled process occurs.

The standard rate constant (k_s) was approximated through Laviron's model, where the assumption is formed that acetaminophen is irreversibly adsorbed [25]. **Equation 3.2** represents the relationship of Laviron's model where E_p is the peak potential, E^o represents the formal potential, α corresponds to the charge-transfer coefficient, n is the number of electrons that are transferred, T symbolises the thermodynamic temperature and finally F being Faraday's constant.

$$E_p = E^0 + \left(\frac{RT}{(1-\alpha)nF}\right) ln\left(\frac{RTk_s}{(1-\alpha)nF}\right) - \left(\frac{RT}{(1-\alpha)nF}\right) lnv \qquad \textit{Eq 3.2}$$

An example of a plot for both the β-CD-modified and activated GCE is illustrated in **Fig 3.11** with both showing a significant linearity. The observed linear behaviour implies there is good agreement with the above equation. The linear regression equation for the modified β-CD/GCE was Ep/mV = (0.0144 ± 0.0011) ln$v$ + (0.325 ± 0.005), compared to Ep/mV = (0.0149 ± 0.0004) ln$v$ + (0.282 ± 0.0020) for the activation GCE. E^0 figures were calculated by plotting E_p as a function of v and extrapolating to v = 0, which resulted in E^0 values of 370 mV and 325 mV for the β-CD/GCE and the activated GCE, respectively. These E^o values and the α value of 0.5 were used in the calculations for the k_s value. Approximated k_s values of (4.3 ± 0.3) × 10^{-3} cm^2 s^{-1} and (3.4 ± 0.2) × 10^{-3} cm^2 s^{-1} were then calculated for the β-CD/GCE and activated GCE, respectively. These values correlate to efficient electron transfer kinetics for both electrodes, with the activated GCE displaying a somewhat lower rate constant.

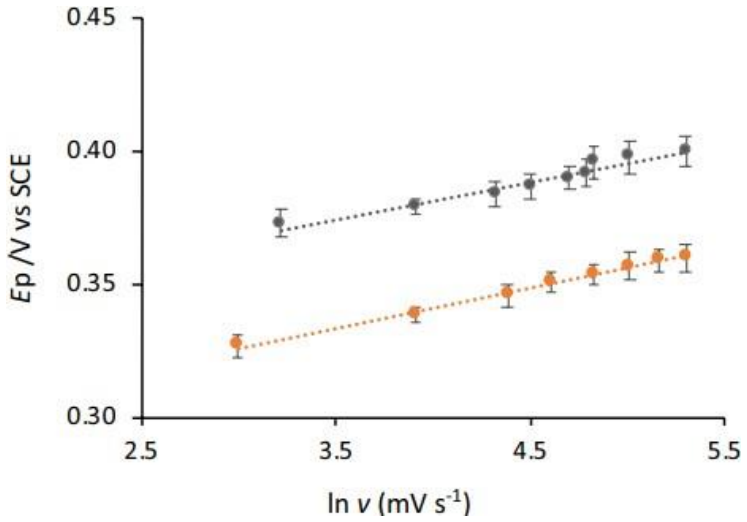

Figure 3.11: Plot of *E*p (oxidation wave) as a function of the logarithm of the scan rate for β-CD modified GCE (grey symbols) and activated GCE (orange symbols), recorded in 0.5 mM acetaminophen.

It can also be noted that the presence of β-CD does not influence significantly the data obtained in **Fig. 3.11.** It does however have some impact on the morphology of the electrodes surface seen previously in **Fig. 3.7** by protecting the surface from considerable etching. It is certain that prolonged etching leads to the widening of peaks as shown in **Fig. 3.9**, this process is

consistent with slower electron kinetics (**Fig 3.9(b)**). Consequently, the slightly higher rate constant obtained for the β-CD/GCE may be linked to the extent of oxidation and to the nature of the oxygenated species that are formed, or to some absorbed β-CD. Taking the slope values and the *n* value as 2, the (1 – α) term was computed as 0.84 resulting in an α value within the 0.0 to 1.0 range, however lying outside the expected value range of 0.4 to 0.7.

3.3.8 Influence of pH

The technique of DVP was used to examine the effect of pH on the oxidation of acetaminophen. DVP was recorded for the modified β-CD electrode at a range of pH values and the corresponding plots are given in **Fig 3.12(a)**. It can be observed that the currents of the peaks become lower when the solution becomes more alkaline, giving a peak current density of 1.8 mA cm^{-2} at a pH of 9.2. In comparison, a higher peak current density of 3.8 mA cm^{-2} is evident at a pH of 6.5.

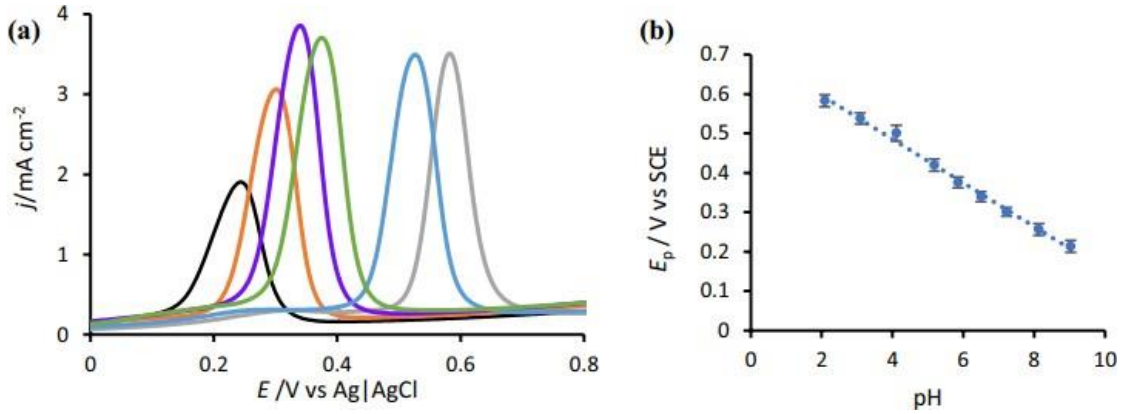

Figure 3.12: (a) Differential pulse voltammograms recorded in 1.0 mM acetaminophen at pH values of 9.0 (black), 7.5 (orange), 6.5 (purple), 5.1 (green), 3.5 (blue) and 2.1 (grey) and **(b)** corresponding plot of peak potential as a function of pH

Acetaminophen exhibits a pK_a of 9.5 and therefore will be become ionised in the more alkaline solutions. This negatively charged or anionic acetaminophen will possess higher water solubility, and this may very well reduce the degree to which it is adsorbed at the electrode-solution interface. As the solution gradually becomes more acidic in nature the acetaminophen becomes more protonated due to the increase of hydronium ions in solution, this is seen for pH

levels lower than 9.2. This finding agrees with the somewhat higher peak currents seen at pH values of 5.5 for which the molecule is neutral in **Fig. 3.12(a).**

The variations of the peak potentials is graphed in **Fig. 3.12(b).** There is an obvious linear relationship between the peak potentials and the pH of the solution. The slope of the linear plot was calculated as 0.055 V which is strongly consistent with the Nernst equation. In scheme 1 it was shown that the oxidation of acetaminophen is a $2e^{-}/2H^{+}$ redox reaction and therefore using the Nernst equation a slope of 0.059V at 298 K is predicted from the Nernst equation. The values of 0.055 V and 0.059 V are undoubtedly in near agreement with one another.

3.3.9 Sensing performance of the β-CD-modified & activated GCE

The sensing performance was categorised and examined based on two important properties: selectivity and sensitivity. The selectivity of a sensor is measured by the sensor's ability to customise specific interactions between species, typically with the use of an immobilising recognition element at the electrode surface, that has a specific binding affinity for the target analyte [26]. In addition, the oxidised product from the redox reaction in the electrochemical cell should be the only product detected, with no detection or indication of any other product i.e., interference free [26]. The property of sensitivity for a sensor can be defined as a measure of the analyte's concentration or amount that is being detected. It may be used as a performance property if it is dependent on the chemical measurement process alone and not on any other factors such as scale factors [27]. The sensitivity measurements reveal how much acetaminophen is being detected at the electrode's surface. Another important parameter is the limit of detection, LOD value, in the determination of acetaminophen.

3.3.9.1 Sensitivity of the β-CD-modified & activated GCE

The sensing ability of the β-CD modified and the activated GCE for the determination of acetaminophen was analysed using DPV measurements. The calibration curves produced by the DVP investigation are illustrated in **Fig. 3.13.** In particular plot **(a)** displays the relationship

between the peak oxidation current for both the modified and activated electrode. This calibration data displays an initial linear progression at the lower concentrations, ranging from 0.1 to 80 μM, while this linear behaviour seems to plateau at higher concentrations, reaching a limiting point which gives an overall curve for the entire range of concentrations. The linear regression of the calibration curves shown in **Fig. 3.13(b)** were recorded as Ip/mA cm^{-2} = (0.0327 ± 0.0006) c/μM + (0.0462 ± 0.0240) for the activated GCE and as for the β-CD modified electrode the obtained values were Ip/mA cm^{-2} = (0.0344 ± 0.0003) c/μM + (0.0004 ± 0.0040), with correlation coefficients >0.99.

The slopes of the above equations were used to calculate the sensitivity of the measurement, determined for the activated GCE as 32.7 ± 0.6 μA cm^{-2} μM^{-1} and for the modified β-CD electrode as 34.4 ± 0.3 μA cm^{-2} μM^{-1}. The matching limit of detection (LOD) values were approximated to be (9.8 ± 0.4) × 10^{-8} M and (9.7 ± 0.4) × 10^{-8} M, respectively. These values were estimated using the standard deviation of the blank and the sensitivity values. Evidently, there is no considerable difference between the activated and the β-CD-modified GCE in the electrochemical detection of acetaminophen. These sensing parameters compare significantly well with numerous other studies involving multiwalled carbon nanotubes (MWCNTs), graphene, nanoparticles and surface modifications using materials such as bismuth [15].

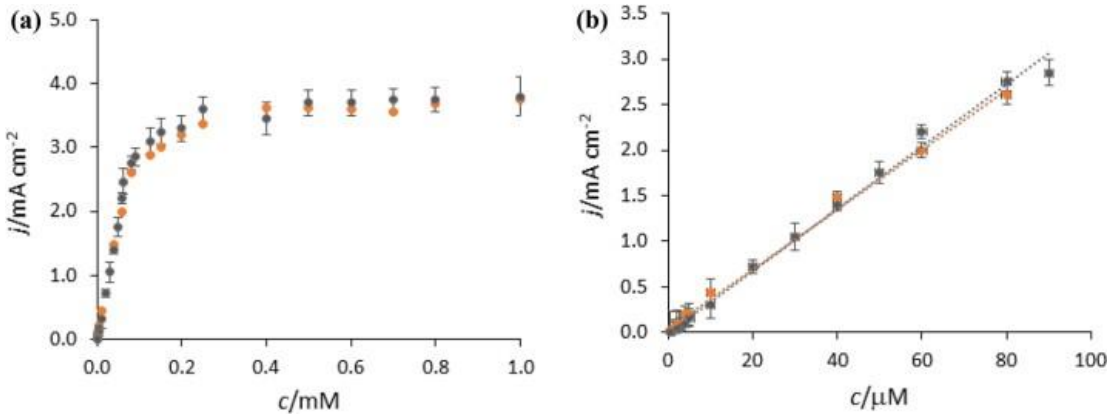

Figure 3.13: Calibration curves recorded over **(a)** a wide concentration range and the **(b)** linear range, using DPV data recorded for the β-CD-modified GCE (grey) and activated GCE (orange).

These sensing parameters are summarised in **Table 3.3** and compared with a number of previous investigations. While the linear region is somewhat lower than some of the reported values, the sensitivities are high at 32.7 and 34.4 μA cm^{-2} μM^{-1} (corresponding to 2.3 and 2.4

μA μM^{-1}). These compare very favourably with reported values of 37.28 μA mM^{-1} [28], 0.618 μA cm^{-2} μM^{-1} [29] and 0.15 μA μM^{-1} [30].

Table 3.3: Data from sensor deployed in real-life commercial paracetamol sample (Panadol) with satisfactory values in comparison to lab analysis of acetaminophen.

Modified electrode	Linear range/μM	LOD/μM	Ref.
MWCNTs/Nafion/GCE	2 – 80	0.5	[31]
Graphene/GCE	0.1 – 20	0.032	[32]
TiO_2Np/MCPE	–	5.2	[33]
Bi/Ag	2 – 20	0.15	[34]
Poly(brilliant green)/CNT/GCE	5 – 200	2.4	[35]
Mesoporous Carbon/GCE	4 –100	0.94	[36]
4-Aminobenzoic/GCE	24 – 240	–	[37]
CNT/Ceramic /GCE	0.2 – 150	0.12	[38]
Activated/β-CD-modified/GCE	0.1 – 80	0.0097	This work

3.3.9.2 The Selectivity of the β-CD-modified GCE

The selectivity of the β-CD/GCE for the detection of acetaminophen was analysed using interference compounds. Caffeine, ascorbic acid, aspirin, uric acid and sorbate were used as the interfering compounds. A resulting voltammogram from the DVP experiments is displayed in **Fig. 3.14**, which was carried out in a neutral solution of 0.025 mM acetaminophen and 0.05 mM caffeine, 0.05 mM aspirin and 0.05 mM ascorbic acid. It is clear from **Fig. 3.14(a)** that the oxidation of acetaminophen is not influenced by the added interferences. The oxidation of caffeine is seen at 1.28 V vs Ag/AgCl and the oxidation of ascorbic acid appears as a broad wave centred at 0.04 V vs Ag/AgCl. However, there is no overlap with the oxidation wave of acetaminophen.

From studying the bar chart in **Fig. 3.14(b)**, it is evidently apparent that the oxidation of acetaminophen is not influenced by the addition of interference compounds at concentrations

of 0.05 mM, which are two-fold higher than the acetaminophen concentration. It is clearly seen that the peak currents recorded for acetaminophen in both the presence and absence of interferents are very similar, indicating a high level of selectivity. Very good selectivity is seen in the presence of caffeine, aspirin, ascorbic acid, uric acid and sorbate, with all interference species with a concentration of 0.05 mM. Furthermore, **Fig. 3.14(a)** highlights the sensor's ability to simultaneously sense and detect acetaminophen and caffeine. This selectivity can be partially linked to the fact that most of the interference species oxidise at different potentials compared to the E_p value of acetaminophen, but it may also be due to the adsorption of acetaminophen that could potentially physically block the interferents from the electrode surface.

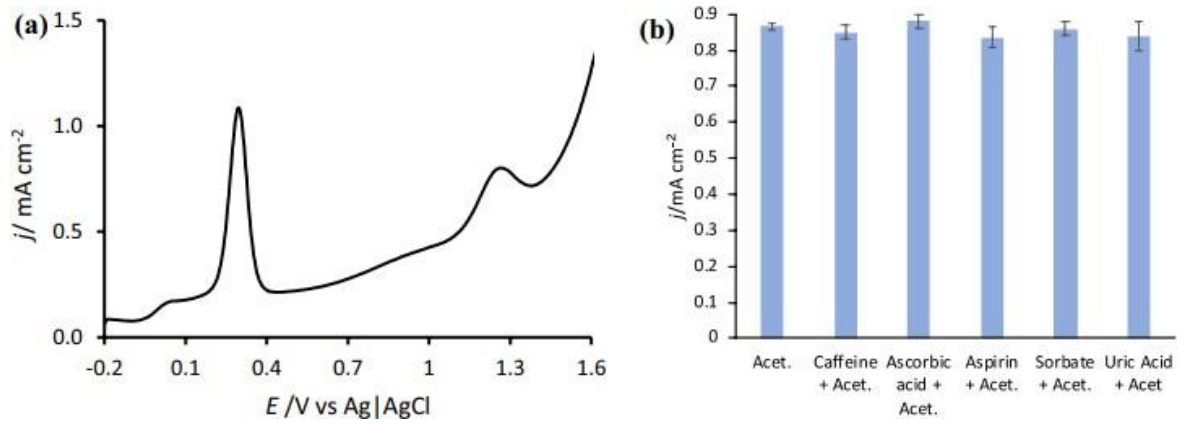

Figure 3.14: (a) DPV recorded in 0.025 mM acetaminophen with 0.05 mM ascorbic acid, 0.05 mM caffeine and 0.05 mM aspirin in a phosphate buffer, at a pH of 7.0, **(b)** acetaminophen (Acet.) peak currents recorded for 0.025 mM acetaminophen in the absence and presence of various interference compounds (0.05 mM).

However, upon increasing the concentration of the interferents, interference was eventually seen with the uric acid where a tenfold excess of uric acid was investigated, the peak current of acetaminophen was reduced from approximately 0.87 mA cm^{-2} to 0.65 mA cm^{-2} corresponding to a 25% peak current reduction.

The sensors capability for detection of acetaminophen in a commercial pharmaceutical tablet which contained caffeine was also tested. The tablet tested was provided by the brand 'Panadol' and was tested using a standard spiking and recovery experiment. A solution of the tablet was made up in phosphate buffer and a range of concentrations were made. The solutions were not further treated and contained various excipients. The sensor was then deployed in these real-life samples that were spiked with the standards and the peak currents obtained were compared

to the values recorded for the acetaminophen standards. The % recovery was excellent with the lower concentrations (97 to 100%, with additions ranging from 0.24 to 1.90 μM), although the high concentrations spikes did not have such great values, instead the recovery values became lower (92.5% with a spike of 19.9 μM). Nonetheless, the data do display satisfactory levels of selectivity for the modified sensor in a complex solution with caffeine and other excipients.

Table 3.3: Data from sensor deployed in real-life commercial paracetamol sample (Panadol) with satisfactory values in comparison to lab analysis of acetaminophen.

Analysis of a commercial paracetamol tablet.

Concentration Added / ∝M	$j_{measured}$ / ∝A cm^{-2}	$j_{expected}$ / ∝A cm^{-2}	% Recovery
0.24	1.86	1.86	100
0.97	4.76	4.81	98.9
1.95	11.4	11.7	97.4
3.90	22.8	23.9	96.2
7.80	38.5	40.6	94.8
9.90	50.0	53.5	93.4
19.9	59.0	65.0	90.7

3.3.10 Comparison of the β-CD and activated GCE

It is apparent from the above experiments and their corresponding data that both the activation of the GCE and its modification with the β-CD, alter the oxidation of acetaminophen. This is seen as the oxidation of acetaminophen changes from a process that is normally governed by a diffusion-controlled event to a process governed by an adsorption-controlled reaction. Moreover, the electrogenerated N-acetyl benzoquinone imine is found to be protected from the extensive hydrolysis reaction by adsorption at the modified electrodes. Similar findings were reported using both the activated and β-CD-modified GCE, evidently concluding that while the β-CD may play a minor role it is indeed the activated GCE that significantly enhances acetaminophen detection. It is well known that the electrochemical oxidation of carbon-based materials, such as the glassy carbon electrode, that undergo polarisation beyond the oxygen evolution reaction, result in the formation of oxygen-containing functional groups [39] due to the greatly oxidising environment alongside the high overpotentials [40].

At high potentials that are commonly seen beyond the oxygen evolution reaction [41] $OH^{\bullet}$ radicals are formed, which then proceed to attack the carbon atoms at the surface. This attack happens at defect sites causing the C-C bonds to begin breaking and various oxygenated atoms to form. The glassy carbon at the electrode surface now exists as microcrystalline graphite with oxide-enriched edge planes which ultimately enhance the electrochemical behaviour of the activated electrode [39]. It seems that the enhanced electrochemical oxidation and detection of acetaminophen can be attributed to these events, providing a simple, cost effective, and eco-friendly method of electrode modification. Indeed, the activation is likely to play an important role in sensing abilities of several published studies where the GCE is polarised to high potentials during modification [15].

3.4 Bibliography

1. Alberti, G.; Zanoni, C.; Losi, V.; Magnaghi, L.R.; Biesuz, R. Current trends in polymer based sensors. *Chemosensors* **2021**, *9*, doi:10.3390/chemosensors9050108.

2. Girek, T.; Koziel, K.; Girek, B.; Ciesielski, W. CD oxyanions as a tool for synthesis of highly anionic cyclodextrin polymers. *Polymers (Basel).* **2020**, *12*, 1–18, doi:10.3390/polym12122845.

3. Han, B.; Yang, B.; Yang, X.; Zhao, Y.; Liao, X.; Gao, C.; Wang, F.; Jiang, R. Host-guest inclusion system of norathyriol with β-cyclodextrin and its derivatives: Preparation, characterization, and anticancer activity. *J. Biosci. Bioeng.* **2014**, *117*, 775–779, doi:10.1016/j.jbiosc.2013.12.001.

4. Healy, B.; Yu, T.; da Silva Alves, D.C.; Okeke, C.; Breslin, C.B. Cyclodextrins as supramolecular recognition systems: Applications in the fabrication of electrochemical sensors. *Materials (Basel).* **2021**, *14*, doi:10.3390/ma14071668.

5. Liao, C. Electrochemical polymerization. *Chem. Bull. / Huaxue Tongbao* **2000**, *63*, 37–41, doi:10.1007/978-3-319-95987-0_3.

6. Huang, D.; Cheng, Y.; Xu, H.; Zhang, H.; Sheng, L.; Xu, H.; Liu, Z.; Wu, H.; Fan, S. The determination of uric acid in human body fluid samples using glassy carbon electrode activated by a simple electrochemical method. *J. Solid State Electrochem.* **2015**, *19*, 435–443, doi:10.1007/s10008-014-2614-9.

7. Videla, H.A. Fundamentals of Electrochemistry. *Man. Biocorrosion* **2018**, 73–120, doi:10.1201/9780203748190-4.

8. Farhat, A.; Keller, J.; Tait, S.; Radjenovic, J. Assessment of the impact of chloride on the formation of chlorinated by-products in the presence and absence of electrochemically activated sulfate. *Chem. Eng. J.* **2017**, *330*, 1265–1271, doi:10.1016/j.cej.2017.08.033.

9. Farhat, A.; Keller, J.; Tait, S.; Radjenovic, J. Assessment of the impact of chloride on the formation of chlorinated by-products in the presence and absence of electrochemically activated sulfate. *Chem. Eng. J.* **2017**, *330*, 1265–1271, doi:10.1016/j.cej.2017.08.033.

10. Hassler, M. Other commonly used biomedical coatings: pyrolytic carbon coatings. *Coatings Biomed. Appl.* **2012**, 75–105, doi:10.1533/9780857093677.1.75.

11. Idris, A.O.; Orimolade, B.O.; Mafa, P.J.; Kuvarega, A.T.; Feleni, U.; Mamba, B.B. Carbon-Nanodots modified glassy carbon electrode for the electroanalysis of selenium in water. *Results Chem.* **2022**, *4*, 100394, doi:10.1016/j.rechem.2022.100394.

12. Ngouoko, J.J.K.; Tajeu, K.Y.; Temgoua, R.C.T.; Doungmo, G.; Doench, I.; Tamo, A.K.; Kamgaing, T.; Osorio-Madrazo, A.; Tonle, I.K. Hydroxyapatite/L-Lysine Composite Coating as Glassy Carbon Electrode Modifier for the Analysis and Detection of Nile Blue A. *Materials (Basel).* **2022**, *15*, doi:10.3390/ma15124262.

13. Zinatullina, K.M.; Kasaikina, O.T.; Kuzmin, V.A.; Khrameeva, N.P.; Pisarenko, L.M. Effect of phosphate buffer solutions on the reactions of glutathione with hydrogen peroxide and peroxyl radicals. *Russ. Chem. Bull.* **2019**, *68*, 1441–1444, doi:10.1007/s11172-019-2574-4.

14. Yi, Y.; Weinberg, G.; Prenzel, M.; Greiner, M.; Heumann, S.; Becker, S.; Schlögl, R. Electrochemical corrosion of a glassy carbon electrode. *Catal. Today* **2017**, *295*, 32–40, doi:10.1016/j.cattod.2017.07.013.

15. Healy, B.; Rizzuto, F.; de Rose, M.; Yu, T.; Breslin, C.B. Electrochemical determination of acetaminophen at a carbon electrode modified in the presence of β-cyclodextrin: role of the activated glassy carbon and the electropolymerised β-cyclodextrin. *J. Solid State Electrochem.* **2021**, *25*, 2599–2609, doi:10.1007/s10008-021-05044-3.

16. Prochowicz, D.; Kornowicz, A.; Lewiński, J. Interactions of Native Cyclodextrins with Metal Ions and Inorganic Nanoparticles: Fertile Landscape for Chemistry and Materials Science. *Chem. Rev.* **2017**, *117*, 13461–13501, doi:10.1021/acs.chemrev.7b00231.

17. Huang, D.; Cheng, Y.; Xu, H.; Zhang, H.; Sheng, L.; Xu, H.; Liu, Z.; Wu, H.; Fan, S. The determination of uric acid in human body fluid samples using glassy carbon electrode activated by a simple electrochemical method. *J. Solid State Electrochem.* **2015**, *19*, 435–443, doi:10.1007/s10008-014-2614-9.

18. Holloway, A.F.; Wildgoose, G.G.; Compton, R.G.; Shao, L.; Green, M.L.H. The influence of edge-plane defects and oxygen-containing surface groups on the voltammetry of acid-treated, annealed and “super-annealed” multiwalled carbon

nanotubes. *J. Solid State Electrochem.* **2008**, *12*, 1337–1348, doi:10.1007/s10008-008-0542-2.

19. Liu, X.; Wang, Y.; Zhan, L.; Qiao, W.; Liang, X.; Ling, L. Effect of oxygen-containing functional groups on the impedance behavior of activated carbon-based electric double-layer capacitors. *J. Solid State Electrochem.* **2011**, *15*, 413–419, doi:10.1007/s10008-010-1100-2.

20. Rana, A.; Baig, N.; Saleh, T.A. Electrochemically pretreated carbon electrodes and their electroanalytical applications – A review. *J. Electroanal. Chem.* **2019**, *833*, 313–332, doi:10.1016/j.jelechem.2018.12.019.

21. SITENKO, A.G. Kinetic Equations. *Fluctuations Non-Linear Wave Interact. Plasmas* 1982, 175–203.

22. Inglezakis, V.J.; Balsamo, M.; Montagnaro, F. Liquid-Solid Mass Transfer in Adsorption Systems - An Overlooked Resistance? *Ind. Eng. Chem. Res.* **2020**, *59*, 22007–22016, doi:10.1021/acs.iecr.0c05032.

23. Pal, N.; Saxena, N.; Mandal, A. Equilibrium and dynamic adsorption of gemini surfactants with different spacer lengths at oil/aqueous interfaces. *Colloids Surfaces A Physicochem. Eng. Asp.* **2017**, *533*, 20–32, doi:10.1016/j.colsurfa.2017.08.020.

24. Nagle, L.C.; Wahl, A.; Ogourstov, V.; Seymour, I.; Barry, F.; Rohan, J.F.; Loughlin, R. Mac Electrochemical discrimination of salbutamol from its excipients in ventolintm at nanoporous gold microdisc arrays. *Sensors* **2021**, *21*, doi:10.3390/s21123975.

25. Randviir, E.P. A cross examination of electron transfer rate constants for carbon screen-printed electrodes using Electrochemical Impedance Spectroscopy and cyclic voltammetry. *Electrochim. Acta* **2018**, *286*, 179–186, doi:10.1016/j.electacta.2018.08.021.

26. Chaubey, A.; Malhotra, B.D. Mediated biosensors. *Biosens. Bioelectron.* **2002**, *17*, 441–456, doi:10.1016/S0956-5663(01)00313-X.

27. sensitivity in metrology and analytical chemistry, A. *IUPAC Compend. Chem. Terminol.* **2008**, *2167*, 5606, doi:10.1351/goldbook.s05606.

28. Wang, L.; Meng, T.; Fan, Y.; Chen, C.; Guo, Z.; Wang, H.; Zhang, Y. Electrochemical study of acetaminophen oxidation by gold nanoparticles supported on a leaf-like zeolitic

imidazolate framework. *J. Colloid Interface Sci.* **2018**, *524*, 1–7, doi:10.1016/j.jcis.2018.04.009.

29. Liu, B.; Ouyang, X.; Ding, Y.; Luo, L.; Xu, D.; Ning, Y. Electrochemical preparation of nickel and copper oxides-decorated graphene composite for simultaneous determination of dopamine, acetaminophen and tryptophan. *Talanta* **2016**, *146*, 114– 121, doi:10.1016/j.talanta.2015.08.034.

30. Kumar, M.; Kumara Swamy, B.E.; Reddy, S.; Zhao, W.; Chetana, S.; Gowrav Kumar, V. ZnO/functionalized MWCNT and Ag/functionalized MWCNT modified carbon paste electrodes for the determination of dopamine, paracetamol and folic acid. *J. Electroanal. Chem.* **2019**, *835*, 96–105, doi:10.1016/j.jelechem.2019.01.019.

31. Li, Z.-Y.; Gao, D.-Y.; Wu, Z.-Y.; Zhao, S. Simultaneous electrochemical detection of levodapa, paracetamol and l-tyrosine based on multi-walled carbon nanotubes. *RSC Adv.* **2020**, *10*, 14218–14224, doi:10.1039/d0ra00290a.

32. Kang, X.; Wang, J.; Wu, H.; Liu, J.; Aksay, I.A.; Lin, Y. A graphene-based electrochemical sensor for sensitive detection of paracetamol. *Talanta* **2010**, *81*, 754–759, doi:10.1016/j.talanta.2010.01.009.

33. Manjunatha, K.G.; Swamy, B.E.K.; Madhuchandra, H.D.; Vishnumurthy, K.A. Synthesis, characterization and electrochemical studies of titanium oxide nanoparticle modified carbon paste electrode for the determination of paracetamol in presence of adrenaline. *Chem. Data Collect.* **2021**, *31*, doi:10.1016/j.cdc.2020.100604.

34. van der Horst, C.; Silwana, B.; Gil, E.; Iwuoha, E.; Somerset, V. Simultaneous Detection of Paracetamol, Ascorbic Acid, and Caffeine Using a Bismuth–Silver Nanosensor. *Electroanalysis* **2020**, *32*, 3098–3107, doi:10.1002/elan.202060389.

35. Ghica, M.E.; Wintersteller, Y.; Brett, C.M.A. Poly(brilliant green)/carbon nanotube-modified carbon film electrodes and application as sensors. *J. Solid State Electrochem.* **2013**, *17*, 1571–1580, doi:10.1007/s10008-013-2040-4.

36. Raoof, J.B.; Chekin, F.; Ojani, R.; Barari, S.; Anbia, M.; Mandegarzad, S. Synthesis and characterization of ordered mesoporous carbon as electrocatalyst for simultaneous determination of epinephrine and acetaminophen. *J. Solid State Electrochem.* **2012**, *16*, 3753–3760, doi:10.1007/s10008-012-1807-3.

37. Yang, G.; Yu, L.; Jia, J.; Zhao, Z. 4-Aminobenzoic acid covalently modified glassy carbon electrode for sensing paracetamol at different temperatures. *J. Solid State Electrochem.* **2012**, *16*, 1363–1368, doi:10.1007/s10008-011-1529-y.

38. Habibi, B.; Jahanbakhshi, M.; Pournaghi-Azar, M.H. Differential pulse voltammetric simultaneous determination of acetaminophen and ascorbic acid using single-walled carbon nanotube-modified carbon-ceramic electrode. *Anal. Biochem.* **2011**, *411*, 167–175, doi:10.1016/j.ab.2011.01.005.

39. Rana, A.; Baig, N.; Saleh, T.A. Electrochemically pretreated carbon electrodes and their electroanalytical applications – A review. *J. Electroanal. Chem.* **2019**, *833*, 313–332, doi:10.1016/j.jelechem.2018.12.019.

40. Yun, T.G.; Sim, Y.; Lim, Y.; Kim, D.; An, J.S.; Lee, H.; Du, Y.; Chung, S.Y. Surface dissolution and amorphization of electrocatalysts during oxygen evolution reaction: Atomistic features and viewpoints. *Mater. Today* **2022**, *xxx*, doi:10.1016/j.mattod.2022.06.023.

41. Ghouri, Z.K.; Elsaid, K.; Badreldin, A.; Nasef, M.M.; Jusoh, N.W.C.; Abdel-Wahab, A. Enhanced oxygen evolution reaction on polyethyleneimine functionalized graphene oxide in alkaline medium. *Mol. Catal.* **2021**, *516*, 111960, doi:10.1016/j.mcat.2021.111960.

Chapter 4: Formation and Characterisation of a CS/GO-modified GCE and its Enantioselective Recognition of L & D Tyrosine

4.1 Introduction

In this chapter, results are presented and discussed on the development of an electrochemical chiral sensor. Chitosan was used as the chiral recognition component, while graphene was incorporated into the sensor to enhance its surface area and to provide a conducting pathway. The D and L enantiomers of tyrosine were used to test the performance of the chiral sensor.

4.2 Experimental

The apparatus and computer software employed during the experiments mentioned in this chapter are previously described in Chapter 2 under Section 2.4. All chemicals were supplied as Analar grade reagents from Sigma-Aldrich and were used without any further purification. All solutions were prepared fresh prior to each experiment. Like all previous experiments pH changes of solutions were carried out with diluted concentrations of HCl and NaOH, and all experiments were conducted at room temperature. A 3 mm glassy carbon electrode (GCE) rod was utilised in all experiments with this rod being encapsulated in epoxy resin and inserted into a Teflon based holder. A copper plate was located at the base of the carbon sample to enable electrical conductivity. Prior to each experiment the GCE was polished and sonicated using the methodology described again in Section 2.4. For the auxiliary electrode a platinum wire (Pt) was used and for the reference electrode a saturated calomel electrode (SCE) was employed during the voltammetry experiments. To analyse the surface of the CS/GO modified GCE and a Hitachi S-3200-N SEM was used whilst investigations into the combination of chitosan and graphene on the CS/GO modified GCE were conducted using a Varian FTS-7000 FTIR spectrometer containing a Pike Miracle ATR diamond, providing ATR-FTIR spectra. Samples were let completely air dry prior to any analysis.

For all cyclic voltammetry experiments a Solartron 1287 Potentiostat was also employed for potentiostatic measurements during the electrodeposition of CS. All the experiments were repeated for at least three times and the standard error ($SE = \rho/n^{1/2}$, where ρ is the standard deviation and n represents the number of repeated experiments) is shown as error bars on the relevant plots.

4.3 Formation of the Chitosan and Graphene Composite

In this section, the approach taken to form the chitosan and graphene composite is described together with the analysis of the resulting composite. In all these experiments an activated GCE electrode was employed. This activation, which was described in Chapter 3 in Section 3.3.1 explains how cycling the bare GCE in a phosphate buffer solution activates the GCE which causes an improvement in the electrochemical performance of the electrode. This activation is caused by changes in the microstructure of the GCE including the formation of new active edge planes and a graphite oxide layer ultimately enhancing adsorption sites of the GCE and therefore sensing ability also.

4.3.1 Electrodeposition of Graphene Nanoplatelets

Electrodeposition of graphene nanoplatelets was carried out using cyclic voltammetry by cycling the GCE electrode from 0.8 to –1.5 V (*vs. SCE*) in an aqueous dispersion of graphene nanoplatelets aided by the presence of 5 mM β-CD. There is clear evidence for the deposition of graphene nanoplatelets, as illustrated in **Fig. 4.1.** Graphene nanoplatelets become chemically modified during the oxidation step in the cyclic voltammetry method to become an altered form of graphene called graphene oxide (GO). The GO contains an array of oxygen functionalised moieties [1]. **Fig. 4.1(I)** shows a typical voltammogram where evidence for the formation of GO at the bare GCE is seen. An anodic or oxidation peak (a) and two smaller cathodic or reduction peaks, (b) and (c), are formed during the cycling process. The continual increase of the peak currents as the number of cycles increase, as depicted in **Fig 4.1(II)**, implies that the deposition of GO on the GCE surface has in fact been accomplished. The anodic peak (a) and the cathodic peak (b) can be attributed to a redox reaction between a pair of oxygen-containing functional groups present on the graphene plane that possess too much stability to become reduced by the means of cyclic voltammetry. The cathodic peak (c) is ascribed to the reduction of GO and this is an irreversible process [2].

Following deposition of the graphene nanoplatelets, the surface of the GCE was analysed using SEM and a typical micrograph is shown in **Fig. 4.2**. Here the presence of the graphene nanoplatelets is clearly shown and confirms that the GCE is modified successfully with the

nanoplatelets. While most of the surface is modified and reasonably uniform, there is some evidence of agglomeration of the graphene nanoplatelets.

(I) **(II)**

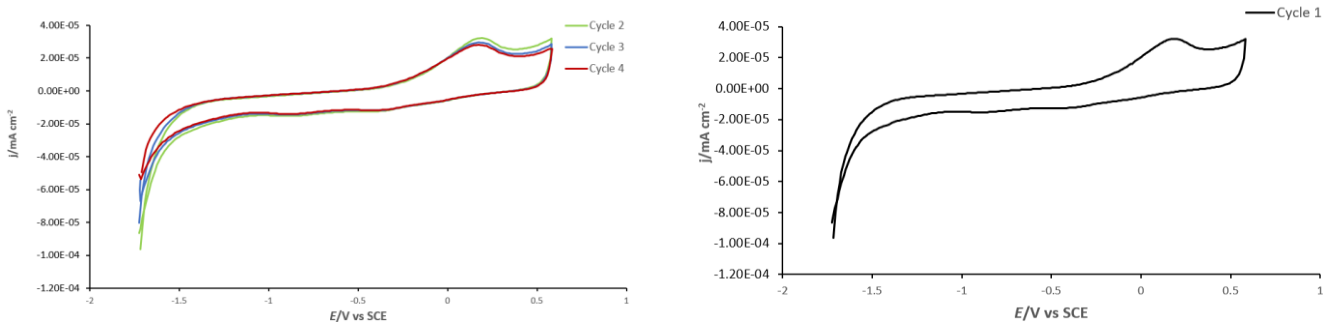

Figure 4.1: Cyclic voltammogram recorded at 50 mV s^{-1} cycled from 0.8 to –1.5 V for 5 cycles in graphene nanoplatelet solution dispersed in 5 mM β-CD solution **(I)** displaying cycle 1 and **(II)** displaying remaining cycles 2 to 4.

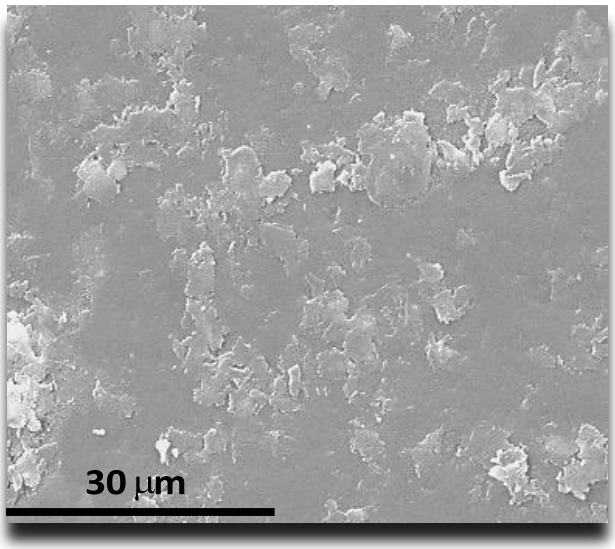

Figure 4.2: SEM micrograph of GCE following the formation of the graphene-modified surface, by cycling from 0.8 to –1.5 V at 50 mV s^{-1} for 10 cycles in the graphene nanoplatelet solution dispersed in 5 mM β-CD solution.

A cyclodextrin solution was used to disperse the graphene nanoplatelets as the use of β-CD can effectively inhibit the process of agglomeration of graphene, enabling individual graphene sheets to be deposited separately layer by layer during the cycling process. The introduction of β-CD as a dispersion solution results in a solution where graphene is more dispersed and consequently more likely to interact with the electrolyte in the electrochemical cell. The presence of β-CD can also act as a bridge which increases the strength of binding interactions between nanoparticles, such as the graphene nanoplatelets, and the glassy carbon surface [3]. In addition, graphene-based materials also possess a high tendency to agglomerate when in contact with polymers due to their large surface area, and as the chitosan hydrogel polymer is deposited after the GO, both the GO and the polymer will unavoidably come in contact within the analyte solution. To tackle this second potential agglomeration phenomenon, the functionalization of the graphene nanoplatelets to form a graphene oxide-like material is ideal. The presence of functional groups, to be exact the oxygen-containing groups, help graphene remain dispersed in the solvent medium, this being the analyte solution [4].

4.3.2 Chitosan Electrodeposition

The electrodeposition of chitosan was achieved through potentiostatic experiments, and the corresponding data are contained in **Fig. 4.3**. In these experiments a constant potential of -1.5 V (*vs. SCE*) was employed to a GCE electrode immersed in a solution of chitosan. On application of the potential, there is an increase in the reduction current and the current continues to increase over a 50 s period. At longer times, the cathodic current begins to decrease. At the end of the 5 min period, the chitosan hydrogel was clearly visible at the GCE.

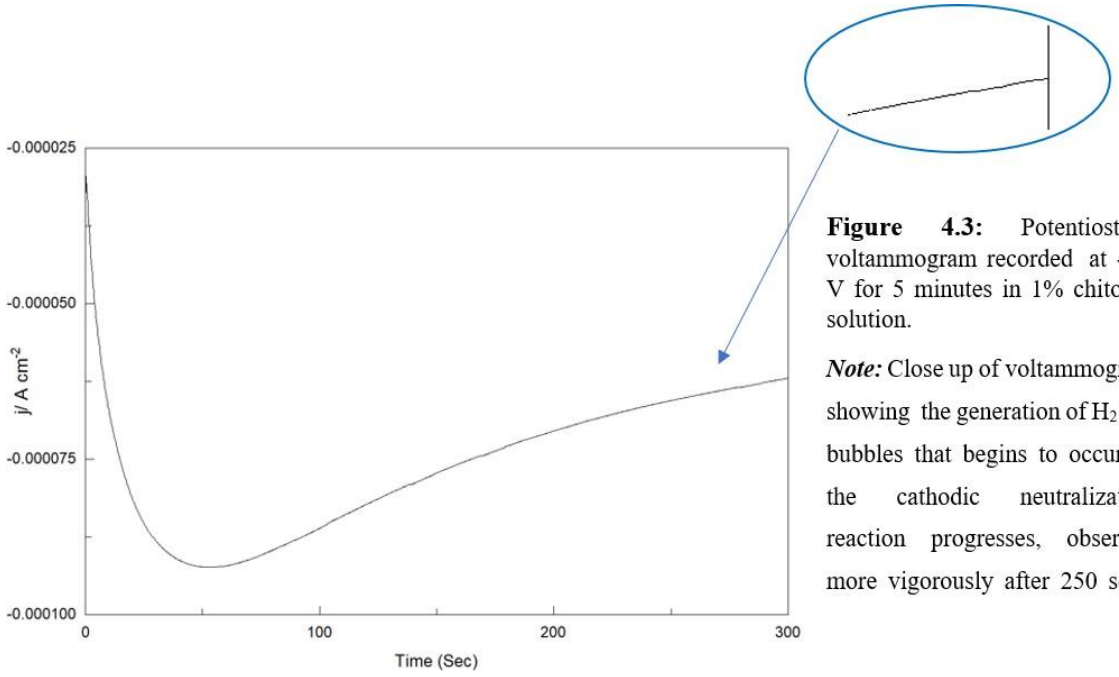

Figure 4.3: Potentiostatic voltammogram recorded at -1.5 V for 5 minutes in 1% chitosan solution.

Note: Close up of voltammogram showing the generation of H_2 gas bubbles that begins to occur as the cathodic neutralization reaction progresses, observed more vigorously after 250 secs.

Chitosan is soluble in slightly acidic media typically with a pH below 6.0–6.5. In this study chitosan was dissolved in an acetic acid solution with an approximate pH value of 3.0. In low pH environments the amino groups of chitosan become protonated resulting in the formation of polymer chains that possess a positive charge. During the electrodeposition process, the reaction given in **Equation 4.1** occurs at the cathode surface which in fact is the surface of the electrode [5,6] to give rise to a pH increase at the electrode solution interface.

$$2H_2O + 2e^- \rightarrow H_2 + 2OH^-. \qquad 4.1$$

As the reaction occurs the acetic acid becomes deprotonated and the pH changes from 3.0 to around 6.0 causing a pH gradient concentrated at a region close to the cathode surface. The pH gradient induces the transition of the chitosan's polymer chains in solution to a more gel-like formation or hydrogel. This reaction then results in the neutralization reaction of the chitosan chains that possess a positive charge. Therefore, the chitosan neutral molecules adjacent to the surface of the cathode become deposited as a chitosan hydrogel on the electrode surface [5,6].

$$Chit - NH_3^+ + OH^- \rightarrow Chit - NH_2 + H_2O. \qquad 4.2$$

It can also be noted that the reaction above in Equation 4.2 produces H_2 gas molecules which exist as gas bubbles during the electrodeposition. The generation of these H_2 bubbles appear as what is referred to as 'noise' during the electrochemical process which visually manifests as a jagged region on the current-time plot [5].

4.3.3 ATR-FTIR Analysis

FTIR studies were performed on chitosan powder, CS-GCE, which represents the electrodeposited chitosan, and a GO/CS-GCE, where the chitosan was electrodeposited at the graphene modified GCE. **Fig. 4.4** shows the FTIR spectra of these three samples collected in the wavenumber range of 4000 – 500 cm^{-1}, while the data are summarised in **Table 4.1**. The pure chitosan powder displays characteristic peaks of the chitosan molecule, as to be expected. The peak of chitosan at 3287 cm^{-1} can be attributed to the stretching vibrations of the OH groups which is overlapped by N-H stretching vibrations also located at that wavenumber. The band located at 2875 cm^{-1} corresponds to the CH_2 symmetrical and asymmetrical stretching vibrations of the chitosan polysaccharide. The peak at 1653 cm^{-1} is the primary amide band, signalling the stretching of a C=O group that is hydrogen bonded to a N-H group of the adjacent intra-sheet chain, with a secondary amide peak is seen at 1580 cm^{-1}. A third amide group band is also present at 1313 cm^{-1}, this peak representing the C-N stretching of this amide group. The vibrations at 1149 cm^{-1} can be attributed to the anti-symmetrical bridge of C-O-C stretching and the in-plane anti-symmetric stretching, whilst the peak at 1026 cm^{-1} corresponds to C-O stretching of the polymer [7,8]. The FTIR spectra of the CS-film electrodeposition onto the GCE (CS-GCE) presented with peaks of a greater intensity primarily in the vicinity of 1550 – 1660 cm^{-1} and in the region from 1300 – 1380 cm^{-1}, when compared to the spectra of the chitosan powder. As the CS-GCE film was fabricated in an acetic acid solution, these regions correspond to the protonation of amides and amines. It can also be noted that there is a minuscule displacement of chitosan feature peaks which may suggest interactions of the polymer's amine groups with the carbonyl groups from the acidic solvent. It has been reported that this displacement can be attributed to the hydrogen bonding between the two functional groups [9]. The FTIR spectra of GO-CS film portrays a mixture of chitosan and GO peaks indicating interactions occurred between chitosan and GO. The board band located at 3287 cm^{-1} can be assigned to a mixture of the amine stretch from chitosan to the OH groups in GO.

The peak at 1063 cm^{-1} corresponds to the C-O-C stretching vibrations, whilst the peak at 1648 cm^{-1} relates to the presence of COOH groups from GO and is downshifted by hydrogen bonding between GO and the ring of chitosan. The peak located at the region of 1560 cm^{-1} is ascribed to the presence of C=C groups from GO and also represents the N-H bonding present in chitosan, the 1407 cm^{-1} peak is assigned to N-H stretching [10].

Table 4.1: Wavenumber and peak assignments for chitosan powder, CS-GCE film and CS/GO-GCE film.

Chitosan Powder **WN (cm^{-1})**	**Assignment**	***CS-GCE Film*** **WN (cm^{-1})**	**Assignment**	***CS-GO Film*** **WN (cm^{-1})**	**Assignment**
3287	N-H , O-H stretching	**3355**	N-H, O-H stretching	**3287**	N-H, O-H stretching
2875	-CH_2 stretching	**2323**	-CH_2 stretching	**2323**	CH_2 stretching
1653	Amide (I)	**2204**	Protonated Amide (I)	**1063**	C-O-C stretching
1580	Amide (II)	**2161**	Protonated Amide (II)	**1407**	N-H stretching
1375	-CH_2 bending	**2025**	Protonated Amide (III)	**1560**	C=C group
1313	Amide (III) (C-N stretching)	**1980**	Protonated Amide (III)	**1648**	C=O group
1149	C-O-C stretching	**1654**	C-O-C stretching		
1027	C-O stretching	**1560**	C-O stretching		

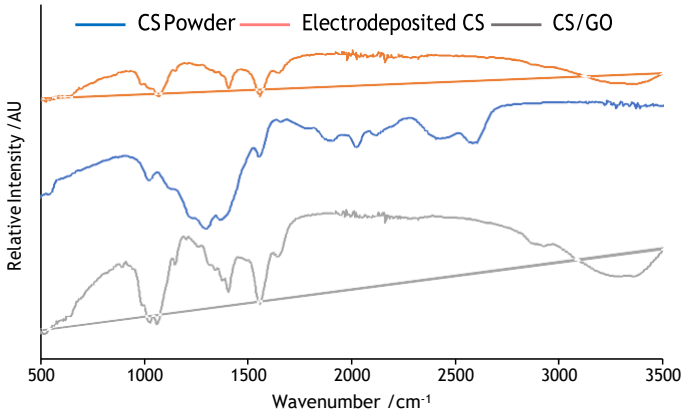

Figure 4.4: FTIR spectra of chitosan powder, electrodeposited chitosan and electrodeposited chitosan with graphene nanoplatelets in the wavenumber region of 3500 – 500 cm^{-1}.

4.3.4 Conductivity Analysis

Information on the conductivity of the materials employed in the fabrication of the chitosan and graphene composite was obtained using potassium ferrocyanide (5 mM $Fe(CN)_6^{3-/4-}$) as an electrochemical probe in 0.1 M NaCl. As depicted from the CV presented in **Fig. 4.5**, the conversion of $Fe(CN)_6^{4-}$ to $Fe(CN)_6^{3-}$ is seen at potentials in the vicinity of 0.10 V to 0.25 V (*vs*. SCE), while the corresponding reduction wave is evident at potentials from 0.0 V to 0.10 (*vs*. SCE). On comparing these voltammograms, it can be seen that the greatest level of conductivity is achieved with the activated GCE that has been modified with GO (GO/GCE). The highest peak current was observed at 0.2 V (*vs*. SCE) with this modified electrode. However, there is only a miniscule peak current difference between the activated GO/GCE and the activated GCE with almost identical voltammograms being observed for both, implying that the activation of the GCE plays an important role in the conductivity of the sensor. Interestingly, both the activated GCE and the activated GCE modified with the graphene nanoplatelets have higher background currents, which are associated with the higher capacitance of these two electrodes.

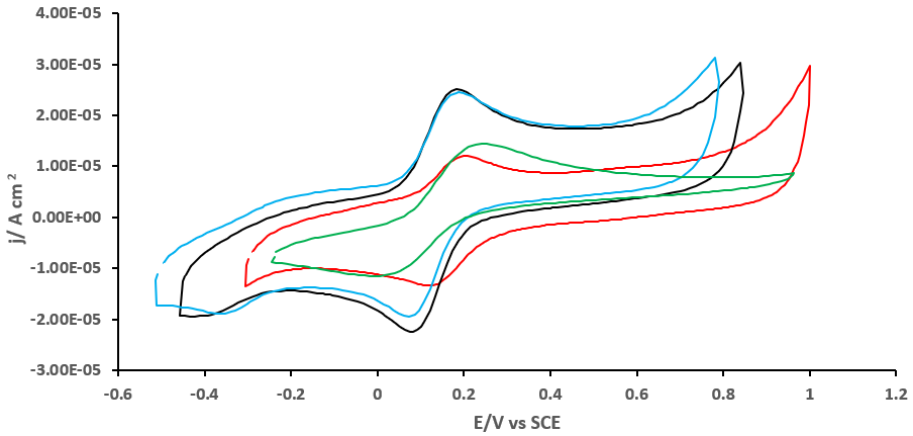

Figure 4.5: Cyclic voltammetry recorded at 50 mV s^{-1} cycled from –0.3 to 1.0 V for 5 cycles displaying cycle 2 in 2 mM $K_4Fe(CN)_6.3H_2O$ solution dissolved in 0.1 M NaCl for **(black)** activated GO/GCE, (red) un-activated bare GCE, (blue) activated GCE and (green) for the CS/GO/GCE.

As discussed in Chapter 3 the GCE is readily activated with this activation accompanied by microstructural changes of the carbon-based electrode surface, such as the formation of new active edge planes and the formation of a graphite oxide layer containing a vast quantity of oxidising groups. The presence of various oxygen-containing functional groups (OFGs) is understood to affect the physiochemical properties such as conductivity of the electrode materials and play a key role in regulating the electrochemical performance of the sensor. However, the underlying mechanism in which OFGs have this effect on conductivity is not entirely understood [11]. During cyclic voltammetry high electrochemical performance of the sensor can be accomplished only if the electronic conductivity is good, which requires the integrity of the sp^2 network to remain unchanged. Many studies examining the relationship between conductivity and OFGs on carbon materials started from a predefined carbon material that is then oxidised. In these scenarios the oxygen atoms present in these groups react with defective regions mainly located at the graphitic oxide edges, and do not disrupt the conjugation of the system and good conductivity is achieved. Such studies are in agreement with the conductivity findings of this study, as following activation OFGs such as hydroxyl, carbonyl and epoxide exist in the edge of the graphitic material non-distributive of the configuration of the system, maintaining a high level of conductivity which can be accounted for by the high peak current seen for the activated GCE.

In contrast, some studies report a decrease in conductivity following oxygen introduction to a carbon material, however this is believed to occur when OFGs exist primarily in the basal plane instead of plane edges following oxidation, leading to a disruption in the network's conjugation [12]. For the activated GO/GCE the addition of a GO does not necessarily increase conductivity as GO displays low levels of conductivity due to its highly disrupted π-system. However, the abundance of OFGs supply GO with an inherent redox activity caused by the fact that some OFGs can be reduced and electrochemically regenerated during an electrochemical process such a cyclic voltammetry [13]. The peak current seen for the activated GO/GCE at about 0.2 V (*vs*. SCE) is only slightly higher in peak current the activated GCE, with this slight increase ascribed to the OFGs acting as signal carries for the redox reaction at the electrode interface where a faster rate of electron transfer is occurring. A much lower peak current is observed for the bare GCE with a peak potential of about at 0.26 V (*vs*. SCE). The absence of OFGs from this un-activated and unmodified GCE result in a decrease in electroactive redox reactions visualised by the dramatic fall in peak current. Interestingly, the CS/GO/GCE-modified electrode has the lowest peak current, implying that the introduction of chitosan to the sensor

results in a significant reduction in the rate of oxidation of the $Fe(CN)_6^{4-}$ to $Fe(CN)_6^{3-}$. The chitosan hydrogel layer will have a significant effect on the diffusion of the $Fe(CN)_6^{4-}$ to the electrode interface and this is consistent with the considerable reduction in the peak current for the CS/GO/GCE-modified electrode The peak potentials, and peak separation are summarised in **Table 4.2**, where it is again evident that the activated GCE and activated GCE/GO have small peak separations, but a much higher peak separation is evident with the added chitosan.

Table 4.2: Summarised peak potentials and peak separation between various experimental steps corresponding to the above cyclic voltammogram.

Electrode	*Ep (Ox) V (vs. SCE)*	*Ep (Red) V (vs. SCE)*	*ΔE_p /mV*
AGCE	0.187	0.074	0.113
Unactivated GCE	0.199	0.123	0.075
CS/GO AGCE	0.240	0.017	0.223
GO AGCE	0.183	0.075	0.108

4.4 Development of the Chitosan and Graphene Composite as a Chiral Sensor

In order to optimise the chitosan and graphene composite to differentiate between the D and L enantiomers of tyrosine (Tyr), a number of parameters were varied and these are now described in turn.

4.4.1 Effect of Chitosan and Solvent Concentration

The effects of chitosan and the solvent (acid) concentration on the hydrogel's enantioseparation ability were analysed, using cyclic voltammetry. In these studies, the GCE was activated and then electrodeposition was employed to give the chitosan hydrogel at the activated GCE electrode. The GO was not added during these initial experiments, with the aim of developing an understanding of the chitosan formulation (chitosan and acid content). Two concentrations

of chitosan solutions were prepared for the formation of the hydrogel, 1% and 2% wt. chitosan solutions, formed by the dissolution of chitosan in an acetic acid aqueous solution. Literature findings concluded that optimum dissolution of chitosan and an ideal diffusion environment for target molecules was achieved typically at these concentrations. It has also been reported that at concentrations higher than 2% it is not possible to obtain a good dissolution of chitosan in solution [14].

Firstly, the effect of the chitosan concentration was investigated, this was carried out by preparing a 1% and 2% chitosan solution, both dissolved in 0.2 M CH_3COOH. A typical CV showing the data recorded at the chitosan modified GCE in 1 mM L-Tyr and D-Tyr dissolved in a pH 7.0 phosphate buffer and recorded at 50 mV s^{-1} by cycling between 0.1 and 1.1 V is shown in **Fig. 4.6**. Here it is seen that the electrodeposited chitosan has only a slight effect on the discrimination of the two enantiomers, with the peak currents and potentials being similar for both the L-Tyr or D-Tyr. These data are summarised in **Table 4.3**, where the average peak separation is shown as a function of the chitosan concentration.

From **Table 4.3** it is evident that the 1% chitosan solution in 0.2 M CH_3COOH yielded a somewhat better enantioseparation result with a peak separation of 9.0 ± 6.3 mV when compared to the 2% value of 5.0 ± 6.1 mV. This can be accounted for by the fact that tyrosine is one of the largest amino acids to exist with a molecular mass of 181.19 Da, just slightly smaller than the largest amino acid of all tryptophan (204 Da). The diffusion of a large amino acid like tyrosine through the mesh size of the chitosan network is undoubtedly affected by an increase in the polymer content. An increase in the chitosan polymer content, with the 2% chitosan solution, results in a larger amount of self-crosslinking of the polymer chains which in turn causes a decrease in the mesh size of the hydrogel [15], with the mesh size referring to the distance between two crosslinked chains [16]. The smaller mesh size makes it increasingly more difficult for tyrosine molecules to diffuse through the hydrogel for detection and the greater degree of chain entanglement/crosslinking sees the solution become more viscous in nature. With increased viscosity, fewer mobile ions can move through the thick hydrogel to carry the electrical charge during the electrochemical process [17]. The lower concentration of tyrosine molecules at the electrode interface and the decreased conductivity of the cell as a result of the increase to 2% chitosan, results in an insufficient interaction of target molecules with the chitosan hydrogel, leading to a decrease in enantioseparation of the sensor when compared to the 1% solution. Moreover, it is clearly evident in **Table 4.3** that there is an increase in the peak potential on comparing the 1% and 2% chitosan solutions. The peak

potential of the L-Tyr is shifted from 584 mV to 609 mV (vs. SCE) giving a 25 mV increase in the peak potential. A similar shift of 20 mV is evident with the D-Tyr on increasing the chitosan concentration to 2%.

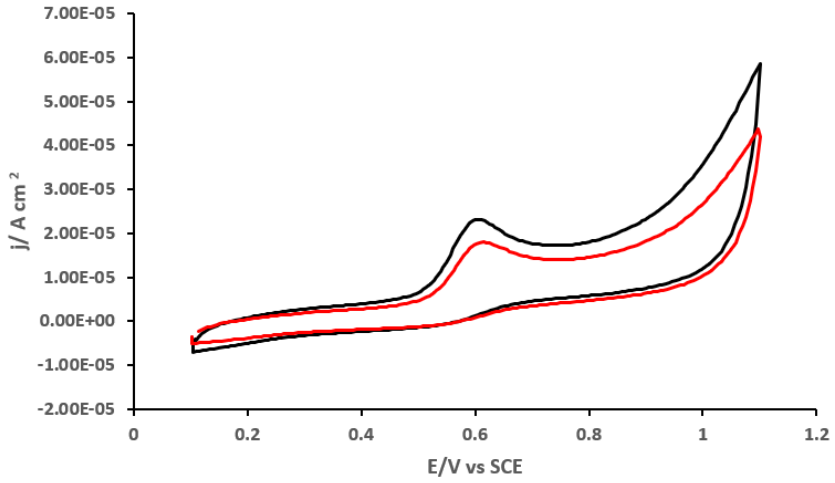

Figure 4.6: Cyclic voltammogram recorded at 50 mV s^{-1} cycled between 1.0 and 1.1 V for 5 cycles in (red) 1mM tyrosine and **(black)** 1mM tyrosine. CV displays a set of L and D data from the table below i.e., 1% wt. CS (CH_3COOH 0.2M) example.

Table 4.3: Chitosan (CS) and solvent concentration analysis data measured using cyclic voltammetry recorded at 50 mV s^{-1} cycled between 0.1 and 1.1 V for 5 cycles in 1 mM L-Tyr or D-Tyr dissolved in a pH 7.0 phosphate buffer. All data given is an average of three values.

Condition	L-Tyr E_p *V (vs. SCE)*	D-Tyr E_p *V (vs. SCE)*	Pot. Difference ΔE_p */V*
1% wt. CS (CH_3COOH 0.2 M)	0.584 ± 0.001	0.592 ± 0.008	0.009 ± 0.006
2% wt. CS (CH_3COOH 0.2 M)	0.609 ± 0.010	0.612 ± 0.019	0.005 ± 0.006
1% wt. CS (CH_3COOH 0.5 M)	0.608 ± 0.007	0.609 ± 0.004	0.004 ± 0.001

Next, the solvent (acid) concentration was analysed, this was examined by comparing two 1% chitosan solutions, one dissolved in a 0.2 M CH_3COOH and the other in 0.5 M CH_3COOH. It can be noted from **Table 4.3** that there is a decrease in enantioseparation with the 0.5 M

CH_3COOH in comparison to the 0.2 M CH_3COOH (both with 1% chitosan). Typically, a higher acid concentration would result in an increase in the reduction in the viscosity of the chitosan solution. This is due to the positively charged chitosan ions becoming neutralised by the high concentration of negative ions in solution, which in turn causes a conformational change where the coil formation of the polymer becomes more compact, lowering viscosity [18,19]. With decreased viscosity a more sufficient interaction between the amino groups of the hydrogel and the tyrosine molecules would occur and give rise to a somewhat higher enantioseparation. Interestingly enough, this was not the case in this study, as for the 0.5 M CH_3COOH a decrease in enantioseparation values was measured. This decrease could be accounted for by the fact that at certain high concentrations acid hydrolysis of chitosan can occur, causing degradation of chitosan. However, hydrolysis of this nature typically occurs at acidic solvent concentrations greater than 0.5 M.

Based on these measurements, a 1% solution of chitosan dissolved in 0.1 M CH_3COOH was chosen for all subsequent experiments.

4.4.2 The Effects of Adding Graphene to the Electrodeposited Chitosan

Although there is evidence of chiral recognition in the data presented in **Table 4.3**, the peak separation between the D and L tyrosine is low, reaching only a maximum of 9 m V. Therefore, the graphene nanoplatelets were added in an attempt to increase these peak separations.

4.4.2.1 Scan Rate Studies

Initially, scan rate studies were performed using 5 mM $Fe(CN)_6^{3-/4-}$ and then the study was extended to L-Tyr to determine if the oxidation of the analytes were under adsorption or diffusion control at the CS/GO-GCE. The data recorded in 5 mM $Fe(CN)_6^{3-/4-}$ is shown in **Fig. 4.7**, where it is seen that the current increases with increasing scan rate, with the oxidation peak potentials in the vicinity of 0.2 V (*vs.* SCE) and the reduction waves centered at about 0.1 V (*vs.* SCE). There is no significant increase in the peak potential with increasing scan rates,

suggesting efficient oxidation and reduction of the ferricyanide redox probe at the CS/GO-GCE. The relationship between the scan rate and the oxidation peak current at the CS/GO-GCE is displayed in **Fig 4.8(a).** A near linear relationship is observed. The linear regression equation of the sensor was deduced as y = 0.0003x + 0.0051 with a R^2 value of 0.78, where y is the peak current and x is the scan rate. The relationship between the logarithm of the oxidation peak current and the logarithm of the scan rate was also analysed, with the slope value of the plot measured as 0.77, as illustrated in **Fig 4.8(b).** As the slope value of 0.77 deviates from the ideal value of 1.0 for a surface or adsorption-controlled process and also deviates from the ideal value of 0.5 for that of a diffusion-controlled process, the redox reactions of the ferricyanide probe is said to be governed by a mixed adsorption-diffusion controlled process at the CS/GO-GCE.

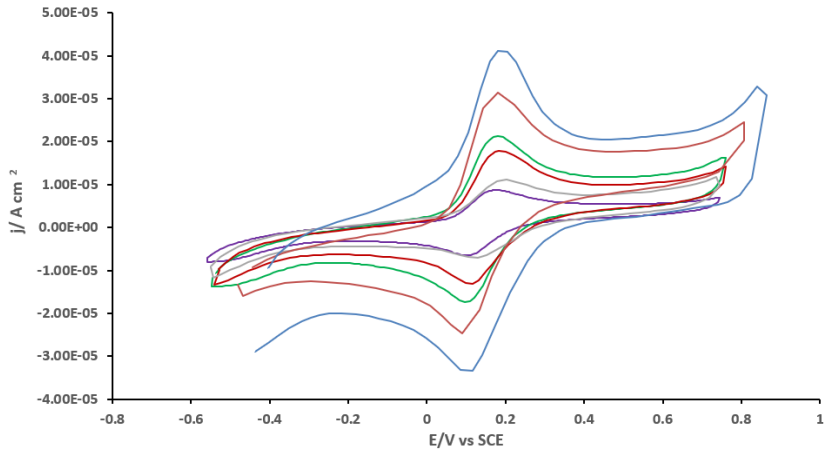

Figure 4.7: Cyclic voltammogram displaying various scan rate studies recorded from 150 mV s^{-1} to 25 mV s^{-1} between –0.3 and 1.0 V (*vs.* SCE) in 0.1 M NaCl with 5.0 mM $Fe(CN)_6^{3-/4-}$ using the CS/GO-modified GCE.

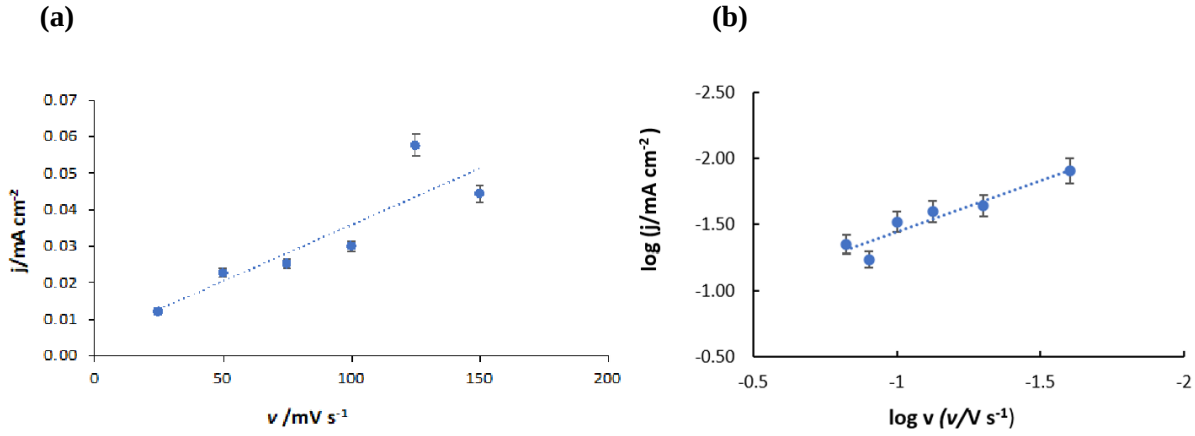

Figure 4.8: (a) Plot of peak current as a function of scan rate and **(b)** logarithm of peak current as a function of the logarithm of scan rate, recorded in 5.0 mM $Fe(CN)_6^{3-/4-}$ and 0.1 M NaCl using the CS/GO-modified GCE.

The overall rate of the adsorption process for an adsorption-diffusion controlled reaction is limited by both phenomena i.e., diffusion from the bulk to the sublayer and adsorption at the interface. In this case, the rates of both phenomena is a mixed kinetic process with no one single rate-determining step [20].

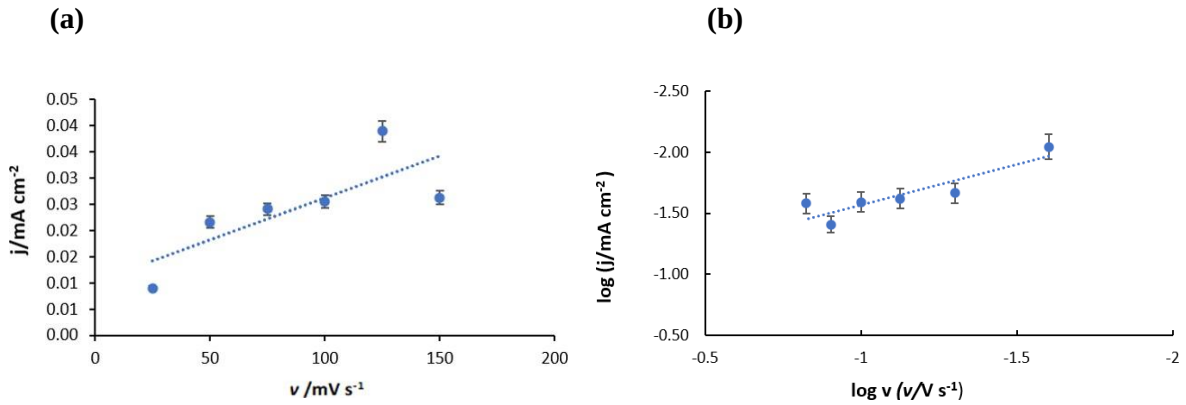

Figure 4.9: (a) Plot of peak current as a function of scan rate and **(b)** logarithm of peak current as a function of the logarithm of scan rate, recorded in 1 mM L-Tyrosine using the CS/GO-modified GCE.

The relationship between the scan rate and the oxidation peak current at the CS/GO-GCE tested in the analyte L-tyrosine is displayed in **Fig 4.9(a).** There is a general linear relationship observed. The linear regression equation was deduced as $y = 0.0002x + 0.0103$ with an R^2 value of 0.6053, where y is the peak current and x is the scan rate, indicating a rather poor linear relationship. The relationship between the logarithm of the oxidation peak current and the logarithm of the scan rate was too analysed, with the slope value of the plot calculated to be 0.65, as illustrated in **Fig 4.9(b).** As the slope value of 0.65 deviates from the ideal value of 1.0 for a surface or adsorption-controlled process and is closer to the ideal value of 0.5 for a diffusion-controlled process, the oxidation of tyrosine is said to be under a diffusion-controlled process at the CS/GO-GCE.

4.4.2.2 The Influence of a Supporting Electrolyte during the electrodeposition of chitosan at the GO/GCE

The ideal supporting electrolyte used in electrochemical measurements will increase the conductivity of a solution by providing the solution with additional ions to transport more charge. In an attempt to increase the enantioseparation of the L-Tyr and D-Tyr, the effect of

different types of supporting electrolytes in the formation of GO/CS/GCE was studied. The supporting salts examined were potassium chloride (KCl) and sodium chloride (NaCl), the quantity of salt used was also examined. The supporting salts were employed in the preparation of the chitosan hydrogel solution. Chitosan is a non-conductive material [21] so the addition of electrolyte ions is paramount for the electrodeposition of chitosan onto the GCE surface.

The results obtained from this study are summarised in **Table 4.4.** The greatest enantioseparation measured in terms of potential difference between the two enantiomers, was achieved with the addition of 0.5 g of KCl, as seen in **Table 4.4.** Both KCl and NaCl are strong electrolytes as they dissociate completely in solution into their constituent ions, for KCl being K^+ and Cl^- ions and NaCl into Na^+ and Cl^-. The preparation of the hydrogel sees the chitosan dissolved in an acetic acid solution, which is a polar solvent. The addition of a polar supporting electrolyte salt dissolved into this polar medium or solvent will result in a greater dissociation of ions of the electrolyte, therefore leading to an increase in conductivity and electrochemical performance. It is well known that KCl has a higher mobility than NaCl, which is related to the size of the hydrated K^+ and Na^+ cations. Consequently, KCl displays better electrical conductivity in solution which leads to a greater flow of charge within the electrochemical cell enhancing the precipitation of chitosan at the GO modified GCE by promoting the reaction descripted in **Equation 2**. Indeed, one study investigating the effect of KCl and NaCl as supporting electrolytes in a water-soluble polymer system, found KCl to possess greater conducting capability than NaCl due to a higher extent of solvation of NaCl in solution in comparison to KCl [21].

It can be seen from **Table 4.4** that the addition of 0.5 g KCl provides a suitable number of ions to enhance conductivity during the formation of the CS/GO/GCE, and the subsequent enantiomer separation. However, a greater quantity of salt resulted in a decreased enantiomer potential difference as observed for the 1.0 g and 1.25 g of both KCl and NaCl. The higher salt concentrations may alter the structure of the electrodeposited chitosan possibly leading to crosslinking and this is turn may affect the enantioselectivity of the CS/GO/GCE.

Table 4.4: Data collected from cyclic voltammetry recorded at 50 mV s^{-1}, cycled between 1.0 to –1.0 V for 5 cycles in 1 mM L-Tyr and D-Tyr solution, displaying the difference in potential for the L and D tyrosine enantiomers. All data is an average of three different experiments.

Supporting Electrolyte		E_p V (*vs.* SCE)		ΔE_p /mV
Salt	g (in 10 mL of CS)	L-Tyr	D-Tyr	
NaCl	0.25	0.676 ± 0.001	0.681 ± 0.001	5.5 ± 1.5
NaCl	0.50	0.676 ± 0.003	0.682 ± 0.007	9.1 ± 3.7
NaCl	1.00	0.662 ± 0.003	0.665 ± 0.001	1.3 ± 0.8
NaCl	1.25	0.677 ± 0.001	0.681 ± 0.001	4.6 ± 0.7
KCl	0.50	0.670 ± 0.004	0.680 ± 0.009	10 ± 7.5
KCl	1.00	0.676 ± 0.004	0.675 ± 0.007	4.1 ± 5.6
KCl	1.25	0.685 ± 0.001	0.689 ± 0.001	2.5 ± 0.7

4.4.2.3 Time Sensitivity of the L & D Tyrosine Diffusion into the Hydrogel

While the addition of supporting electrolyte can enhance the enantioselectivity, the maximum peak separation is 10 mV. Aiming to increase this peak separation further, or alter the peak currents, the CS/GO/GCE was immersed in the L- and D-Tyr for different periods of time to enable a greater interaction between the amino acid and the CS. In all the previous sections, once the CS/GO/GCE was formed it was immersed in the phosphate buffer with the amino acid and the experiments were carried out immediately. The influence of the immersion period on the peak current is illustrated in **Fig 4.10(a) and (b)** and peak potential separation values for the L- and D-Tyr enantiomers are given in **Table 4.5.** It can be observed from **Fig 4.10(a)** that a gradual increase in peak current was recorded up until approximately 17 min for the D enantiomer, where after this point a gradual decrease can be seen. Therefore, optimal levels of detection were recorded once the CS/GO - modified GCE was left to sit in the D Tyr solution for 17 min prior to carrying out cyclic voltammetry on that analyte solution. During this waiting time tyrosine molecules have more time to diffuse from the bulk solution into the hydrogel film. The nature of the hydrogel is thick, elastic and viscous due to the self-crosslinking present during formation [22] meaning diffusion into the material would most likely require a certain

amount of time. The gradual decrease in peak current after the 17 min period can be attributed to the fact that the hydrogel becomes heavier as it is exposed for longer periods of time to the electrolyte. Indeed, the hydrogel begins to peel off and separate from the surface of the GCE after long immersion periods (typically over 17 min).

Fig 4.10(b) illustrates the L enantiomer results, tested using an identical experimental methodology and time periods as the D enantiomer. Similar findings were observed and the optimal immersion period was determined at 20 min, deviating from the D enantiomer time of 17 min. From the literature the diffusion of the tyrosine molecules into the hydrogel matrix is believed to be a time dependent or time sensitive process. Diffusion of a solute within a hydrogel is affected by the existence of polymer chains, in which they create a network with open spaces in-between the chains. The dimension of these spaces is referred to as the 'mesh size' of the network and cavity sizes vary from nano to microscopic [23]. It is these crevices filled with aqueous solution that the tyrosine molecules must diffuse through, and as they can be rather tiny cervices in size contained within a crosslinked network of larger polymer chains, the rate of the diffusion process is ultimately altered. Therefore, when dealing with hydrogel materials optimum sensing ability for the target molecules can be accomplished once the diffusion process is given a suitable time to occur prior to electrochemical detection using the modified electrode.

Interestingly, as evident in **Fig. 4.10**, there is a significant different of the peak currents for both the L and D enantiomers. The peak current after a 20-min immersion period is 24.4 μA for the L enantiomer and 19.2 μA for the D enantiomer to give a ratio of I_L/I_D of 1.27 which compares very favourably with literature values [24][25].

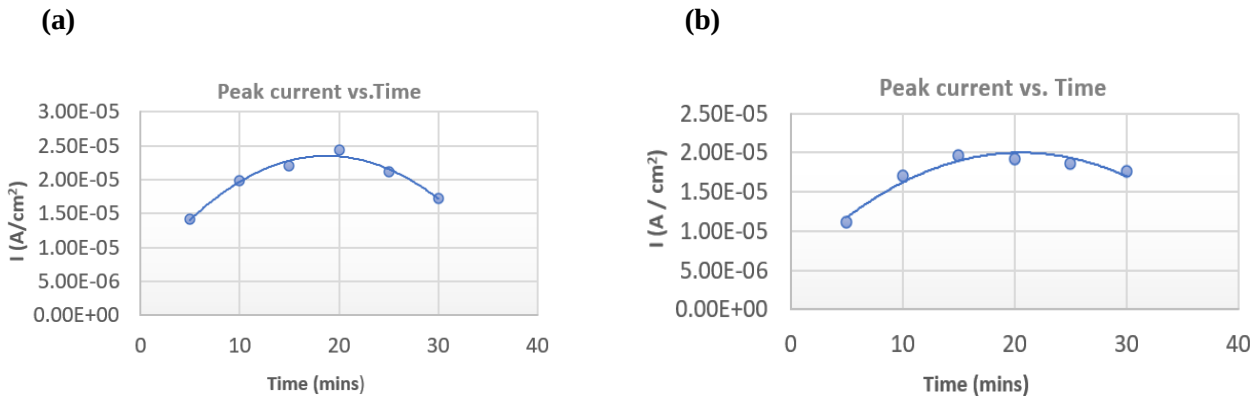

Figure 4.10: Time sensitive diffusion of tyrosine into the hydrogel matrix for **(a)** L enantiomer and **(b)** D enantiomer displaying the influence of the immersion period of peak current.

	ΔE_p /mV	*Ip*(L-Try)/*Ip*(D-Try)
CS/GO-GCE (17 mins immersion time)	163	1.45
	221	1.33
	80	1.56

Table 4.5: CV data displaying peak potential separation values between the L-Tyr and D-Tyr. CV recorded at 50 mV s^{-1} cycled from 0.1 to 1.1 V for 5 cycles each for 1mM D-Tyr and L-Tyr.

Fig 4.11 shows the analysis of the enantio-separation of the L and D tyrosine enantiomers with the GO/CS-modified electrode, conducted using cyclic voltammetry. The CV illustrates an example of achieved enantioseparation between the two enantiomers in which the enantiomers oxidise at different potentials. As seen from the CV, L-tyrosine had a large cathodic peak estimated at 0.8 V (*vs*. SCE) whereas the D-enantiomer had a smaller oxidised signal at about 0.85 V (*vs*. SCE). This increased potential separation of the two enantiomers was accomplished due to the longer immersion periods. However, as shown in **Table 4.5** there is considerable variations in the peak separations, indicating different extents of diffusion of the D- and L-Tyr throughout the chitosan hydrogel.

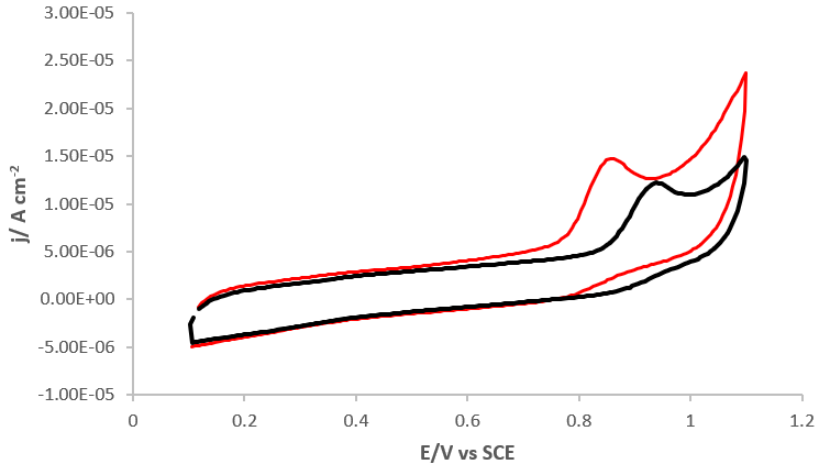

Figure 4.11: Cyclic voltammetry recorded at 50 mV s^{-1} cycled from 0.1 to 1.1 V for 5 cycles in 1mM D-tyrosine solution **(black)** and in a 1Mm L-tyrosine solution (red).

The chitosan hydrogel was formed through self-crosslinking as discussed in Section 1.3.3 and is therefore a self-assembled helical structure in solution. Chitosan is a natural chiral polymer and typically molecular chirality can shift to supramolecular chirality in such self-assembled formations, retaining characteristics of molecular chirality mainly through hydrogen bonding, π-π stacking and electrostatic interactions [26]. It is clear from all the results presented that the chitosan hydrogel has a higher binding affinity towards L-Tyr than D-Tyr. The binding interaction between the hydrogel and the L enantiomer occurs at a lower potential, indicating that the interaction with L-Tyr is more thermodynamically favoured by the modified electrode, hence preferential binding towards L-Tyr was observed and enantioselectivity achieved. Furthermore, the higher peak currents observed during the immersion experiments in the presence of L-Tyr, **Fig. 4.10**, suggest that higher quantities of L-Tyr are bound within the CS/GO/GCE, which is again consistent with the same findings, that L-Tyr is preferentially bound by the hydrogel.

Enantiomer recognition is mainly achieved through non-covalent interactions between the solute and the active site i.e., between the amino acid and complementary regions covalently bound to the polymer system. The self-binding interactions within the hydrogel network itself are composed mainly of hydrogen bonds and the non-covalent binding that occurs between tyrosine molecules and the hydrogel can be attributed to short range hydrogen bonding and π-π interactions. These short-range directional interactions are believed to be responsible for stereoselective binding. Moreover, steric hindrance that results from the spatial arrangement of the binding region or active site is thought to contribute to chiral recognition also. Furthermore, the swelling of the hydrogel can be triggered by the concentration of bound effector or guest molecules [27,28]. As the hydrogel binds more favourably towards L-Try a greater number of L-Tyr molecules will adsorb at the surface. This increase in effector molecule concentration triggers a larger swelling phenomenon of the hydrogel and consequently more L-Tyr molecules can diffuse into the hydrogel for detection. This phenomenon can account for the larger peak currents observed for L-Try when compared to the lower peak current seen for D-Try, **Fig. 4.8**. Natural polymers such as chitosan have previously been reported to display greater binding towards L enantiomers of amino acids, for example Takara et al. [28] examined the adsorption of tyrosine onto chitosan films and concluded that a higher affinity for the L-Tyr was achieved by the chirality of the chitosan. Another study using similar materials to this study, developed a chiral sensor based on a type of multiwalled carbon nanotubes (MWCNTs) and a modified

chitosan material which led to the modified GCE displaying a preferential combination with L tryptophan over D tryptophan [29].

4.4.2.4 Reusability of the GO/CS-modified GCE Sensor

The reusability of the sensor was investigated using cyclic voltammetry as seen by the voltammogram in **Fig 4.12**, with reusability referring to the number of consecutive analyses that can be conducted using one electrode [30]. For reusability analysis of the GO/CS-modified GCE, the sensor was developed following the usual experimental steps, such as GCE activation, GO electrodeposition and CS electrodeposition and then tested in a solution of L-tyrosine. Following this '1st use testing' as illustrated in **Fig 4.12** the electrode was removed from the tyrosine solution, gently rinsed with deionised water and then placed back into the same solution and let sit for 5 min. After 5 min the same modified electrode was tested in the same solution for the determination of L-Try with this testing step referred to as '2nd use testing'. This procedure was continued two more times with subsequent testing results seen as 3rd use and 4th use in the CV. It is clearly evident that after the first testing in the tyrosine solution, the sensing ability of the modified electrode dramatically decreases with subsequent use. The peak current for the first use was recorded at 0.625 V (*vs*. SCE) and is a significantly higher peak in comparison to the peak current recorded at 0.655 V (*vs*. SCE) for the second use of the electrode, which is a much lower and smaller peak. It can also be noted that the oxidation peak of L-Try has shifted slightly in potential from the 1st to the 2nd use by 0.03 V (*vs*. SCE). The 3rd use shows an extremely low current at approximately 0.65 V (*vs*. SCE), with the 4th use resulting in no levels of detection.

The slight increase in potential from the 1st to the 2nd use indicates that more energy was required to bring about oxidation of L-Try on the pre-used sensor during the second round of testing. The decrease in L-Try sensing and the slight potential increase may be related to the fact that some of the oxidised product may still be present at the electrode surface following the first use. The oxidised product may possibly have become embedded within the thick chitosan hydrogel and remained there even after the electrode was rinsed with deionised water. The remains of oxidised product means there is less surface area available for the diffusion of new tyrosine molecules onto the modified-GCE surface hence the significant decrease in

tyrosine determination. Furthermore, as an oxidised product is present on the surface during the next round of cyclic voltammetry, this product cannot be readily oxidised again therefore the process requires a higher potential to bring about some oxidation of fresh tyrosine molecules.

There are several products of tyrsoine oxidation that have been proposed in the literature with the dominant ones being 3,4-dihydroxyl-L-phenyalainine also know as DOPA and dimers of tyrsoine [31]. It has been reported that the oxidation of tyrosine by cyclic voltammetry is an equal electron-proton transfer process [32] and is irreversible due to the absence of a reduction peak during the reverse scan. The proposed oxidation is described in Scheme 1.

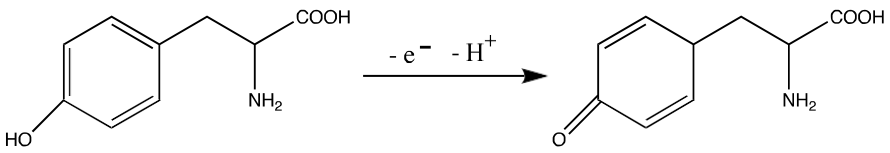

Scheme 1: Oxidation of Tyrosine [32].

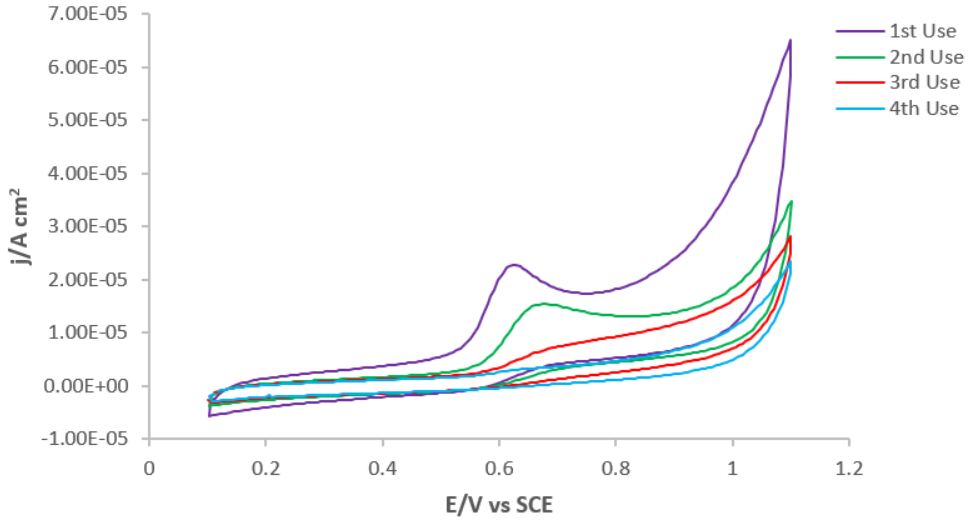

Figure 4.12: Cyclic voltammetry recorded at 50 mV s^{-1} cycled between 0.3 V to 1.1 V for 5 cycles displaying cycle 2, in 1 mM L-Try solution. Consecutive testing was carried out under identical conditions and solution.

4.5 Bibliography

1. Ray, S.C. *Application and Uses of Graphene Oxide and Reduced Graphene Oxide*; Elsevier Inc., 2015;

2. Chen, L.; Tang, Y.; Wang, K.; Liu, C.; Luo, S. Direct electrodeposition of reduced graphene oxide on glassy carbon electrode and its electrochemical application. *Electrochem. commun.* **2011**, *13*, 133–137, doi:10.1016/j.elecom.2010.11.033.

3. Zang, X.; Liang, L.; Wang, X.; Li, C.; Li, P.; Shao, Q.; Cao, N. β-Cyclodextrin Anchor NiCo2S4 on Graphene to Enhance Electrochemical Performance of Supercapacitor. *Energy Technol.* **2022**, doi:10.1002/ente.202200490.

4. Matencio, A.; Hoti, G.; Monfared, Y.K.; Rezayat, A.; Pedrazzo, A.R.; Caldera, F.; Trotta, F. Cyclodextrin monomers and polymers for drug activity enhancement. *Polymers (Basel).* **2021**, *13*, 1–18, doi:10.3390/polym13111684.

5. Geng, Z.; Wang, X.; Guo, X.; Zhang, Z.; Chen, Y.; Wang, Y. Electrodeposition of chitosan based on coordination with metal ions: In situ -generated by electrochemical oxidation. *J. Mater. Chem. B* **2016**, *4*, 3331–3338, doi:10.1039/c6tb00336b.

6. Nawrotek, K.; Grams, J. Understanding electrodeposition of chitosan–hydroxyapatite structures for regeneration of tubular-shaped tissues and organs. *Materials (Basel).* **2021**, *14*, 1–14, doi:10.3390/ma14051288.

7. S. Dassanayake, R.; Acharya, S.; Abidi, N. Biopolymer-Based Materials from Polysaccharides: Properties, Processing, Characterization and Sorption Applications. *Adv. Sorption Process Appl.* **2019**, doi:10.5772/intechopen.80898.

8. Dahmane, E.M.; Taourirte, M.; Eladlani, N.; Rhazi, M. Extraction and Characterization of Chitin and Chitosan from Parapenaeus longirostris from Moroccan Local Sources. *Int. J. Polym. Anal. Charact.* **2014**, *19*, 342–351, doi:10.1080/1023666X.2014.902577.

9. Frick, J.M.; Ambrosi, A.; Pollo, L.D.; Tessaro, I.C. Influence of Glutaraldehyde Crosslinking and Alkaline Post-treatment on the Properties of Chitosan-Based Films. *J. Polym. Environ.* **2018**, *26*, 2748–2757, doi:10.1007/s10924-017-1166-3.

10. Gea, S.; Sari, J.N.; Bulan, R.; Piliang, A.; Amaturrahim, S.A.; Hutapea, Y.A. Chitosan/graphene oxide biocomposite film from pencil rod. *J. Phys. Conf. Ser.* **2018**,

970, doi:10.1088/1742-6596/970/1/012006.

11. Peng, Y.; Chen, Z.; Zhang, R.; Zhou, W.; Gao, P.; Wu, J.; Liu, H.; Liu, J.; Hu, A.; Chen, X. Oxygen-Containing Functional Groups Regulating the Carbon/Electrolyte Interfacial Properties Toward Enhanced K+ Storage. *Nano-Micro Lett.* **2021**, *13*, 1–15, doi:10.1007/s40820-021-00722-3.

12. Jerigová, M.; Odziomek, M.; López-Salas, N. "We Are Here!" Oxygen Functional Groups in Carbons for Electrochemical Applications. *ACS Omega* **2022**, *7*, 11544–11554, doi:10.1021/acsomega.2c00639.

13. Ambrosi, A.; Chua, C.K.; Bonanni, A.; Pumera, M. Electrochemistry of graphene and related materials. *Chem. Rev.* **2014**, *114*, 7150–7188, doi:10.1021/cr500023c.

14. Payet, L.; Ponton, A.; Léger, L.; Hervet, H.; Grossiord, J.L.; Agnely, F. Self-diffusion in chitosan networks: From a gel-gel method to fluorescence recovery after photobleaching by fringe pattern. *Macromolecules* **2008**, *41*, 9376–9381, doi:10.1021/ma801192q.

15. Bradley, K.T.; Westlund, N.K. 乳鼠心肌提取 HHS Public Access. *J Neruosci Res* **2017**, *95*, 1336–1356, doi:10.1007/s10439-016-1768-2.Alginate-chitosan.

16. Campbell, K.T.; Wysoczynski, K.; Hadley, D.J.; Silva, E.A. Computational-Based Design of Hydrogels with Predictable Mesh Properties. *ACS Biomater. Sci. Eng.* **2020**, *6*, 308–319, doi:10.1021/acsbiomaterials.9b01520.

17. Subbiah, B.; Morison, K.; Morison, K.R. Effect of viscosity on electrical conductivity in liquid foods Hydrodynamic cavitation View project Create new project "Physical Properties of model food systems" View project Effect of viscosity on electrical conductivity in liquid foods. **2017**.

18. Huang, C.; Chen, S.; Ruhsing Pan, J. Optimal condition for modification of chitosan: A biopolymer for coagulation of colloidal particles. *Water Res.* **2000**, *34*, 1057–1062, doi:10.1016/S0043-1354(99)00211-0.

19. Rinaudo, M.; Pavlov, G.; Desbrières, J. Solubilization of Chitosan in Strong Acid Medium. *Int. J. Polym. Anal. Charact.* **1999**, *5*, 267–276, doi:10.1080/10236669908009742.

20. Staszak, M. A Linear Diffusion Model of Adsorption Kinetics at Fluid/Fluid Interfaces.

J. Surfactants Deterg. **2016**, *19*, 297–314, doi:10.1007/s11743-016-1789-8.

21. Martins, A.M.; Eng, G.; Caridade, G.; Mano, F.; Reis, R.L. Electrically Conductive Chitosan/Carbon Sca ff olds for Cardiac Tissue Engineering. **2014**.

22. Bartnikowski, M.; Wellard, R.M.; Woodruff, M.; Klein, T. Tailoring hydrogel viscoelasticity with physical and chemical crosslinking. *Polymers (Basel).* **2015**, *7*, 2650–2669, doi:10.3390/polym7121539.

23. Axpe, E.; Chan, D.; Offeddu, G.S.; Chang, Y.; Merida, D.; Hernandez, H.L.; Appel, E.A. A Multiscale Model for Solute Diffusion in Hydrogels. *Macromolecules* **2019**,*52*, 6889–6897, doi:10.1021/acs.macromol.9b00753.

24. Luo, H.; Li, H.; Ge, Q.; Cong, H.; Tao, Z.; Liu, M. An electrochemical sensor for enantiorecognition of tyrosine based on a chiral macrocycle functionalized rGO. *Microchem. J.* **2021**, *164*, 105949, doi:10.1016/j.microc.2021.105949.

25. Zou, J.; Yu, J.G. Chiral recognition of tyrosine enantiomers on a novel bis-aminosaccharides composite modified glassy carbon electrode. *Anal. Chim. Acta* **2019**, *1088*, 35–44, doi:10.1016/j.aca.2019.08.018.

26. Yang, J.; Wu, D.; Fan, G.C.; Ma, L.; Tao, Y.; Qin, Y.; Kong, Y. A chiral helical self-assembly for electrochemical recognition of tryptophan enantiomers. *Electrochem. commun.* **2019**, *104*, 106478, doi:10.1016/j.elecom.2019.06.004.

27. Schneider, H.J.; Strongin, R.M. Supramolecular interactions in chemomechanical polymers. *Acc. Chem. Res.* **2009**, *42*, 1489–1500, doi:10.1021/ar800274u.

28. Takara, E.A.; Vega-Hissi, E.G.; Garro-Martinez, J.C.; Marchese, J.; Ochoa, N.A. About endothermic sorption of tyrosine on chitosan films. *Carbohydr. Polym.* **2019**, *206*, 57–64, doi:10.1016/j.carbpol.2018.10.102.

29. Li, Z.; Mo, Z.; Yan, P.; Meng, S.; Wang, R.; Niu, X.; Liu, N.; Guo, R. Chiral electrochemical recognition of tryptophan enantiomers at a multi-walled carbon nanotube-: N -carboxymethyl chitosan composite-modified glassy carbon electrode. *New J. Chem.* **2018**, *42*, 11635–11641, doi:10.1039/c8nj01814f.

30. Finšgar, M.; Majer, D.; Maver, U.; Maver, T. Reusability of SPE and Sb-modified SPE sensors for trace Pb(II) determination. *Sensors (Switzerland)* **2018**, *18*, doi:10.3390/s18113976.

31. Recky, J.R.N.; Serrano, M.P.; Laura, M.D.; Lorente, C. Free Radical Biology and Medicine Oxidation of tyrosine: Antioxidant mechanism of L -DOPA disclosed. *Free Radic. Biol. Med. J.* **2021**, *165*, 360–367.

32. Cheng, H.; Chen, C.; Zhang, S. Electrochemical behavior and sensitive determination of L-tyrosine with a gold nanoparticles modified glassy carbon electrode. *Anal. Sci.* **2009**, *25*, 1221–1225, doi:10.2116/analsci.25.1221.

Chapter 5: Conclusions

5.1 General Conclusions

The results presented in Chapter 3 clearly show that activation of the GCE surface gives rise to an efficient and cost-effective electrochemical sensor for the detection of acetaminophen. During the proposed electropolymerisation of β-CD at the GCE surface, it was discovered that the typical potential window applied during cyclic voltammetry resulted in the activation and oxidation of GCE surface. This activation significantly improved the electrochemical performance of the sensor, enhancing the detection of acetaminophen. Results and findings conclude that acetaminophen is adsorbed at the activated surface with this adsorption also protecting the oxidised acetaminophen product from extensive hydrolysis. Within the literature there are numerous studies that have also investigated the electropolymerisation of β-CD at the GCE surface, however many fail to investigate the role of the activation process in relation to improved sensor sensitivity, with this enhancement typically only related to the electropolymerisation process. Therefore, when modifying glassy carbon electrodes or indeed other carbon-based electrodes by cycling between high and low potentials it is clearly important to perform control experiments to separate the effects of the potential activation of the carbon-based that occurs during the modification steps.

In Chapter 4, it was found that a CS/GO composite can serve as a chiral sensor enabling the enantioselective discrimination of L- and D-Try. The addition of graphene appears to enhance the conductivity of the sensor. Nevertheless, the chitosan, while acting as a dependable chiral material enabling good enantioselectivity, greatly reduces the conductivity of the sensor. It was also clear that diffusion of the analyte within the chitosan was relevant and greater enantioselective discrimination was achieved by allowing time to enable the diffusion of the Try within the chitosan hydrogel. Nevertheless, a greater understanding of these diffusion processes within the hydrogel matrix is needed, given some of the large variations seen in the peak potentials of the D- and L-Try. Furthermore, the CS/GO has rather poor long-term stability in water with the dissolution of the hydrogel.

5.2 Future Work

The CS/GO modified GCE was tested for the enantioselective recognition of tyrosine enantiomers with good selectivity being achieved. However, further work is needed to develop a better understanding of the diffusion of the tyrosine amino acid within the hydrogel matrix

and the role played by the hydrogel in this diffusion process. As the CS/GO is immersed in water it swells and ultimately dissolves from the surface. Crosslinking could be used to stabilise the CS/GO sensor and extend its applications as a chiral sensor in water, and this would be an interesting future study. Other future work would possibly involve the application of the CS/GO-GCE sensor for the electrochemical differentiation of other amino acid enantiomers, such as tryptophan. Tryptophan is similar in size to tyrosine, as previously mentioned in Chapter 4, and would therefore be a likely match for the mesh size of the chitosan polymer of the CS/GO-GCE. Likewise, by using larger and smaller analytes more mechanistic data could be obtained linking the mesh size of chitosan with the size and charge of the amino acid or analytes.

Published Papers:

1) **Healy, B**., Rizzuto, F., de Rose, M., Yu, T., Breslin, C.B. Published: J. Solid State Electrochemistry, 2021, 25(10-11), pp. 2599–2609.

Title: *Electrochemical determination of acetaminophen at a carbon electrode modified in the presence of β-cyclodextrin: role of the activated glassy carbon and the electropolymerised β-cyclodextrin*

2) da Silva Alves, D.C., **Healy, B**., Yu, T., Breslin, C.B.

Materials, 2021, 14(13), 3655

Graphene-based materials immobilized within chitosan: Applications as adsorbents for the removal of aquatic pollutants

3) **Healy, B**., Yu, T., da Silva Alves, D.C., Okeke, C., Breslin, C.B.

Materials, 2021, 14(7), 1668

Cyclodextrins as supramolecular recognition systems: Applications in the fabrication of electrochemical sensors

4) da Silva Alves, D.C., **Healy, B**., Pinto, L.A.A., Cadaval, T.R.S., Breslin, C.B.

Molecules, 2021, 26(3), 594

Recent developments in Chitosan-based adsorbents for the removal of pollutants from aqueous environments